ICT | ILLINOIS CENTER FOR TRANSPORTATION

Reducing Concrete Cure Times for Bridge Substructure Components and Box Culverts

Prepared By
Faisal Qadri
Nishant Garg, PhD
University of Illinois Urbana-Champaign

A report of the findings of

ICT PROJECT R27-213
Reducing Concrete Cure Times for Bridge Substructure Components and Box Culverts

Illinois Center for Transportation

September 2023

1. Report No. FHWA-ICT-23-013	2. Government Accession No. N/A	3. Recipient's Catalog No. N/A
4. Title and Subtitle Reducing Concrete Cure Times for Bridge Substructure Components and Box Culverts		5. Report Date September 2023
		6. Performing Organization Code N/A
7. Authors Faisal Qadri and Nishant Garg (https://orcid.org/0000-0001-9292-8364)		8. Performing Organization Report No. ICT-23-018 UILU-2023-2018
9. Performing Organization Name and Address Illinois Center for Transportation Department of Civil and Environmental Engineering University of Illinois at Urbana-Champaign 205 North Mathews Avenue, MC-250 Urbana, IL 61801		10. Work Unit No. N/A
		11. Contract or Grant No. R27-213
12. Sponsoring Agency Name and Address Illinois Department of Transportation (SPR) Bureau of Research 126 East Ash Street Springfield, IL 62704		13. Type of Report and Period Covered Final Report 8/16/20–9/30/23
		14. Sponsoring Agency Code
15. Supplementary Notes Conducted in cooperation with the U.S. Department of Transportation, Federal Highway Administration. https://doi.org/10.36501/0197-9191/23-018		

16. Abstract

This report investigated pathways to reduce concrete curing time while maintaining mechanical and durability performance. Among several options such as admixtures, supplementary cementitious materials, and low water-to-cement ratio, researchers explored two mix designs in a field demonstration project. For Stage I of the project, a low water-to-cement ratio concrete mixture was used. For Stage II, the use of calcium-silicate-hydrate (C-S-H) based seeds was explored. Concrete laboratory mixtures containing C-S-H seeds X1 and X2 exhibited increased early-age strength and reduced permeability. Based on these findings and the Illinois Department of Transportation acceptance of X2 as a Type S admixture, a field demonstration project was conducted on a box culvert near Armstrong, Illinois. The X2 concrete mix design was compared to a low water-to-cement ratio concrete mix design. Results showed that the X2 mixture with C-S-H seeds consistently demonstrated higher strength than the low water-to-cement concrete mixture, suggesting that seed-based admixtures can provide additional benefits for reducing curing times. The recommended dosage of X2 is 5 fl oz/cwt for optimal performance in reducing cure time.

17. Key Words Compressive Strength, Acceleration, C-S-H Seeds, Open Porosity, Fly Ash, Concrete, Electrical Resistivity, Formation Factor	18. Distribution Statement No restrictions. This document is available through the National Technical Information Service, Springfield, VA 22161.		
19. Security Classif. (of this report) Unclassified	20. Security Classif. (of this page) Unclassified	21. No. of Pages 64 + appendices	22. Price N/A

Form DOT F 1700.7 (8-72)   **Reproduction of completed page authorized**

ACKNOWLEDGMENT, DISCLAIMER, MANUFACTURERS' NAMES

EXECUTIVE SUMMARY

The main objective of this research was to investigate how to reduce the concrete curing time from 7 days to 3 days for bridge substructure components and box culverts and still maintain the required mechanical and durability performance. For this objective, the effect of water-to-cement (w/c) ratio and fly ash replacement with ordinary Portland cement (OPC) on strength development and microstructure refinement were evaluated. Additionally, the potential of using calcium-silicate-hydrate (C-S-H) based seeds, specifically X1 and X2 products, were evaluated. These seeds were commercially available and were tested in a series of laboratory experiments to evaluate their performance. The results were then compared to laboratory control mixtures to assess the effectiveness of the seeds. In addition to the lab tests, one seed type, X2, was tested in the field on a box culvert near Armstrong, Illinois, to determine its performance in real-world conditions.

The laboratory tests revealed that X1 had a slightly accelerating effect on the reaction kinetics of the cementitious pastes, resulting in a higher degree of hydration, as measured by total cumulative heat recorded from isothermal calorimetry. This finding was seen at all dosages up to 30 fl oz/cwt, with higher dosages also resulting in a finer microstructure, as indicated by reduced open porosity values. X1 also seemed to limit the diffusion of chloride ions into the cement pastes and reduce water sorptivity.

In contrast, X2 had a slightly retarding effect on the reaction kinetics of the cementitious pastes at the beginning of hydration. However, over a three-day period, it also resulted in a higher degree of hydration, as shown by the total cumulative heat from calorimetry. The optimal dosage for reducing open porosity was 14 fl oz/cwt, at which the lowest value of 10% was recorded. Thermogravimetry data showed an increase in bound water with increasing dosage of these seeds, suggesting a finer microstructure. Concrete mixtures containing X2 at dosages of 0 (control), 7, and 14 fl oz/cwt had increased early-age strength and reduced permeability, as indicated by the formation factor. There were strong correlations observed between various measurement parameters, including total mass loss via thermogravimetry, cumulative heat, open porosity, formation factor, and compressive strength.

X2 was selected for further testing in the field based on these laboratory findings and the acceptance of X2 as a Type S admixture by Illinois Department of Transportation (IDOT). To supplement the laboratory findings, a series of concrete mixtures were cast in the field to ascertain the range of variability for permeability. Based on this range, a low water-to-cement ratio concrete mixture was selected for the demo project. A demo project was then conducted under two stages, one with and one without X2, to compare the effect of using seeds in the field. The mixtures containing X2 consistently had higher strength than control mixes. Finally, there were clear relationships between compressive strength and formation factors for all mixes deployed in the field, suggesting resistivity-based rapid testing can be used as an approximate indicator of mechanical strength development. It should be noted, however, that the relationship between formation factor and strength is highly mix-dependent and formation factors should not be compared across different mixes.

Overall, the results of this study suggest that seed-based admixtures have the potential to enhance the strength and microstructure of concrete, leading to reduced curing times. The type and dosage of the admixture are important factors that should be carefully considered based on desired performance, cost, and feasibility. Based on lab and field testing, X2 at a dosage of 5 fl oz/cwt performed well in reducing concrete cure time, achieving early strength gain, and reducing porosity.

TABLE OF CONTENTS

LIST OF FIGURES

LIST OF TABLES

CHAPTER 1: INTRODUCTION

BACKGROUND

Curing, which is typically done after concrete placement, is primarily responsible for maintaining the desired moisture and temperature conditions in the bulk of concrete for maximum hydration. Maximum hydration, in turn, leads to reduced porosity, which directly affects strength and durability aspects such as permeability and freezing and thawing (Kosmatka & Wilson, 2016). Given the importance of curing, several practical and useful guidelines have been published over the years (American Concrete Institute, 2016; Taylor, 2013).

According to Illinois Department of Transportation specifications, several types of concrete construction have a curing period of up to seven days. IDOT's *Standard Specifications for Road and Bridge Construction* (2022) require cast-in-place substructures and cast-in-place box culverts to cure for seven days. For precast structural members and precast box culverts, the producer has the option to discontinue curing when the concrete has attained 80% of the mix design strength or after 7 days of curing (IDOT, 2022).

The American Association of State Highway and Transportation Officials (AASHTO) allows curing time less than 7 days in some cases. AASHTO LRFD Bridge Design Specifications states that for other than top slabs of structures serving as finished pavements and Class A (HPC) concrete, the curing period may be terminated when test cylinders cured under the same conditions as the structure indicate that concrete strengths of at least 70% of that specified have been reached (AASHTO, 2020).

Considering that concrete curing is based on a Type I or Type IL cement achieving a specific strength and not on a certain level of porosity or durability, there is room to tailor the cure time to a set level of porosity. However, quantifying porosity (which is intrinsically linked to durability) in cementitious materials is not straightforward (Berodier & Scrivener, 2015). Complexity arises from the fact that pores in concrete can span multiple scales, ranging from a few nanometers (gel pores) to a few microns (capillary pores) or a few millimeters (air voids). Figure 1 presents a comparison between porosity, permeability, and strength. Porosity is defined as the measure of the volume of voids in concrete, and permeability is defined as the rate of flow of moisture through concrete.

RESEARCH OBJECTIVE

Curing concrete is important to achieve a high level of hydration and a well-refined microstructure. A dense microstructure leads to reduced porosity and improved transport properties, such as lower permeability in the cement matrix. Traditional curing methods can be time-consuming and costly. The objective of this research is to develop a concrete mix design that requires less curing time than the usual seven days, without sacrificing mechanical strength or durability.
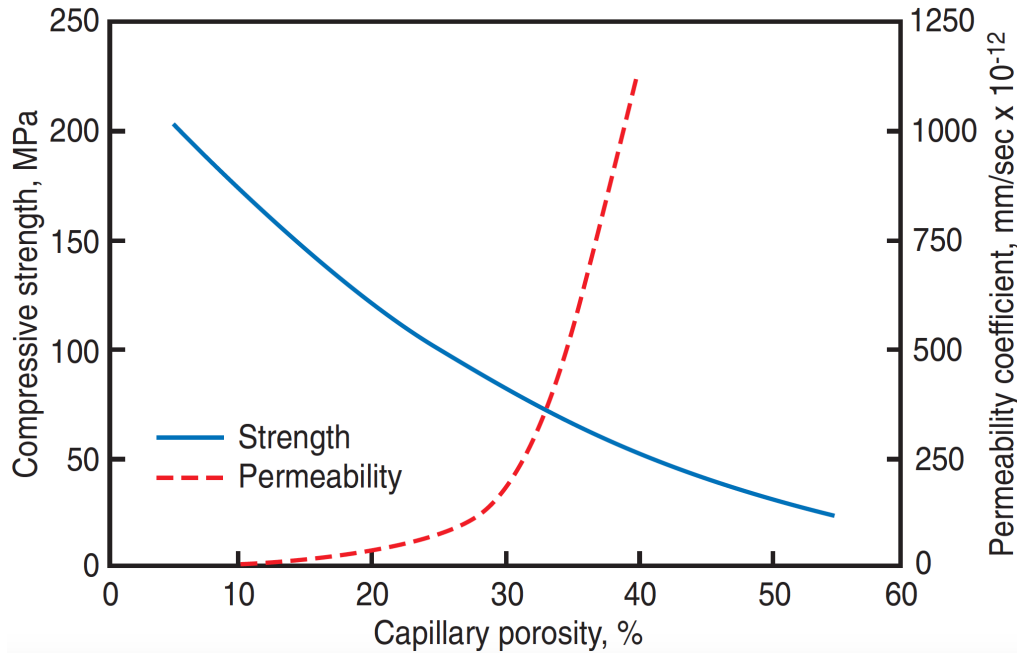
Figure 1. Graph. A comparison plot, adapted from the PCA handbook (Kosmatka & Wilson, 2016), presents the interdependence of several concrete properties such as strength, permeability, and porosity. Historical data in the plot were originally reported by Powers (1958).

This study evaluated two approaches to reduce curing time. The first approach was to evaluate the water-to-cement (w/c) ratio and the fly ash replacement with ordinary Portland cement (OPC) on strength development and microstructure refinement based on collected data from concrete mixtures obtained from the field. The second approach was to evaluate a new kind of seed-based chemical. Commercially available C-S-H (calcium silicate hydrate) seed-based chemical admixtures were added to cement paste and concrete mixtures and were evaluated based on their performance on strength, kinetics, and transport properties. These admixtures are called X1 and X2. X1 is designed to develop very high strength (< 16 hours), and the supplier recommended it to be used for precast applications. However, X2 is designed to develop high strength at an early age (1 day) and a late age (28 days). For this reason, X2 is recommended to be used for cast-in-place concrete where very early strength is not a big concern. This study aims to evaluate the performance of both admixtures within a few days after casting.

The abovementioned approaches were evaluated based on the strength, kinetics, and transport properties of concrete. To do this, the researchers will prepare cement paste mixtures in the lab and test them using various techniques such as isothermal calorimetry, open porosity, sorptivity, and thermogravimetry analysis (TGA). They will also evaluate concrete samples from both the field and the lab for their compressive strength, center-point flexural strength, and surface electrical resistivity at different ages. They will discuss the results of these tests in detail later in this report. Based on the results, the researchers will provide recommendations for reduced curing times that can be applied to concrete bridge substructure components and concrete box culverts without compromising strength and permeability.

CHAPTER 2: LITERATURE REVIEW

PRACTICAL PERSPECTIVE

Several criteria are used to evaluate concrete performance such as fresh properties, strength, and durability aspects. Strength is the most important criterion in most cases, because contractors commonly rely on achieving a certain value of strength, which is then used to decide further actions such as opening the road to traffic or removing the formwork of any structural element (Todd et al., 2017; Das et al., 2020), saving time and money. From a practical perspective, achieving high strength early reduces concrete curing time, which in turn saves labor costs and materials. In addition, reducing curing time allows drivers to use roads earlier, saving on logistic costs required from the contractors due to road closures. Moreover, a continuous pace of construction can be achieved, allowing for earlier finish times and formwork removal (Ferreira & Jalali, 2010). Regarding the criteria for opening roads to traffic in the US, state departments of transportation (DOTs) require achieving a certain flexural or compressive strength, which varies among DOTs. For example, Illinois DOT requires a minimum flexural strength 4.5 MPa (650 psi) or a minimum compressive strength 24.1 MPa (3,500 psi) (IDOT, 2022), whereas Michigan and Indiana require a minimum flexural strength 3.8 MPa (550 psi) (MDOT, 2020; INDOT; 2022).

CONCRETE CURING AND MICROSTRUCTURE ENHANCEMENT

Necessity for Curing

Concrete curing is required to enhance the degree of cement hydration and to densify its microstructure. OPC concrete achieves full hydration and full strength gain at 28 days after casting, and it needs at least seven continuous days of moist curing to achieve full strength (Price, 1951). Figure 2 demonstrates that the concrete was cured in a moist environment for seven days and then was kept in air until day 28 to achieve an equivalent compressive strength of concrete that continuously moist cured for 28 days. From this process, the available specifications decide the required curing times based on strength only, and without considering durability issues.

Elongated curing time is tedious and expensive. Different approaches have been used to enhance curing processing or performance of concrete such as increasing strength and lengthening service against premature damage. For example, internal curing technology has been used to enhance curing by providing extra water that gets adsorbed from the prewetted lightweight aggregates. This technology enhances the hydration of cement and achieves high early strength (Qadri & Jones, 2020). However, this technique requires special preparation for the aggregates prior to casting. Another approach to enhance cement hydration and concrete performance is to use supplementary cementitious materials (SCMs), as explained in the next subsection.
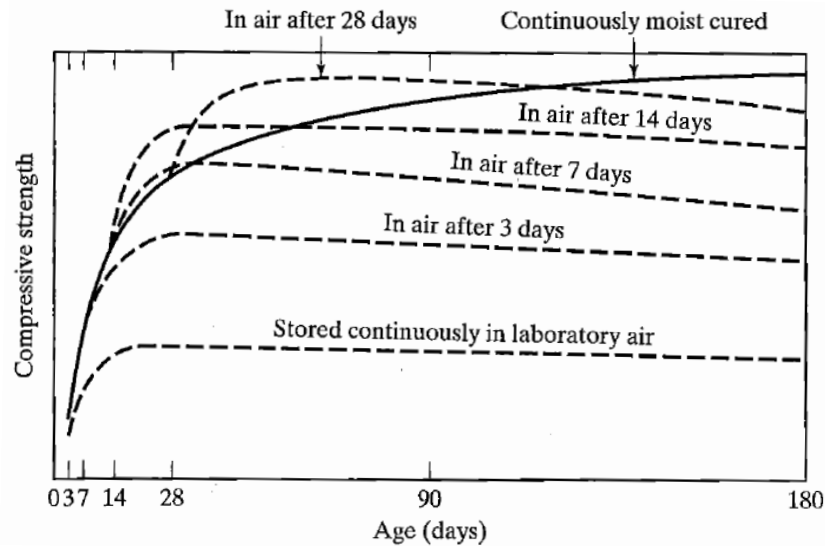
Figure 2. Graph. Compressive strength of concrete at different ages and curing levels.

Source: Price (1951)

Supplementary Cementitious Materials and Microstructure Enhancement

Supplementary cementitious materials (SCMs) like fly ash, blast furnace slag, and silica fume are commonly used to enhance concrete performance (Juenger et al., 2019; Lothenbach et al., 2011). Using SCMs is a good approach to improve long-term strength; however, the main limitation is low early strength (e.g., three days). One possibility is to use silica fume, which plays a great role in refining the microstructure of concrete because of its small particle size and high surface area (Amin, Tayeh, & Agwa, 2020; Chaudhary & Sinha, 2020). Also, silica fume consumes calcium hydroxide and produces additional C-S-H, further increasing strength (Song et al., 2010). However, silica fume continues to be an expensive SCM and, thus, is not a very good solution for reducing the cure time of concrete. Moreover, traditional SCMs such as fly ash are experiencing high demand due to declining supply, and newer SCMs such as calcined clays may be a viable solution (Garg & Skibsted, 2014, 2015; Garg & Wang, 2012; Romero & Garg, 2022).

Chemical Admixtures and Rheological Properties

Alternatively, chemical admixtures are used to control the rheological properties of fresh concrete as well as the setting times and strength of hardened concrete. Water reducers, air entrainers, viscosity modifiers, shrinkage reducers, retarders, and accelerators are different chemical admixtures used to control fresh and hardened concrete properties (Ramachandran, 1996; Hanehara & Yamada, 1999; Houst et al., 2008; Aïtcin, 2016). In particular, *accelerators* are used to control setting times, strength development, or both, depending on the chemical compositions of the used accelerator (Hewlett & Liska, 2019). Accelerators play a great role in enhancing the rate of cement hydration in mortar and concrete. For example, using accelerators is a good solution for increasing the production rate in precast concrete plants due to the ability to remove formwork earlier. Also, accelerators are encouraged in cold weather, as they hasten hydration reactions and subsequently prevent the delay in strength development (Karagöl et al., 2013; Aïtcin, 2016; Kanchanason & Plank, 2019). Additionally,

accelerators can provide great value in small jobs, such as concrete pavement patching or repair where the job should be completed within a few hours before opening the road for traffic (Todd et al., 2017; Qadri & Jones, 2020).

In general, accelerators affect cement hydration by shortening the setting time and increasing the rate of strength development (Cheung et al., 2011; Shanahan, Sedaghat, & Zayed, 2016). Accelerators are divided into two main categories: rapid-set accelerators and accelerators of setting and hardening (Hewlett & Liska, 2019). In the first category, the dissolution of the tricalcium aluminate (C3A) phase in ordinary Portland cement is accelerated, which significantly reduces setting time. Mechanistically, the silicates and aluminates in the solution are dissolved by the rapid-set accelerators, which results in interference with the C3A-gypsum reaction (Hewlett & Liska, 2019). Also, high-temperature development is accompanied by the reaction of C3A, which promotes the reaction of tricalcium silicate (C3S) and causes early strength development. Nevertheless, long-term strength is compromised when this type of accelerator is used (Hewlett & Young, 1983). Alkali metal oxides, silicates, aluminates, and carbonates are some examples of these accelerators. However, these accelerators are limited to niche applications such as shotcrete. The second category (accelerators of setting and hardening) are primarily made of acids that influence C3S hydration as opposed to C3A hydration (Hewlett & Liska, 2019). These accelerators could either affect setting time or hardening, or both simultaneously, in a hydrating cement, depending on chemical composition. For example, while calcium nitrate ($Ca(NO_3)_2$) only affects setting and sodium thiocyanate (NaSCN) only affects hardening, calcium chloride ($CaCl_2$) affects both setting and hardening simultaneously. Further, the calcium chloride accelerator takes advantage of its small anion size (0.27 nm), which penetrates the silicate particles easier than formate and nitrite, whose anion sizes are 0.34 nm and 0.45 nm, respectively. For these reasons, calcium chloride is commonly used as a highly effective accelerator. Yet, using chloride-based accelerators in reinforced concrete promotes steel corrosion, resulting in major durability problems. These problems occur because of the development of cracks in concrete, which are caused by swelling-induced corrosion of reinforcing steel (Galan & Glasser, 2015; Vehmas, Kronlöf, & Cwirzen, 2018). To avoid any corrosion and potential durability issues, several chloride-free accelerators have been introduced to the market. Most of these accelerators are calcium salts, which tend to have superior performance compared to other metal salts by causing early supersaturation of the solution with $Ca(OH)_2$, which is due to the excess production of Ca^{2+} ions. This mechanism results in lowered setting times. For example, calcium nitrate ($Ca(NO_3)_2$) and calcium nitrite ($Ca(NO_2)_2$) have been widely studied as examples of chloride-free calcium-based accelerators (Justnes & Nygaard, 1995). Moreover, some researchers reported that some ordinary accelerators could compromise the elastic modulus by 20% as well as the ultimate compressive strength (Galobardes et al., 2014; Wei et al., 2022).

SEED ADDITIVES IN CONCRETE

Nano Seeds

Nano seeds or nano particles were introduced into the concrete industry almost a decade ago to accelerate and enhance hydration (Land & Stephan, 2012). There are several kinds of nano seeds such as those made of quartz, aluminum oxide (Korpa & Trettin, 2007; Mondal et al., 2010), titanium

oxide (Gaitero et al., 2010), or C-S-H–based seeds (Nicoleau et al., 2013). Several studies have been conducted to investigate the influence of adding nano seeds into cement paste and concrete. The studies found that nano seeds form new nucleation sites that promote the formation of hydration products on their surfaces, instead of forming hydration products on cement particles surfaces (Alizadeh et al., 2009; Thomas et al., 2009; Nicoleau et al., 2013; John et al., 2019; Wang et al., 2020). Figure 3 illustrates this phenomenon. The illustration demonstrates that nano seeds (C-S-H in this study) alter the location of the formation of the product. Growth of hydration products on the seeds instead of the clinker's surface prevent the inhibition of C_3S dissolution, which in turn accelerates cement hydration (John, Matschei, & Stephan, 2018; Magarotto, Zeminian, & Roncero, 2010; Thomas et al., 2009). Providing additional nucleation sites reduces the kinetic energy required to form hydration products and subsequently accelerates hydration (Wang et al., 2020). Figure 3 illustrates how introducing foreign seeds tends to accelerate cement hydration.
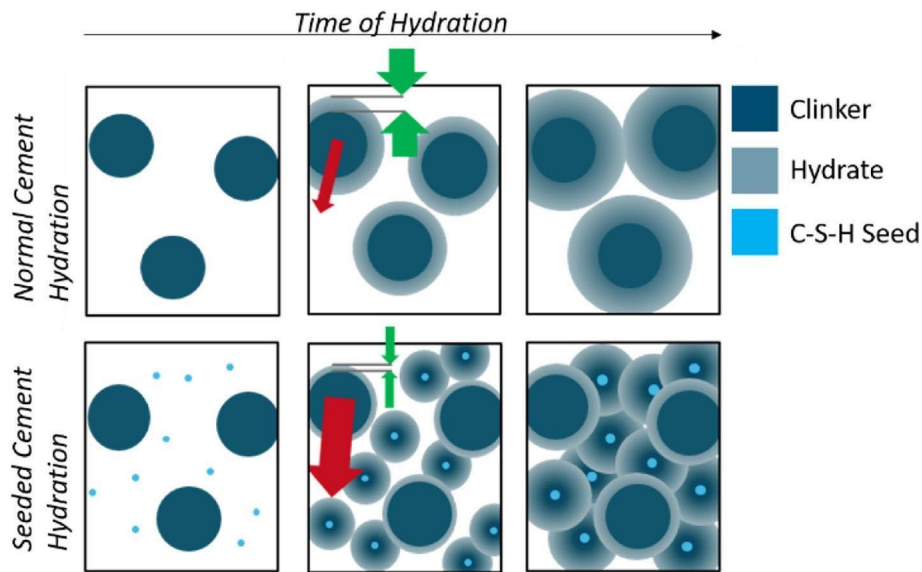
Figure 3. Graph. Schematic representation of the influence of nucleation seeding of C-S-H seeds on cement hydration. The green arrows indicate the different thicknesses of the hydration products formed on the surface of the clinker particles. The red arrows display concentration gradients.

Source: John et al. (2018)

The total energy required to form new phases is assumed to consist of interfacial free energy (positive) and bulk free energy (negative), which are responsible for the surface formation and phase transformation, respectively, according to the classical theory of nucleation (Balluffi, Allen, & Carter, 2005; Das et al., 2020). Any phase forms when the energy overcomes a certain value (called critical free energy), which is the peak on the curve presented in Figure 4. External nucleation sites tend to reduce the critical free energy so that the cement hydration is hastened (Balluffi et al., 2005; Das et al., 2020). Some researchers have proven that cement hydration is enhanced when nano seeds are added through isothermal calorimetry. They found that the amount of heat liberated increases earlier due to the shortened induction period of hydration (Garg, Gomez, & White, 2017; Land & Stephan, 2018; Wang et al., 2020). The molecular structure of the C-S-H hydrate phase was investigated by ^{29}Si

magic angle spinning (MAS) nuclear magnetic resonance (NMR) when nano-silica particles were added into cement paste at dosages of 1% and 3%. The degree of polymerization and chain length increased with the addition of the nano-silica particles (Moon et al., 2016). Moreover, the seed particle's morphology played a key role in the kinetics and nano structure of the C-S-H phase. Finer seeds tend to accelerate cement hydration more effectively than coarse seeds (Alizadeh et al., 2009; Thomas et al., 2009; Land & Stephan, 2012; Land & Stephan, 2015, 2018; Sharma et al., 2019) in addition to forming more Q2 species in the C-S-H hydrate product (John et al., 2019).
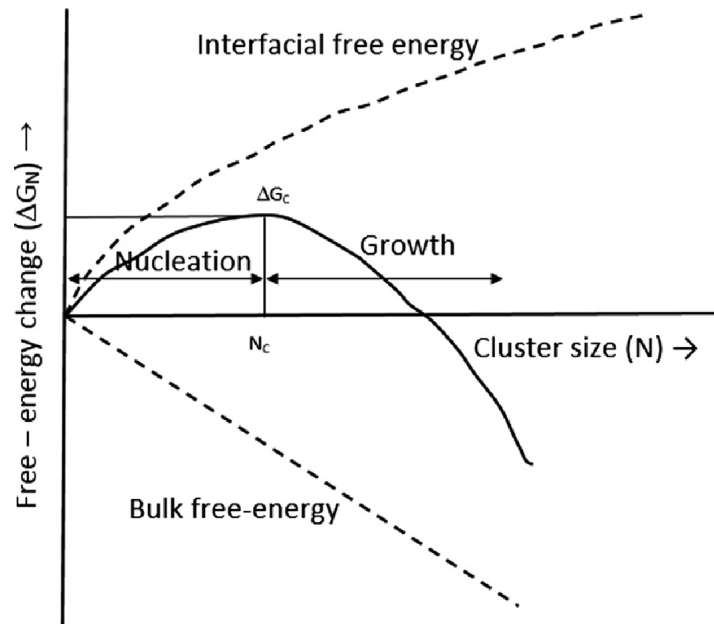
Figure 4. Graph. Free energy versus particle size.

Source: Das et al. (2020)

C-S-H Seeds as a Chemical Admixture

The C-S-H seed-based chemical admixture is gaining interest in the research community for its potential to enhance early cement hydration (John et al., 2018). It has been reported that introducing C-S-H seeds into the cement matrix enhances the kinetics and strength of cementitious mixes (Alzaza et al., 2022; Chen et al., 2023; Hubler, Thomas, & Jennings, 2011; Haoxin Li et al., 2020; Hui Li, Xiao, Yuan, & Ou, 2004; Theobald & Plank, 2022; Xu, Li, & Yang, 2020; Zhang, Yang, & Li, 2020). One of the key advances has been the stabilization of C-S-H particles through polyelectrolytes, which have been reported to be essential for the synthesis of active and stable C-S-H suspensions (Nicoleau et al., 2013). Moreover, these new seed-based admixtures can be cost-effective given that their synthesis involves nontoxic ingredients, which do not necessitate precaution or special lab requirements to deal with these materials (Bräu et al., 2012). A series of recent studies have found this seeding approach to be highly effective in accelerating reaction kinetics as well as improving early strength development (Li et al., 2004; Pedrosa et al., 2020). Yet, there have been limited studies on the impact of C-S-H seeds on pore-structure refinement and durability of cementitious systems (Wyrzykowski et al., 2020). Hence, there is a need to further explore their impact on cementitious pore structure and durability.

THERMAL SHOCK IN CONCRETE

Thermal shock is a criterion that needs some attention at early removal of formwork in the case of reduced cure time. Exposure to thermal shock may happen if the formwork is removed too early, where the surface of the structural element is still warm due to ongoing hydration. This shock usually occurs because of the temperature difference between the structural element's surface and its surroundings. This finding means that early removal of formwork increases the risk of having thermal shock, while increasing the time prior to formwork removal reduces the risk of having thermal shock (Bonneau & Aitcin, 2002). Zhang et al. (2013) stated that maximum cracking happens at the surface due to having the lowest degree of hydration and lowest tensile strength. Cracking risk decreases by 20% to 40% per day of stripping time (formwork removal time) postponement. Zhang et al. (2013) conducted a comparison between two mixtures prepared with OPC mixed at 0.45 w/c and 0.55 w/c, respectively. They observed that cracking risk is a little higher for mixtures mixed at 0.45 w/c than 0.55 w/c due to its relatively higher temperature rise associated with hydration. This observation might need some attention in concrete pavement as the high degree of hydration obtained in concrete mixtures prepared with accelerators might exhibit a significant difference in temperature between the pavement and the environment. A finite-element analysis conducted by Schrag, Qadri, and Jones (2021) for early-strength concrete patching found that delayed ettringite formation could result due to the high temperature > 70°C (158°F) when concrete hydration accelerated. Surface cracking may additionally result due to the thermal gradient between the core of the concrete pavement and the outer surface of the pavement (Schrag et al., 2021). In general, thermal shock is more significant in structural components covered with formwork from all sides than in pavements that have free exposure to air at casting.

CHAPTER 3: MATERIALS AND METHODS

ABBREVIATIONS

Table 1 provides the common measurement units and their explanations.

Table 1. Abbreviations Used in the Data Analysis

Abbreviation	Definition
psi	Pound per square inch
fl oz/cwt	Fluid ounce per 100 pounds of cement
kohm-cm	Kilo ohm*centimeter
mw/g	Milliwatt per gram
j/g	Joule per gram
mw/g.hrs	Milliwatt per gram per hour
(i, mm)	Water absorption in millimeter
$(s, \sqrt{min})$	Initial rate of absorption in square root of minutes

MATERIALS

This research used Type I OPC as the main cementitious material, Class C fly ash (FA), and commercially available C-S-H seeds X1 and X2 as strength-enhancing admixtures. Both chemical admixtures contain highly nano-crystalline C-S-H particles dispersed in different mediums. X1 meets ASTM C494 for Type S-specific performance admixtures (ASTM C494/C494 M-17, 2020). This admixture is usually used in the precast concrete applications as it enhances the very early age strength development. X2 meets ASTM C494 for Type S-specific performance admixtures (ASTM C494/C494 M-17, 2020). This admixture is usually used in cast-in-place concrete applications, as it increases strength at the early and late ages. The X-ray diffraction (XRD) patterns of the dried C-S-H seeds (X1) after drying in the oven for 48 hours at 105°C (221°F) are presented in Figure 5. These XRD patterns are compared to synthetic C-S-H samples obtained from two independent studies (Garg et al., 2019; Baral et al., 2022). Specifically, the C-S-H patterns of Ca/Si 1.4 (Garg et al., 2019) and 1.3 (Baral et al., 2022) are largely similar with major peaks at 29.4° and 32° as well as 29.4° and 32.01°, respectively. The XRD pattern of the C-S-H X1 also displays two major peaks at 29.6° and 32.06° with a narrow line width. Based on these observations, the researchers consider that these seeds likely contain highly crystalline C-S-H particles.

Concrete cylinders and beams were collected from the field to conduct center-point flexural and compressive strength tests in addition to conducting electrical resistivity testing. Different cement pastes and concrete mixtures were prepared in the lab to conduct several experiments. The following subsection briefly explains each sample size and preparation.
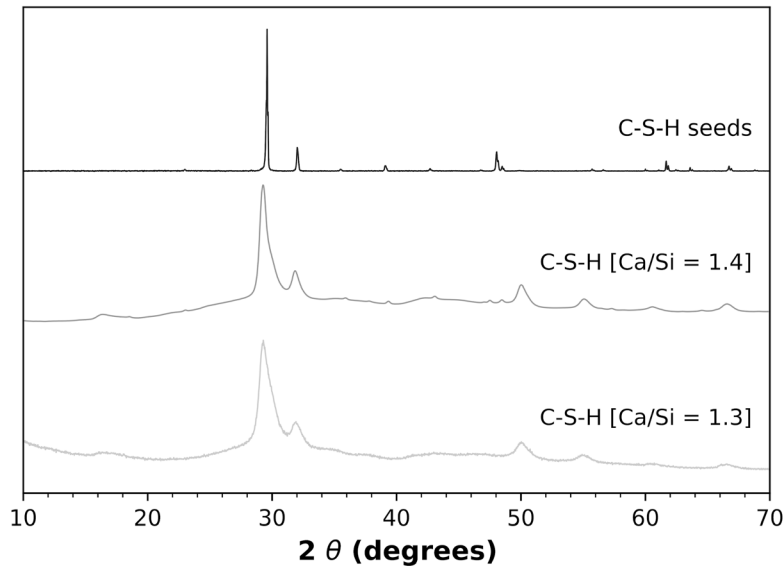
Figure 5. Graph. XRD pattern of the oven-dried commercially available X1 (top), compared with synthetic C-S-H gel of Ca/Si = 1.4 (Garg et al., 2019) and a synthetic C-S-H gel of Ca/Si = 1.3 (Baral et al., 2022).

Laboratory Work

Eight cement paste mixtures were prepared with Type I OPC, X1, and water at a w/c ratio equal to 0.40. The X1 doses increased from 0 to 30.17 fl oz/cwt of the cement. Please note that fluid ounces (fl oz) is the amount of the admixture, typically measured in US customary fluid ounces, that is equal to 29.5735 mL per fluid ounce. Hundredweight (cwt) refers to the quantity of cement, measured in units of 100 lb (approximately 45.36 kg). These mixtures were evaluated consistently by isothermal calorimetry, open porosity, sorptivity, chloride ion diffusion, and TGA. These methods will be explained later in this chapter.

The X2 strength-enhancing chemical admixture was evaluated in cement paste and concrete mixtures at different ages using Type I OPC and water at a w/c ratio equal to 0.48. Three mixtures were prepared with 0, 7, and 14 fl oz/cwt of X2 strength-enhancing chemical admixture. All cement paste mixtures were evaluated consistently by isothermal calorimetry, open porosity, and TGA. One more experiment was designed to evaluate cement paste mixtures prepared with Type I OPC, X2, and water at a w/c equal to 0.40. The mixtures were cured for three days. This experiment intended to evaluate a series of dosages to identify whether there is a threshold of added dosage of this admixture.

All cement paste specimens mixed with X1 and X2 were prepared by adding the materials to a 50 mL centrifugal vial and stirring them in a vortex mixer for 2 minutes at 3,000 revolutions per minute.

Moreover, three concrete mixtures prepared with and without X2 using dosages of 0, 7, and 14 fl oz/cwt were evaluated. These mixtures were evaluated by compressive strength, electrical resistivity, and formation factor. Fifteen 10.16 × 20.32 cm (4 × 8 in.) cylinders were cast for each mixture and

covered with plastic lids for the first day. After that, the cylinders were demolded and moved to the curing room (relative humidity = 95%, temperature = 23°C [73.4°F]). These cylinders were kept there until the day of testing. The mixtures were compared with field-based data. Table 2 presents the proportions for the concrete mixtures cast in the lab using OPC and X2 mixed at a w/c ratio equal to 0.48.

Independent experiments were conducted in this project to answer specific questions. For example, open porosity was conducted for a control and two OPC/FA (75% OPC and 25% FA) cement paste mixtures to examine the effect of fly ash on refining the microstructure over time. Also, a control and OPC/FA cement paste mixtures were prepared with and without the X2 admixture. This experiment intended to understand the effect of the X2 on OPC/FA (75% OPC and 25% FA) compared to the control mixture. All mixtures in the experiments were mixed with a w/c ratio = 0.40 and the dosage of X2 was 17 fl oz/cwt. Lastly, a chloride ion diffusion experiment was conducted to study the effect of w/c ratio on refining microstructure.

Table 2. Proportions of the Concrete Mixtures Cast in the Lab

Ingredient	Amount		
	M0	M7	M14
Cement kg (lb)	276 (609)	276 (609)	276 (609)
Water kg (lb)	164 (362)	163 (360)[1]	162 (358)[1]
Fine Aggregate[2] kg (lb)	512 (1,128)	512 (1,128)	512 (1,128)
Coarse Aggregate[2] kg (lb)	790 (1,742)	790 (1,742)	790 (1,742)
X2 Admixture mL/cwt (fl oz/cwt)	0	207 (7)	414 (14)

1: It was assumed 70% of the chemical admixture is water.
2: Aggregates in the dry state.

Field Work

Several concrete mixtures were cast in the field, and samples were collected for analysis. Table 3 presents the proportions for each concrete mixture. The fresh properties, including slump, air content, concrete temperature, and air temperature of each concrete mixture, were collected at the time of casting and are summarized in Table 4.

Table 3. Concrete Mixture Proportions Collected from the Field

Concrete Mixtures	Quantity Batched per Cubic Yard											
	Cement, kg (lb)	Fly Ash, kg (lb)	Water, L (gal)	FA[6], kg (lb)	CA[7], kg (lb)	AEA[8], mL (fl oz)	Water Reducer, mL (fl oz)	Accelerator or Retarder, mL (fl oz)	HRWR[9], mL (fl oz)	Water Reducer and Retarder, mL (fl oz)	VMA[10], mL (fl oz)	RCA[12], mL (fl oz)
SI Mix 75-25 OPC/FA[1]	194 (435)	67 (147.5)	103 (27.1)	560 (1,235)	834 (1,840)	237 (8)	600 (20.3)	–	–	–	–	–
SI Mix 75-25 OPC/FA+ ACC[1]	194 (435)	67 (147.5)	103 (27.1)	560 (1,235)	834 (1,840)	237 (8)	600 (20.3)	6,122 (207) (A)	–	–	–	–
SI Mix OPC[1]	259 (570)	–	102 (27)	569 (1,255)	832 (1,835)	177 (6)	577 (19.5)	–	–	–	–	–
SI Mix OPC + ACC[1]	259 (570)	–	102 (27)	569 (1,255)	832 (1,835)	177 (6)	577 (19.5)	6,122 (207) (A)	–	–	–	–
PC Mix OPC[2]	315 (695)	–	108 (28.6)	582 (1,282)	766 (1,689)	92 (3.1)	–	–	1,026 (34.7)	–	–	–
DS Mix 60-40 OPC/FA[3]	171 (378)	116 (256)	105 (27.7)	537 (1,184)	799 (1,762)	455 (15.4)	–	1,115 (37.7) (R)	376 (12.7)	650 (22)	367 (12.4)	–
Field Demo Stage I OPC[4]	286 (630)[11]	–	107 (28.3)	533 (1,174)[11]	831 (1,831)[11]	192 (6.5)	654 (22.1)	467 (15.8) (R)	840 (28.4)	–	–	–
Field Demo Stage II OPC + X2[5]	286 (630)[11]	–	119 (31.5)	529 (1,166)[11]	822 (1,812)[11]	296 (10)	651 (22)	186 (6.3) (R)	420 (14.2)	–	–	932 (31.5)

1: Cast on 10/21/2020 (IDOT Class SI structural mix design)

2: Cast on 3/31/2021 (IDOT Class PC precast concrete structural mix design)

3: Cast on 6/17/2021 (IDOT Class DS drilled shaft mix design for mass concrete pour)

4: Cast on 5/12/2022 (Box culvert field demo project near Armstrong, IL using experimental mix without X2)

5: Cast on 7/21/2022 (Box culvert field demo project near Armstrong, IL using experimental mix with X2)

6: Fine aggregate

7: Coarse aggregate

8: Air-entraining admixture

9: High-range water reducer

10: Viscosity modifying admixture

11: Theoretical batch weight provided since actual batch weight was unavailable.

12: Rheology-controlling admixture (X2). (X2 = 31.5 fl oz/6.3 cwt = 5 fl oz/cwt)

Table 4. Concrete Mixture Fresh Properties

Concrete Mixtures	Slump, cm (in.)	Air Content %	Concrete Temperature °C (°F)	Air Temperature °C (°F)	Water-to-Cement Ratio[2]
SI Mix 75-25 OPC/FA	12.7 (5.0)	5.7	23 (73)	8 (46)	0.39
SI Mix 75-25 OPC/FA + ACC	–	5.3	21 (70)	8 (46)	0.41
SI Mix 100 OPC	8.3 (3.25)	7.6	23 (73)	10 (50)	0.40
SI Mix 100 OPC + ACC	–	8.2	23 (73)	10 (50)	0.41
PC Mix 100 OPC	12 (4.75)	6.4	14 (58)	5 (41)	0.35
DS Mix 60-40 OPC/FA	20.3 (8.0)	7.0	19 (67)[1]	23 (74)	0.37
Field Demo Stage I OPC	16.5 (6.5)	5.1	31 (88)	33 (91)	0.38
Field Demo Stage II OPC + X2	12 (4.75)	5.4	27 (80)	18 (65)	0.42

1: Contractor added ice to the concrete mixture.

2: The calculated water-to-cement ratio includes water from the admixtures. It was assumed 70% of the chemical admixture dosage was water.

Twenty-four 10.16 × 20.32 cm (4 × 8 in.) cylinders and six 15.24 × 15.24 × 50.8 cm (6 × 6 × 20 in.) beams were cast and collected for the SI mix 75-25 OPC/FA, SI mix 75-25 OPC/FA + ACC, SI mix 100 OPC, and SI mix 100 OPC + ACC concrete mixtures. The mixtures were cast at a ready-mix concrete plant in Peoria, Illinois. Cylindrical samples were used to conduct compressive strength and surface electrical resistivity testing, and the beams were used to conduct center-point flexural strength testing. The cylinders and beams were demolded on the first day after casting and kept in water until reaching seven-day wet curing. Then, all samples were removed and surface moisture dried. During testing for compressive strength and surface electrical resistivity, the same cylinders were used to conduct both tests on days 1, 2, 3, and 7. On day 14, dried cylinders were accidentally used during the electrical resistivity testing. Therefore, three cylinders were returned to the water bath. At later ages, the remaining nine dried cylinders were used to conduct compressive strength testing at days 14, 52, and 97, and the three wet cylinders were used to conduct electrical resistivity testing at all remaining ages.

Twenty-seven cylinders and six beams were cast and obtained from a precast concrete plant (PC mix 100 OPC) in Champaign, Illinois. Twenty-one cylinders were kept sealed in the mold until compressive strength testing; however, beams for the center-point flexural strength test were demolded on the first day after casting and kept dry until the day of testing. Three cylinders were demolded on the first day after casting and kept in water for conducting electrical resistivity testing at all ages.

Twenty-seven cylinders and six beams were cast and collected from concrete mixtures prepared for casting a drilled shaft (DS mix 60-40 OPC+FA) for a new bridge in Peoria, Illinois. The cylinders and beams were demolded on the first day after casting and wet cured in water for seven days from the day of casting. Then, all samples were moved and kept dry except for three cylinders, which were kept in water to conduct surface electrical resistivity testing.

Three cylinders from PC mix 100 OPC and three cylinders from DS mix 60-40 OPC+FA concrete mixtures were kept dry by leaving them in the mold for 90 days. Then, they were moved to water for seven days to get saturated before conducting the electrical resistivity and formation factor tests.

This experiment was conducted to understand the effect of long- and short-term curing on electrical resistivity and formation factor measurements. The results for this experiment are presented in Tables 11 and 13 in Appendix A.

The last two concrete mixtures were called Field Demo Stage I 100 OPC and Field Demo Stage II 100 OPC + X2. The demo project is described in detail in the specification attached in Appendix B as the following: The demo project shall consist of the construction of a cast-in-place box culvert using Class SI concrete with a cure period in the range of 24 to 72 hours for Stage I and Stage II, as well as construction of trial batches for concrete testing with disposal of the excess concrete. The work shall be according to the applicable portions of Section 540 of the Standard Specifications (IDOT, 2022). These concrete mixtures were supplied by a ready-mix concrete plant in Paxton, Illinois, for construction of a box culvert located near Armstrong, Illinois. The stage I concrete mixture was an experimental mixture with no X2 chemical admixture, whereas the stage II concrete mixture contained the X2 strength-enhancing chemical admixture, as presented in Table 3. At that time, the cost of casting one cubic yard of stage I concrete mixture was $1,225 for labor and materials, whereas the cost of casting one cubic yard of stage II concrete mixture was $1,250. Thus, the C-S-H-based chemical admixture added cost was $25 per one cubic yard. Twenty-one 10.16 × 20.32 cm (4 × 8 in.) cylinders were cast and collected for stage I and stage II concrete mixtures at different times. These cylinders were demolded after one day and were kept in water for compressive strength and electrical resistivity testing. Six beams were also cast and tested by IDOT using a portable beam breaker capable of center-point flexural testing. The beams were demolded the next day and placed in a water bath.

Figure 6 presents a map of the State of Illinois and illustrates where the concrete mixtures were obtained. Location 1 is Peoria, location 2 is near Armstrong, and location 3 is Champaign. Figure 7 presents some specimens collected from the field.
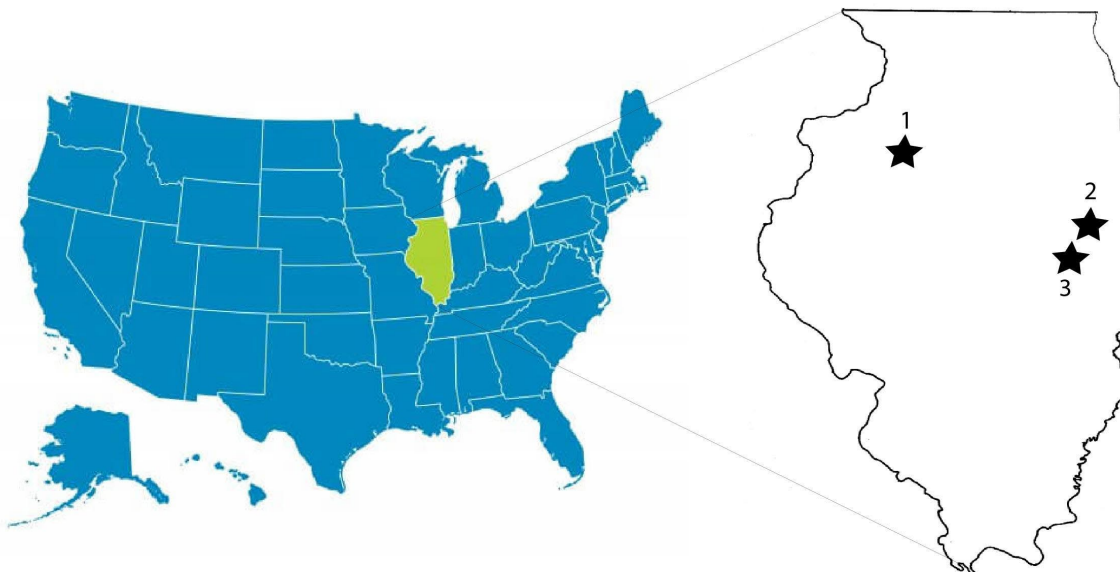
Figure 6. Map. A map of Illinois extracted from a US map. Location 1 is Peoria, location 2 is near Armstrong, and location 3 is Champaign.

a) Beam and cylinder test specimens cast in the field

b) Curing tanks used to store the specimens

c) Box culvert demo project near Armstrong, Illinois

Figure 7. Photos. a) Beam and cylinder test specimens cast in the field, b) the curing tanks used to store the specimens (curing medium was lime water: water and calcium hydroxide), and c) a box culvert demo project near Armstrong, Illinois.

Source: Figure partially modified and reproduced from Qadri and Garg (2023).

METHODS

Fresh Properties

Slump

AASHTO T 119 (2018) and ASTM C143 (2012) were used to measure slump for fresh concrete mixtures. The fresh concrete is poured in three layers into a damp Abrams cone seated and clamped to a flat base. Each layer is rodded 25 times, making sure the rod penetrates the whole layer and reaches the layer below. Then, the cone is lifted, and the vertical difference between the top of the cone and the center of the top surface of the displaced fresh concrete is measured and recorded to the nearest 6.4 mm (0.25 in).

Air Content

AASHTO T 152 (2019) and ASTM C231 (2009) were used to measure air content in the fresh concrete mixtures. A type-A meter and type-B meter were used in this project. Concrete is placed in three layers into the measuring bowl with a known volume. Each layer is rodded 25 times, making sure the rod penetrates the whole layer and reaches the layer below. The measuring bowl is tapped with a hammer 10 to 15 times after placing each layer. Then, the excess concrete is stroked using a rod, making sure the surface is flat before covering the measuring bowl. Water is introduced to a predetermined height, and the predetermined air pressure is applied. The reduction in the amount of water due to the applied pressure determines the air content in the concrete.

Strength

Compressive Strength

AASHTO T 22 (2017) and ASTM C39 (2018) were used to measure the compressive strength of the collected concrete cylinders.

Flexural Strength

AASHTO T 177 (2017) and ASTM C293 (2016) were used to measure the flexural strength of the collected concrete beams for all testing. The field demo project used the same flexural test except a portable hand pump beam breaker did the actual break.

Cement Hydration Kinetics

Isothermal Calorimetry

The TAM Air isothermal calorimeter instrument manufactured by TA Instruments was used to monitor the heat liberated from cement paste specimens during hydration. This test was conducted for 72 hours to monitor heat flow evolution and cumulative heat for the cement paste hydration at 23°C (73.4°F). The samples were prepared by mixing 10 g (0.022 lb) cement with water at a w/c ratio equal to 0.4 in addition to any added chemical admixtures. After mixing, the specimens were immediately inserted into the instrument's channels to minimize missing heat liberation at the dissolution phase of cement hydration.

Microstructure Analysis

This analysis examines microstructure refinement, including pore size distribution, pore volume, and pore connectivity.

Surface Electrical Resistivity and Formation Factor

An electrical surface resistivity apparatus composed of steel electrodes (Wenner probe method) was used to measure the resistivity of cylindrical concrete samples. Out of the four electrodes, the outer two electrodes applied electrical current and the inner two electrodes measured the potential difference in a cylindrical concrete specimen following ASTM C1760 (2012). At the time of testing, the wet concrete cylinder was wiped with a dry cloth to keep the surface dry before starting the test. Before putting the cylinder inside the measuring chamber, a conductive gel was applied at each probe's tip to make sure there was proper conductivity between the concrete and the probes. The instrument gave an average of eight measurements taken twice from four sides of the concrete cylinder. Electrical resistivity testing was conducted just before compressive strength testing at the required age, and three replicates of concrete cylinders were measured at each age. Figure 8 demonstrates schematically how the Wenner probe device measures electrical resistivity.
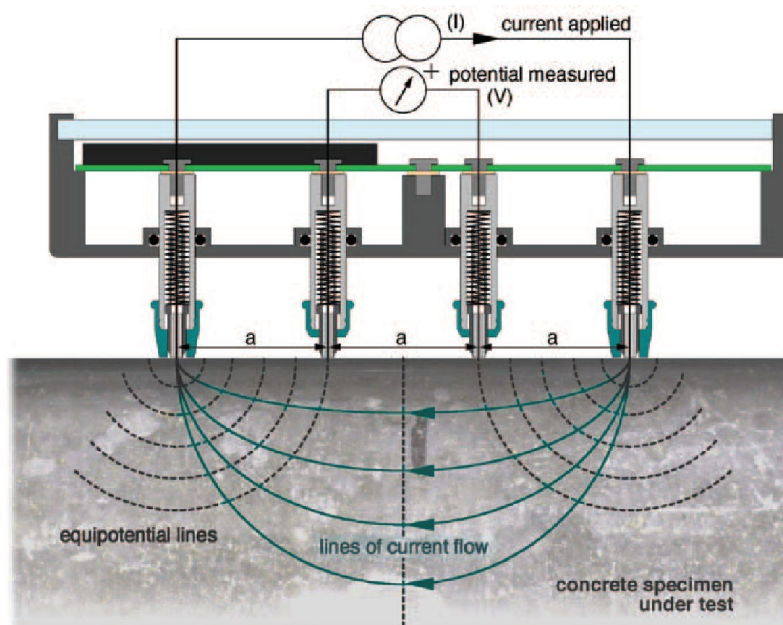
Figure 8. Schematic. An illustration of how the Wenner probe device measures electrical resistivity.

Source: Proceq (2011)

Electrical resistivity is a function of the ions' conductance dissolved in the pore solution of concrete. This measurement reflects the microstructure's connectivity and porosity. Porosity represents the gel and capillary pores formed due to formation of C-S-H gel in the hydrated cement and due to the consumption of unbound water reacting with cement, while connectivity, which is an empirical parameter, represents how much pores are connected with each other. The porosity volume and its connectivity affect the required potential to move a certain electrical current, which eventually

affects electrical resistivity. Electrical resistivity increases in the fine microstructure, where the porosity volume is low and less connected. With low porosity and tortuous microstructure, fewer conductive ions exist to transfer the electrical current, resulting in higher electrical resistivity. The electrical resistivity technique is useful for predicting the quality of concrete permeability instead of conducting costly tests such as the rapid chloride permeability test (Rupnow & Icenogle, 2012), and it is typically used as a quality-control measurement in the field to monitor the variability of concrete mixtures (Spragg et al., 2013).

An electrical current passes through the pore solution in concrete. Based on this phenomenon, electrical resistivity results seem to be biased to the dissolved ions in the pore solution and their conductivity. *For example, two identical concrete microstructures filled with different pore solutions could give different electrical resistivity results.* With this, the formation factor parameter is used instead of electrical resistivity, where the former is a function of porosity and connectivity of pores (Weiss et al., 2020). The formation factor is determined by dividing (normalizing) the obtained bulk electrical resistivity value by its pore solution resistivity, as presented in Figure 9 (Weiss et al., 2016). Figure 10 illustrates the formation factor as a function of the porosity and connectivity of the microstructure (Weiss et al., 2016).

$$\rho_T = \rho_0 \cdot \frac{1}{\phi\,\beta}$$

Figure 9. Equation. Electrical resistivity is a function of pore solution resistance, porosity, and pore connectivity.

Source: Spragg et al. (2013)

$$\phi\beta = \frac{1}{F}$$

Figure 10. Equation. The formation factor is a function of porosity and connectivity in the pore structure.

Source: Spragg et al. (2013)

- ρ_T: bulk electrical resistivity ($\Omega.m$)

- ρ_0: pore solution electrical resistivity ($\Omega.m$)

- *F:* formation factor

- β: connectivity parameter for pore structure

- $\emptyset$: porosity parameter of the cement paste

Pore solution resistance can be calculated in different ways. This study calculates it by using an online software developed by Bentz (2007) at the National Institute of Standards and Technology based on mixture constituents and proportions. Figure 11 presents a screenshot of the pore solution

conductivity calculator. To calculate the elemental composition of the used cementitious materials and chemical admixtures, X-ray florescence (XRF) is used to identify and quantify these elements. XRF was performed by an XRF spectrometer (Shimzadu EDS-7000). The powder cement and liquid chemical admixtures were placed in a sample cell and wrapped well with a thin film (ultralene), prior to exposing it to the X-ray source from a Rhodium anode with a collimator size of 10 mm (0.4 in.). The spectra were acquired between 0 and 40 KeV conditioned in a helium atmosphere.

Mixture Proportions

Material	Mass (kg or lb)	Na_2O content (mass %)	K_2O content (mass %)	SiO_2 content (mass %)
Water	160.0	Not applicable	Not applicable	Not applicable
Cement	400.0	0.2	1.0	Not applicable
Silica fume	20.0	0.2	0.2	99.0
Fly ash	0.0	0.2	0.2	50.0
Slag	0.0	0.2	0.5	Not applicable

Estimated system degree of hydration (%): 70

Hydrodynamic viscosity of pore solution relative to water: 1.0

Curing: Saturated ◉ Sealed ○

Compute   **Estimated pore solution composition (M):**

K+: 0.0

Na+: 0.0

OH-: 0.0

Estimated pore solution conductivity (S/m): 0.0

Effective water-to-cement ratio: 0.5   Free alkali ion factor: 0.75

Reset all values to defaults

Figure 11. Screenshot. Pore solution conductivity calculator.

Source: Bentz (2007)

Helium Pycnometry

Open porosity, which counts only the connected pores and excludes the isolated pores of the cement paste samples, was measured using the AccuPyc 1330 Pycnometer device. The device contains a chamber with a known volume (6.37 cm^3 [0.389 in^3]) where the sample was inserted, and the volume of the occupied chamber was measured after the injection of helium gas. Figure 12 presents the helium pycnometry device and its chamber in addition to a cement paste specimen. The samples were prepared by casting the cement paste into a 10 × 10 × 40 mm (0.39 × 0.39 × 1.57 in.) small mold (cuvette), and the mold was sealed-cured using parafilm for one day. After the first day of sealed curing, the samples were moved to a water container to attain full saturation until the day of testing.

a) AccuPyc 1330 Pycnometer device

b) Chamber and a cement paste specimen

c) Close up of a cement paste specimen

Figure 12. Photos. a) AccuPyc 1330 Pycnometer device, b) chamber and a cement paste specimen, c) close up of a cement paste specimen.

At the time of testing, several steps were required to measure the open porosity. The sample was taken out of the water and wiped out using a dry cloth to assure a saturation-surface dry state (SSD). Then, the mass was measured immediately before placing it into the pycnometer's chamber to measure the volume. In the SSD state, the measured volume represents the cement paste and the water-filled open pores. After that, the sample was transferred into an oven and dried for 24 hours at 105°C (221°F). Bulk density was determined with the mass and volume measured in the SSD state.

The next day, the procedures performed for the saturated sample were repeated for the same sample after drying. In the dry state, the measured volume is the true volume of the cement paste excluding the empty open pores. The measured mass and volume of the dry sample represent the true density of the cement paste. For each mixture, three replicates were cast and measured to obtain statistically the average and standard deviation of the measurements.

A ratio taken between the bulk density and true density represents the volume occupied by the solid material. Several studies provided the formula in Figure 13 to estimate the open porosity of the cement paste (Das, Singh, & Pandey, 2007; Gluth & Hillemeier, 2013; Krus, Hansen, & Künzel, 1997).

$$\eta = \left(1 - \frac{\rho_{bulk}}{\rho_{true}} \right) 100\%$$

Figure 13. Equation. Open porosity volume as a function of the bulk and true densities.

- ρ_{bulk}: cement paste sample density represents the cement paste and water-filled open pores and its mass.

- ρ_{true}: cement paste sample density represents the cement paste and empty open pores and its mass.

Transport Properties

Chloride Ion Diffusion

ASTM C1556 (2016) was used to monitor the chloride ion diffusion in cement paste specimens. Cement paste samples were cast in a 10 × 10 × 40 mm (0.39 × 0.39 × 1.57 in.) mold (cuvette) and sealed-cured for a certain period. Then, samples were removed from the cuvettes and coated with epoxy resin from all faces except the top face, which should be exposed to the solution, prior to soaking them in a sodium chloride solution (165 g NaCl per 1 L of water) for a certain age. At the end of the soaking period, the samples were washed and dried for one day. After drying, samples were cut into 2 mm ± 0.5 mm (0.08 in. ± 0.02 mm) slices using a small lab-based saw-cutting machine and ground using mortar and pestle. The chloride content was measured using the XRF technique instead of using ASTM C1152 (2020) because it is easier, faster, and more accurate to measure chloride content since it can detect chlorine content at a very low detection limit (approximately 10 ppm). XRF was performed by an XRF spectrometer (Shimzadu EDS-7000). The ground slides of cement paste were placed in a sample cell and wrapped well with a thin film (ultralene), prior to exposing it to the X-ray source from a Rhodium anode with a collimator size of 10 mm (0.4 in.). The spectra were acquired between 0 and 40 KeV conditioned in a helium atmosphere. A modification was made for this method. After curing the specimens for a certain time and drying them for one day, the specimens were sealed with epoxy and were not exposed to calcium hydroxide. Figure 14 illustrates the procedures used to conduct the chloride ion diffusion experiment using the XRF technique.
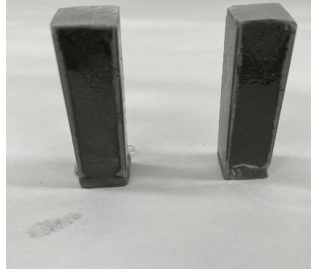
a) Cement paste specimens coated with epoxy
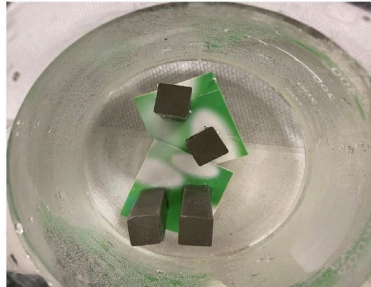
b) Sample kept for seven days in sodium chloride solution

c) 2 mm (0.079 in.) sliced layer

d) Sliced layers kept in sample cups ready for XRF measurements

Figure 14. Photos. a) Cement paste specimens coated with epoxy, b) sample kept for seven days in sodium chloride solution, c) a sliced layer, and d) sliced layers are ground and kept in sample cups ready for XRF measurements.

Water Sorptivity

The sorptivity of the cement paste samples was evaluated by measuring the rate of water absorption following ASTM C1585 (2013). The water absorption of hydraulic cement paste was measured by monitoring the rate of mass increase as a function of time. Small cubes of 10 × 10 × 10 mm (0.39 × 0.39 × 0.39 in.) of cement paste were cast in a plastic mold. Then, these molds were covered with a plastic sheet to avoid any moisture loss from the samples before initiation of the sorptivity test.

All cement paste specimens were conditioned similarly to provide an accurate comparison. To perform the sorptivity experiment, five specimens of cement paste from each mixture were cast and kept in the molds for 72 hours after casting. After 72 hours, the samples were sealed with epoxy resin from all surfaces except one surface, which was kept free for measurement. After, the specimens were moved to a vacuum desiccator for 24 hours to prevent carbonation and to prevent excessive moisture from entering the specimens. On the day of testing (the following day), the samples were taken from the desiccator to polish the uncoated surface using silicon carbide sheets with grit 400, 600, and 1200 to assure that the surface was flat and to remove any excess epoxy from the exposed surface. Some modifications were made in the sample preparation such as doing this test on cement paste samples instead of concrete. Additionally, the sealed samples were kept in a vacuum desiccator for 1 day instead of 15 days. These modifications were conducted for the sake of doing the experiment at an early age and to resemble early field conditions as closely as possible.

The weights of the specimens were measured just before putting the specimens in water and were not immersed more than 2 mm (0.079 in.). Then, the weights of the samples were measured at minutes 2, 5, 10, 15, 20, 30, 45, 60, 75, 90, 120, 150, 180, 240, and 360 and on days 2, 3, 4, 5, 6, and 7. The rate of absorption was determined for each cement paste mixture, as presented in the equation in Figure 15. The equation normalized the weight of absorbed water to the area of exposed surface and water density.

$$I = \frac{m}{d \times A}$$

Figure 15. Equation. Water absorption.

- I: the absorption

- m: the mass change with time (g)

- A: the area of the exposed surface (mm^2)

- d: density of the water (0.001 g/mm^3)

The collected data points were plotted against the square root of time to make sure the curves have a linear trend. The initial and secondary rates of absorption were defined by taking the slopes of the best-fit lines between hours 0 and 6 and days 1 and 7, respectively.

Phase Assemblage

Once the cement is mixed with water, chemical reactions take place where the reactants convert into hydration products. Several phases form due to this reaction such as C-S-H gel, calcium hydroxide, monosulfoaluminate (AFm), ettringite (AFt), and other minor phases.

Thermogravimetric Analysis

Thermogravimetric analysis (TGA) is used to identify and quantify the crystalline and non-crystalline hydration products formed due to hydration of cement. In particular, this test is used to monitor the formation of new phases or the diminishing of other phases due to the interaction of chemical and mineral admixtures with OPC.

The Q50 TGA instrument was used to conduct TGA experiments. A sample of 20 ± 5 mg of ground cement paste cured for a certain age was placed in a platinum crucible. Then, the crucible was inserted into the instrument and heated in a nitrogen atmosphere from 20°C (68°F) to 1000°C (1832°F) at a rate of 20°C (68°F) per minute.

Several steps were required to prepare the sample prior to conducting the TGA experiment. The intention of the sample preparation was to remove free water and to stop hydration. The cement paste sample was crushed using a mortar and pestle and then sieved to collect the ground cement particles smaller than 40 μm. The collected ground material was soaked in a flask filled with isopropanol alcohol and stirred using a magnetic rod for 20 minutes. Then, this material was filtered using two filter papers placed in a Büchner funnel fixed with a Büchner flask and attached to a suction hose to separate the ground material from the isopropanol. Finally, the extracted ground material was washed with diethyl ether to remove any deposited isopropanol alcohol adsorbed on the hydrated phases. Then, the ground material was kept in an oven at 60°C (140°F) for 8 to 10 minutes (Scrivener, Snellings, & Lothenbach, 2016). The prepared sample was brought immediately to the TGA instrument to start the experiment.

CHAPTER 4: RESULTS AND DISCUSSION

This chapter presents all data collected for cement paste and concrete mixtures using X1 and X2 chemical admixtures. The chapter is divided into two main sections: lab and field data and their results.

LAB DATA

Compressive Strength

Three mixtures, one prepared with OPC (control mixture) and two seeded with X2 at dosages of 7 and 14 fl oz/cwt, were cast in the lab (refer to Table 2). Concrete cylinders were collected to analyze their compressive strength development, as presented in Figure 16.
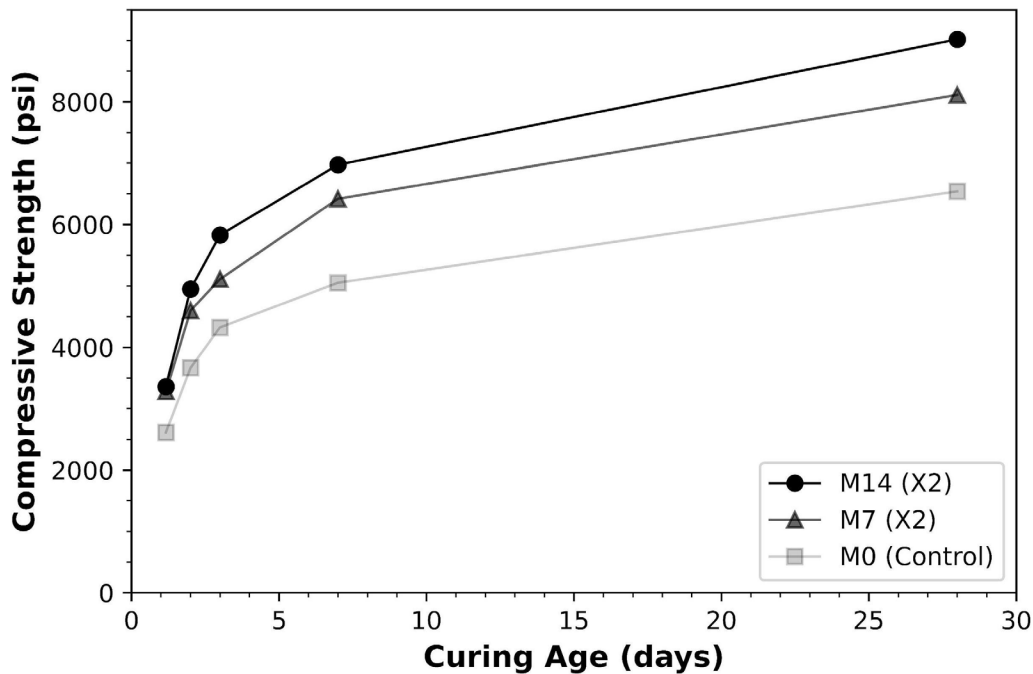
Figure 16. Graph. Compressive strength development for concrete mixtures at days 1, 2, 3, 7, and 28 (M0 = control, M7 = 7 fl oz/cwt, M14 = 14 fl oz/cwt).

Compressive strength was measured for M0, M7, and M14 mixtures at days 1, 2, 3, 7, and 28 (see Figure 16). Two main observations were found. First, among the three mixtures, M0 achieved the lowest compressive strength, while M14 achieved the highest at all ages. Second, the strength difference between M7 and M14 was very small initially, while the difference became bigger the third day after casting. The difference between the control mixture and the seeded mixtures continued growing on day 7 and onward.

On the first day, the control mixture achieved 17.2 MPa (2,500 psi), whereas the M7 mixture achieved 22.4 MPa (3,250 psi), which means that M7 achieved a 30% strength increase when it was

seeded. In addition, the compressive strength obtained in the M0 mixture on day 7 can be obtained by day 3 when M0 is seeded, as demonstrated in mixtures M7 or M14. By day 28, M0 obtained a strength of 45.2 MPa (6,550 psi), while M7 and M14 obtained strengths of 55.8 MPa (8,100 psi) and 62.1 MPa (9,000 psi), respectively. These values demonstrate a 24% and 38% strength increase in M7 and M14 when compared to the control mixture. Here, introducing C-S-H seeds in concrete mixing increases the strength significantly at early and late ages.

Electrical Resistivity and Formation Factor

The electrical resistivity and formation factors were measured for concrete mixtures M0, M7, and M14 (mentioned in Table 2) at days 1, 2, 3, 7, and 28, as presented in Figure 17. The electrical resistivity of all concrete mixtures increased with time, which confirms that further hydration takes place and further refinement of the microstructure occurs. Two major observations were made, as shown in Figure 17(a). First, among the three mixtures at all ages, electrical resistivity was lowest in M14 and highest in M0. Second, the difference in electrical resistivity between the M7 and M14 mixtures is slightly different because they were both seeded.

Regarding the formation factor, Figure 17(b) displays an opposite trend to that of electrical resistivity. M14 obtained the highest formation factor, while M0 obtained the lowest at all ages. M7 obtained a formation factor on day 3 almost equal to what M0 obtained on day 7, with M14 having the highest formation on day 3 and staying the highest throughout. Based on the equation from Figure 10, the higher the formation factor, the lower the porosity or the more tortuous the microstructure.

The obtained data from the formation factor concurred with the data obtained from compressive strength, where the seeded mixtures had the highest compressive strength and formation factor. Here, electrical resistivity seems to be unreliable when comparing concrete mixtures' quality, in which these mixtures have different pore solutions. Including the pore solution resistivity in the calculations significantly changes the conclusion about the microstructure of the cement paste. When electrical resistivity data is considered, M0 seemed to have the most refined microstructure. However, the formation factor showed M0 to have the least refined microstructure when normalized with its pore solution resistivity. These results prove that direct resistivity measurements cannot be used to compare specimens of different concrete because resistivity tests are dependent on the conductivity of the concrete's pore solution. Referring to the formation factor's equation in Figure 10, the theory of formation factor comes into play to normalize the resistivity measurements for each concrete based on each's pore solution. Furthermore, the formation factor is inversely proportional to porosity and pore connectivity (i.e., transport properties), and thus, the greater either gets, the smaller the formation factor.

Several studies have investigated the effect of adding nano particles on the mechanical properties of concrete. Adding nano silica, nano alumina, or nano silver particles into concrete increases electrical resistivity (Asaad et al., 2018; Hosseini et al., 2014). However, there were no studies investigating the effects of C-S-H seeds for determining the electrical resistivity and formation factor. The present study is unique in directly addressing this issue.
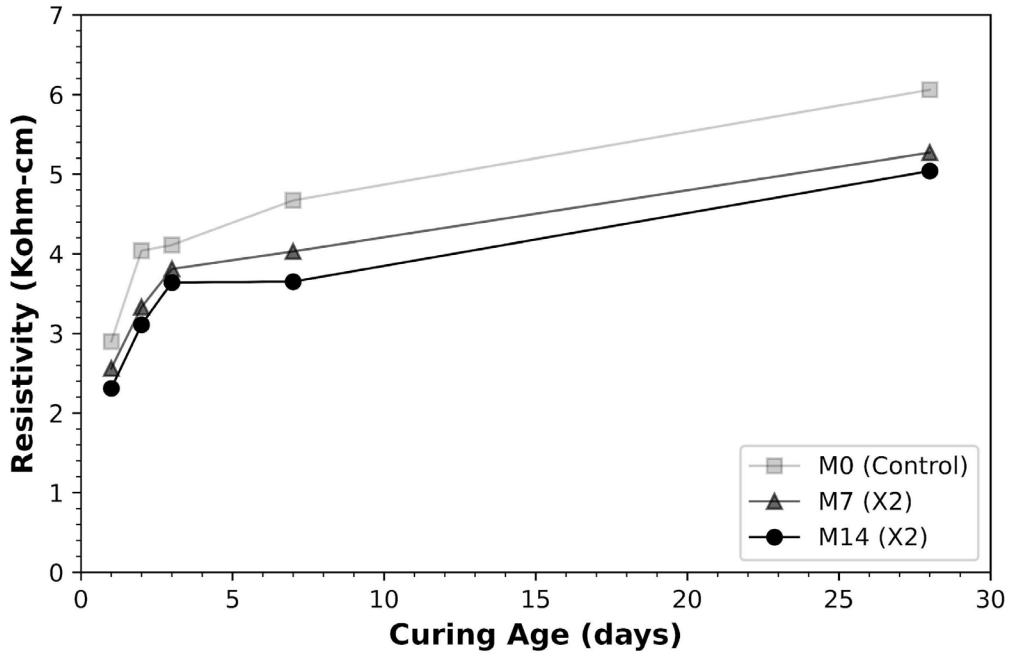
a) Electrical resistivity for concrete mixtures
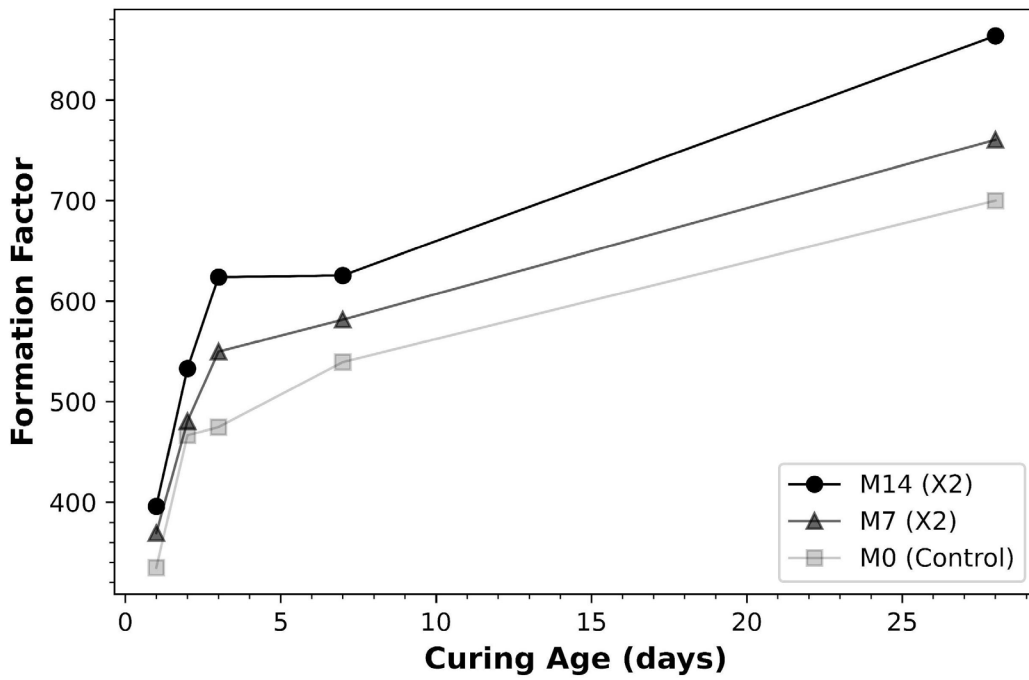
b) Formation factor for concrete mixtures

Figure 17. Graphs. a) Electrical resistivity for concrete mixtures at days 1, 2, 3, 7, and 28, b) formation factor for concrete mixtures at days 1, 2, 3, 7, and 28 (M0 = Control, M7 = 7 fl oz/cwt, M14 = 14 fl oz/cwt).

Isothermal Calorimetry

X1

Data were collected for eight cement paste mixtures mixed with X1 dosages added from 0 to 30.17 fl oz/cwt, as presented in Figure 18. The mixtures were first explained in Chapter 3 under the subtitle "Laboratory Work." The experiment stopped once a steady-state trend was obtained, indicating that most of the fast-reacting, anhydrous phases had reacted. To provide an accurate comparison, the obtained heat values were normalized to the weight of the cement content (10 g) in each paste.

The heat flow of all seeded mixtures was compared with the control mixture, as presented in Figure 18(a). Two major observations can be made. First, seeded mixtures accelerate the occurrence of the first peak and decrease the induction period when the dosage of the X1 increased. The reduction in the induction period may be due to the enhanced nucleation of hydration products because of the presence of seeds. Second, this behavior is accompanied by an increase in initial peak heights, which indicates that a larger amount of hydration products hydrated at a certain time. After the acceleration period, the deceleration period started in all mixtures, and after almost 30 hours, the heat flow became a steady state in all mixtures, indicating the last stage in the hydration reaction development. Figure 18(b) presents the cumulative heat of all mixtures. The cumulative heat was higher in all seeded mixtures than in the control mixture. These results confirm that hydration was enhanced.

The times to the minima and maxima peaks for all mixtures were extracted from Figure 18(a) and presented in Figure 18(c) and Figure 18(d). There was a reduction in the times for minima peaks (from 1.2 hours to 0.8 hours) with an increase in X1 dosage until 21.55 fl oz/cwt, but there was little increase after this dosage by 0.84 hours. The times to the maxima peaks decreased (from 7.12 hours to 5.54 hours) with the addition of X1. With the addition of 30.17 fl oz/cwt X1, the time decrease is 1.58 hours when compared to the 0 fl oz/cwt mixture.

Moreover, the acceleration rate increased with the addition of X1. The acceleration rate was calculated as the slope between the high and low points during the acceleration stage. The acceleration rate increased from 1.80 to 2.75 mW/g.hrs with the increase of the X1 dosage, as presented in Figure 18(e). This increase indicated that the time span between the initial and final setting times is becoming shorter with the addition of C-S-H seeds. Lastly, the total degree of hydration is plotted in Figure 18(f) and shows that it increased linearly with the increase of the X1 dosage. For example, the total degree of hydration for the 30.17 fl oz/cwt mixture was 324 J/g compared to 290 J/g in the control mixture with 0 fl oz/cwt after three days.

Several researchers have investigated the impact of adding C-S-H seeds on kinetics. Most recently, Pedrosa et al. (2020) studied the effect of adding C-S-H seeds into oil well cement paste mixtures via isothermal calorimetry and nanoindentation. They used a different commercial product, as opposed to the X1 used here, but their overall results indicated that increasing seed dosage resulted in a higher degree of nucleation and hydration. Thus, given the strong agreement between these results, the researchers can conclude that C-S-H seeds are viable admixtures to accelerate hydration kinetics and increase the overall degree of hydration in cementitious systems.
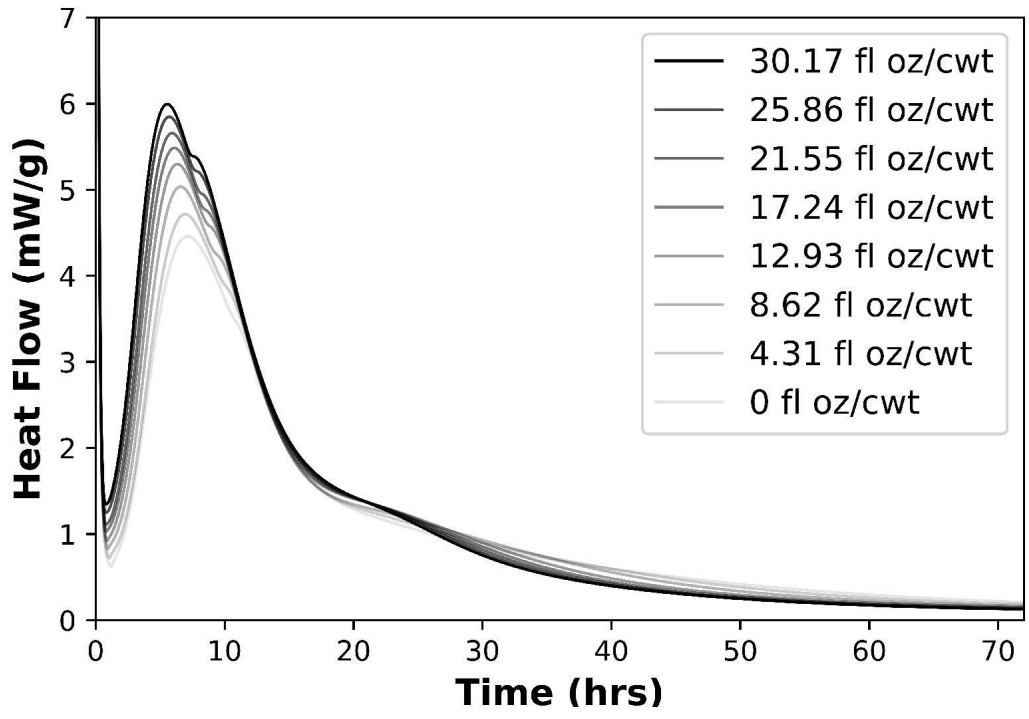
a) Heat flow development
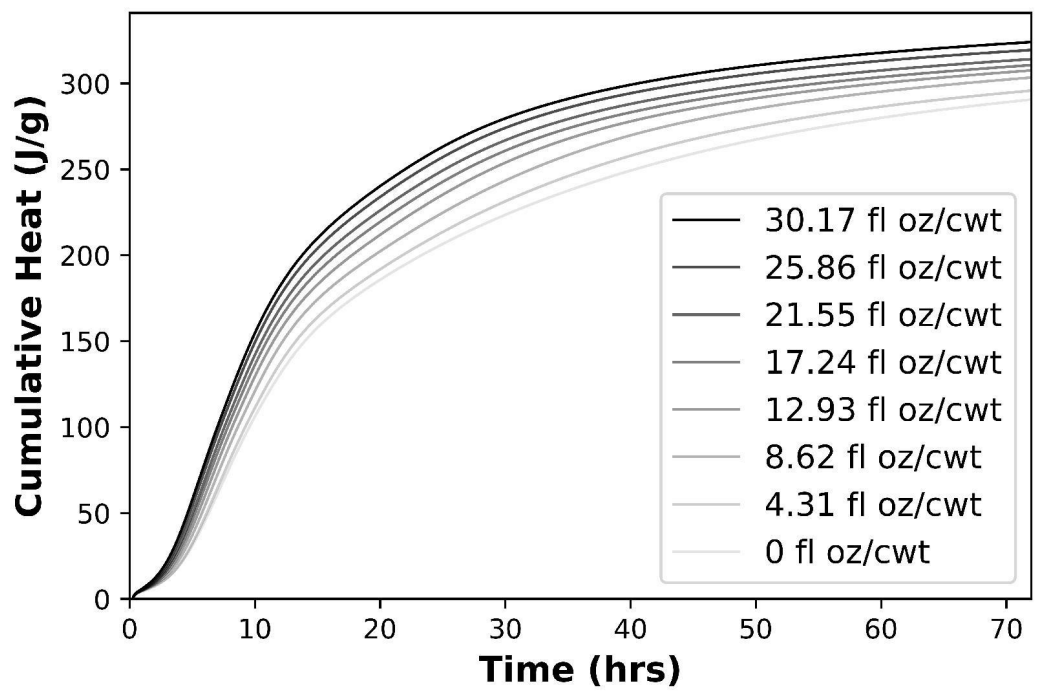
b) Cumulative heat development
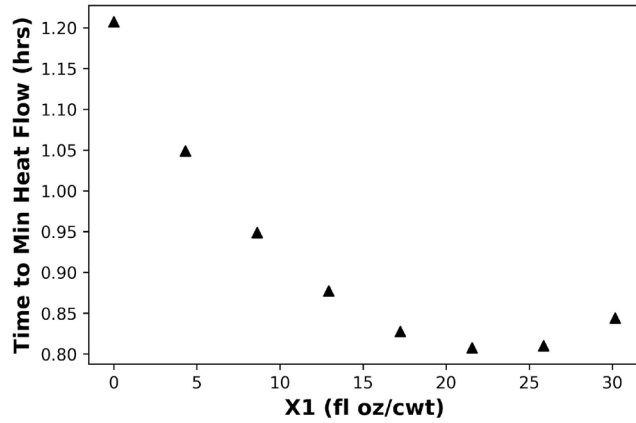
c) Time to minimum heat flow
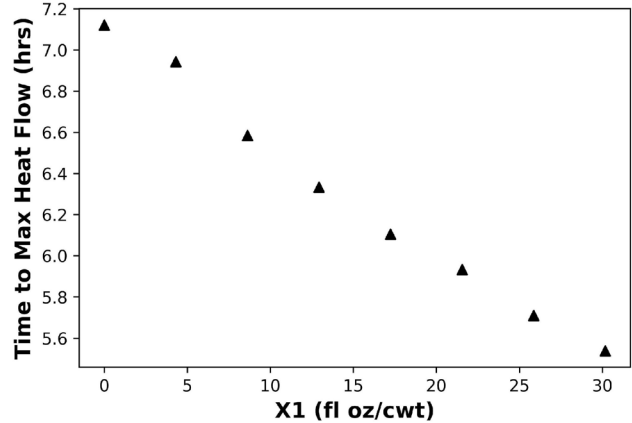
d) Time to maximum heat flow
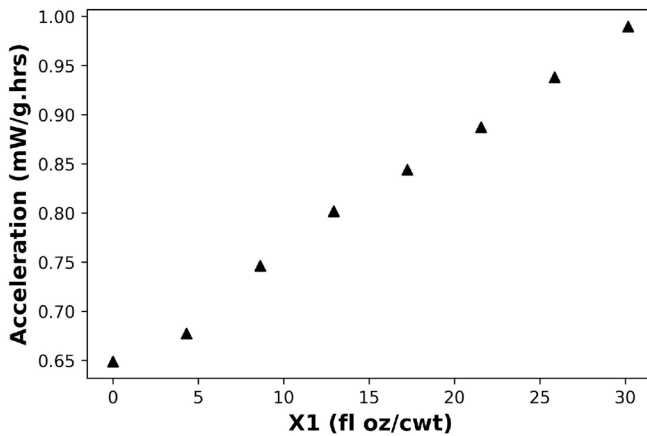
e) Acceleration rate
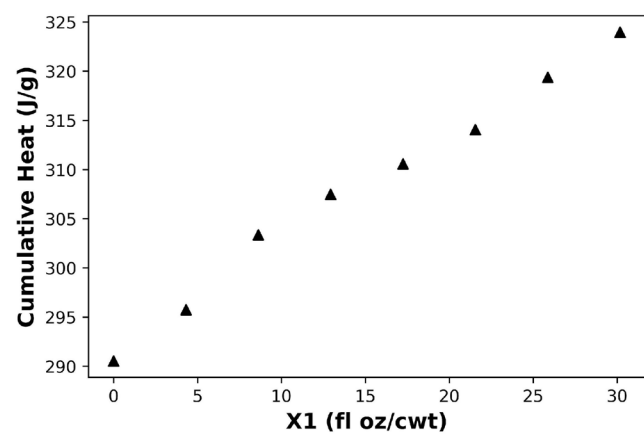
f) Total degree of hydration

Figure 18. Graphs. a) Heat flow development for cement paste mixtures mixed with X1, b) cumulative heat development for cement paste mixtures with X1, c) time to minimum heat flow versus X1 dosages, d) time to maximum heat flow versus X1 dosages, e) acceleration rate versus X1 dosages, f) total degree of hydration versus X1 dosages. The dosages of X1 in all graphs range from 0 to 30.17 fl oz/cwt. The data were collected for three days after hydration.

X2

Data were collected for six cement paste mixtures mixed with X2 at dosages added from 0 to 15 fl oz/cwt, as presented in Figure 19. The mixtures were first explained in Chapter 3 under the subtitle "Laboratory Work." After a steady-state trend was obtained, indicating that most of the fast-reacting anhydrous phases had occurred, the experiment stopped after 72 hours. To provide an accurate comparison, the obtained values were normalized to the weight of the cement content (10 g) in each paste.

Figure 19(a) presents the heat development data for all cement paste mixtures with and without X2. Unlike when X1 was used, the X2 retarded the initial hydration peak with increased dosage, meaning there was an increase in the induction period with the addition of C-S-H seeds. The retardation is due

to using polycarboxylate to disperse the nano C-S-H seeds to avoid having them agglomerated (Sun et al., 2017). Similar to what the researchers observed in the X1 results, the height of the initial peak seemed to increase with the addition of X2, which confirms that there was additional hydration product precipitation when the mixtures were seeded. Moreover, with the addition of up to 6 fl oz/cwt of X2, the initial peak was accompanied by a shoulder just after the peak. This shoulder, however, was switched to before the peak when the dosage was 9 fl oz/cwt and more. This behavior indicated that the phase assemblage at that time of hydration was influenced by the addition of C-S-H at an early age. The cumulative heat of all cement paste mixtures is presented in Figure 19(b). All seeded mixtures demonstrated higher cumulative heat than the control mixture, meaning that the degree of hydration is higher at an early age when the cement paste was seeded with X2.

The times of the minima and maxima peaks were extracted from Figure 19(a) and presented in Figure 19(c) and Figure 19(d). With the increase of the X2 dosage, both the times to minima and maxima increased. For example, the time to minima peak increased from 1.64 to 3.4 hours, following a steady-state rate when a dosage of 15 fl oz/cwt was used when compared to the 0 fl oz/cwt. The time to the maxima did not increase following a steady-state rate. The time jumped from 9.2 to 12.5 hours when 6 fl oz/cwt was used compared to 0 and 3 fl oz/cwt. It then increased at a steady rate up to 16.4 hours when 15 fl oz/cwt dosage was used. This admixture retards cement hydration, so the acceleration rate was not plotted.

Finally, the total degree of hydration increased when the cement paste was seeded with X2, as presented in Figure 19(e). After 72 hours of hydration, in comparison to the control mixture of 0 fl oz/cwt, the total degree of hydration increased from 292 J/g to 305 J/g when the dosage of 3 fl oz/cwt was used, equivalent to a 4.5% increase. Furthermore, the total degree of hydration increased up to 325 J/g when the dosage was increased from 3 to 15 fl oz/cwt, equivalent to an 11.3% increase.
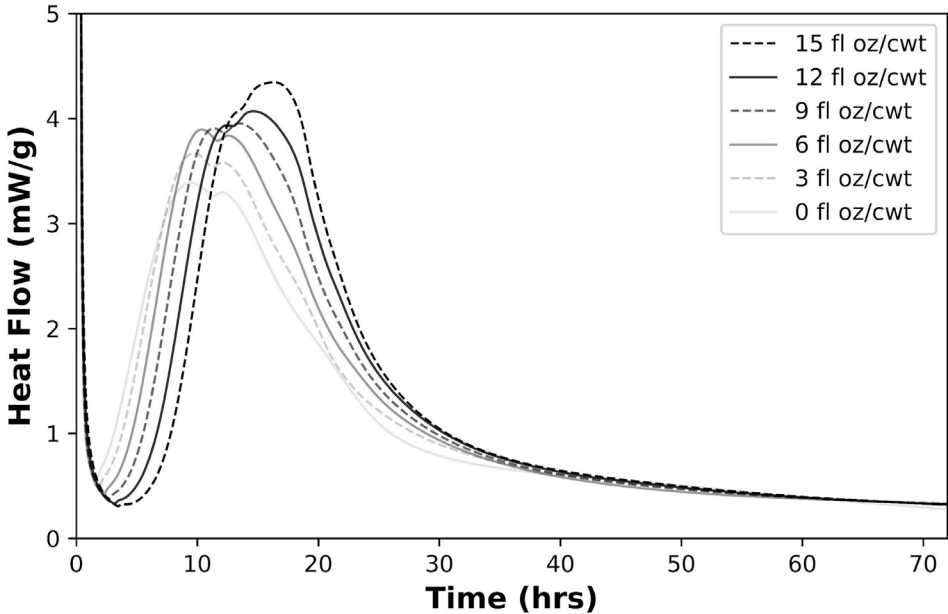
a) Heat flow development
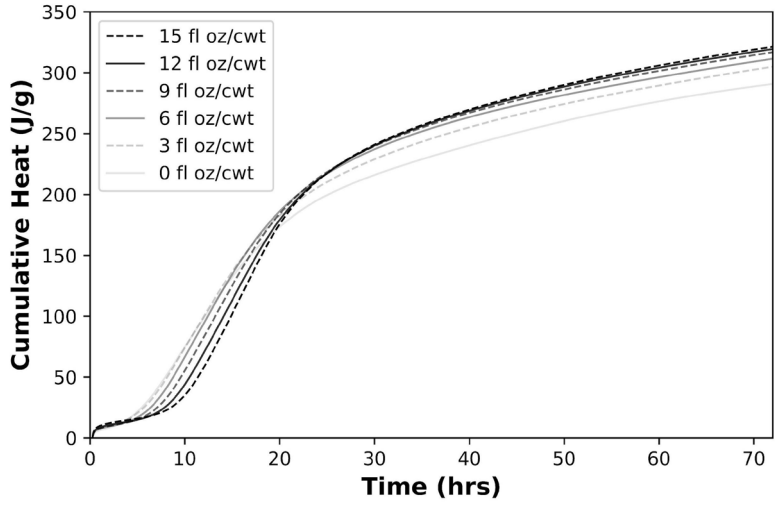
b) Cumulative heat development
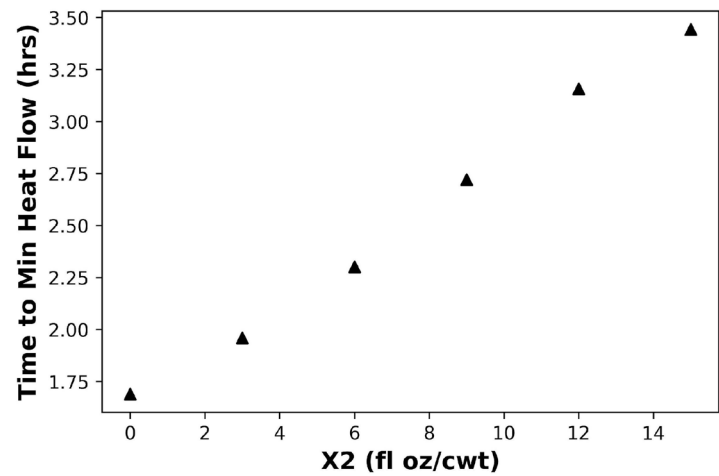
c) Time to minimum heat flow
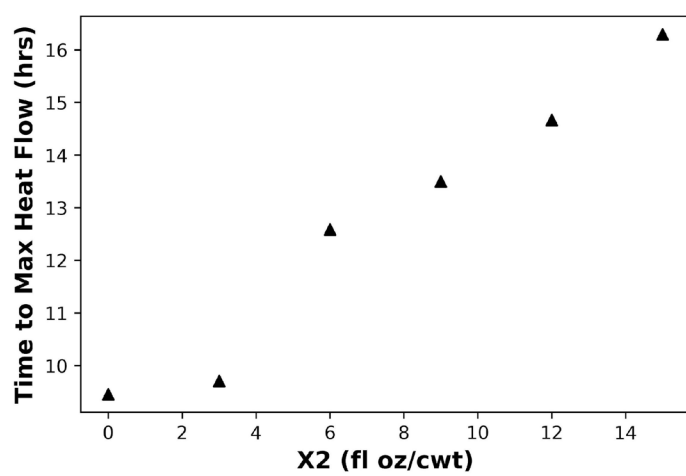
d) Time to maximum heat flow
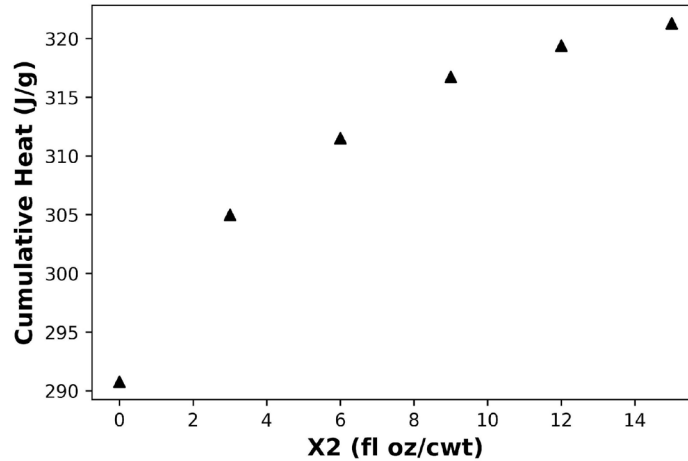
e) Total degree of hydration

**Figure 19. Graphs. Isothermal calorimetry data for cement paste samples at doses 0, 3, 6, 9, 12, and 15 fl oz/cwt after 72 hours: a) heat flow development, b) cumulative heat development, c) time to minimum peak, d) time to maximum peak, and e) total degree of hydration. The data were collected for 72 hours after hydration.**

Open Porosity Using Helium Pycnometry

Porosity starts once cementitious materials are mixed with water, as capillary porosity develops due to the consumption of water. Gel porosity develops due to the precipitation of C-S-H gel. However, porosity decreases with time as more cementitious materials react and more hydration products precipitate. Porosity is a key factor in characterizing the performance of the cement paste matrix because it influences other mechanical properties such as strength, creep, and shrinkage as well as transport properties of paste such as diffusion and permeability (Jennings et al., 2008). Among techniques used to characterize porosity, helium pycnometry seemed to be a good technique to measure the open porosity volume of cementitious pastes (Nguyen et al., 2019). This technique has the advantage of using helium gas, where helium molecules can penetrate most of the open pores because they are 0.22 nm in size and are smaller than 0.28 nm water vapor molecules (Krus, Hansen, & Künzel, 1997). The main limitation of this technique is that it cannot measure pore size distribution, but it is still a reasonable method for determining bulk and open porosity (Aligizaki, 2005), which is strongly correlated to cementitious permeability (Marsh & Day, 1984).

The open porosity experiment was conducted several times for different purposes. All mixtures prepared in this experiment were first explained. Open porosity was measured after three days of casting for cement paste mixtures prepared with different dosages of X1 and X2. Figure 20 presents the open porosity for cement paste mixtures prepared with different dosages of X1, a w/c ratio equal to 0.40, and cured for three days. With the addition of the X1 dosage, the open porosity decreased from 15.5% to 10.9%. Additionally, the decrease in porosity was steep until the dosage addition of 12.93 fl oz/cwt was reached because the porosity decreased to 11.8%. However, the open porosity kept decreasing at a gradual pace in the range of 12.93 fl oz/cwt to 30.17 fl oz/cwt, but it was not significant in contrast to before the 12.93 fl oz/cwt addition.
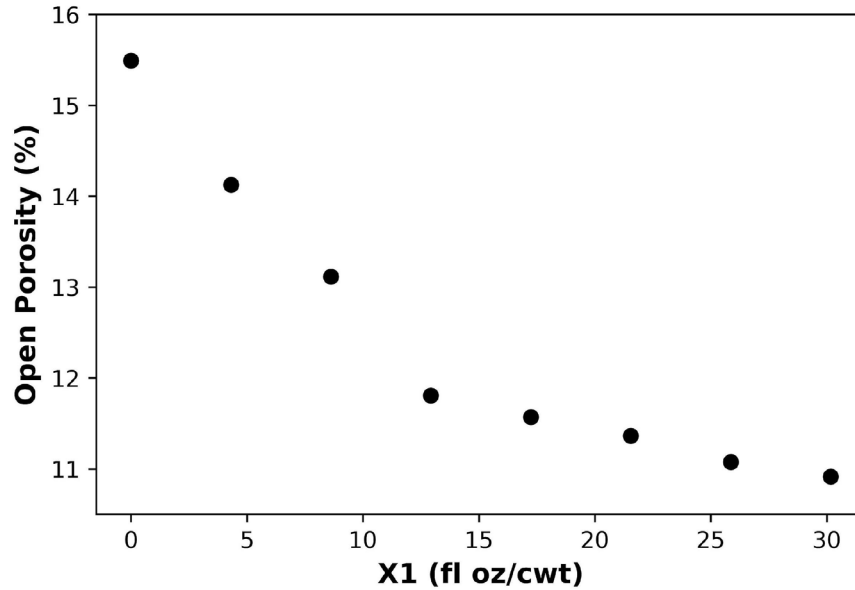
Figure 20. Graph. Open porosity as a function of X1 dosage for all cement paste mixtures mixed with 0 to 30.17 fl oz/cwt by cement weight at the age of three days. Each measurement had three replicates, and the error bars represent the standard deviation.

X2 was investigated in two experiments. The first experiment evaluated the addition of C-S-H seeds at different dosages into the cement paste mixed with a w/c ratio equal to 0.40 and cured for three days, as presented in Figure 21. A major observation in this experiment is that the open porosity decreased from 15.5% to 19% by adding X2 until the dosage of 12.93 fl oz/cwt was reached, whereas it increased back to 13.8% when the dosage increased from 12.93 to 30.17 fl oz/cwt. This behavior opposed what the researchers found when using X1, where porosity kept decreasing with the addition of X1 until 30.17 fl oz/cwt. Figure 22 presents the data for cement paste of a control (M0) and two cement paste mixtures seeded with X2 with dosages of 7 fl oz/cwt (M7) and 14 fl oz/cwt (M14) mixed at a w/c ratio equal to 0.48 and cured at different ages (refer to Table 2). The porosity development for the three cement paste mixtures was measured at days 1, 2, 3, 7, and 28. The data indicate a reduction in open porosity over time for all three mixtures. On the first three days of hydration, the open porosity volumes were close to each other, but this trend changed after the third day. On the seventh day, a gap difference between M0 and both M7 and M14 started to develop, and this gap increased after the seventh day. For example, the open porosity decreased from 15% in the control mixture to 12.5% in the seeded mixtures on the seventh day. Interestingly, M7 demonstrated the least porosity at all ages among the three mixtures. Moreover, the open porosity decreased steeply in the first seven days in all mixtures, while the decreasing rate became smoother from day 7 until day 28. The reduction in the open porosity in the first three days is almost equal to the reduction in the open porosity between day 3 and day 28. This finding proves that most microstructure refinement happened at an early age. Last, the obtained porosity in M0 after seven days can be obtained approximately after days 4 and 5 in M7 and M14, respectively.
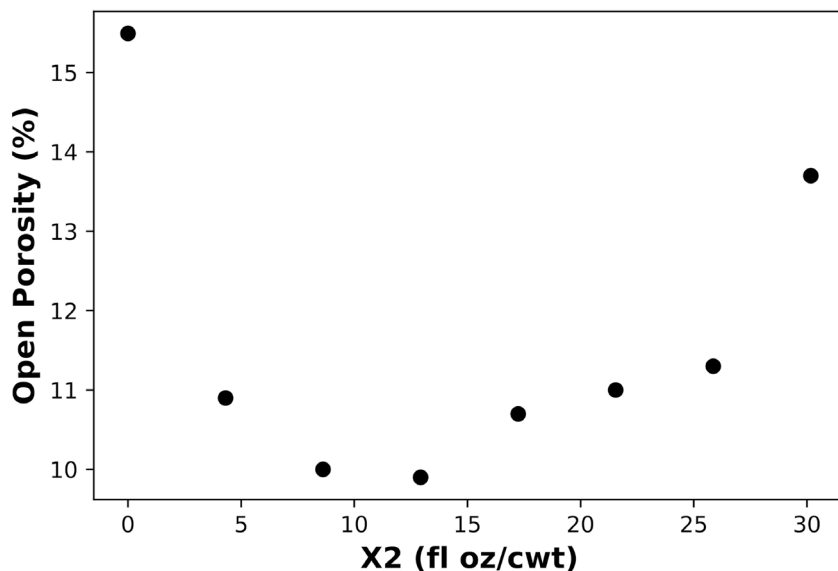
Figure 21. Graph. Open porosity versus X2 dosage (0 to 30.17 fl oz/cwt) for cement paste mixtures.
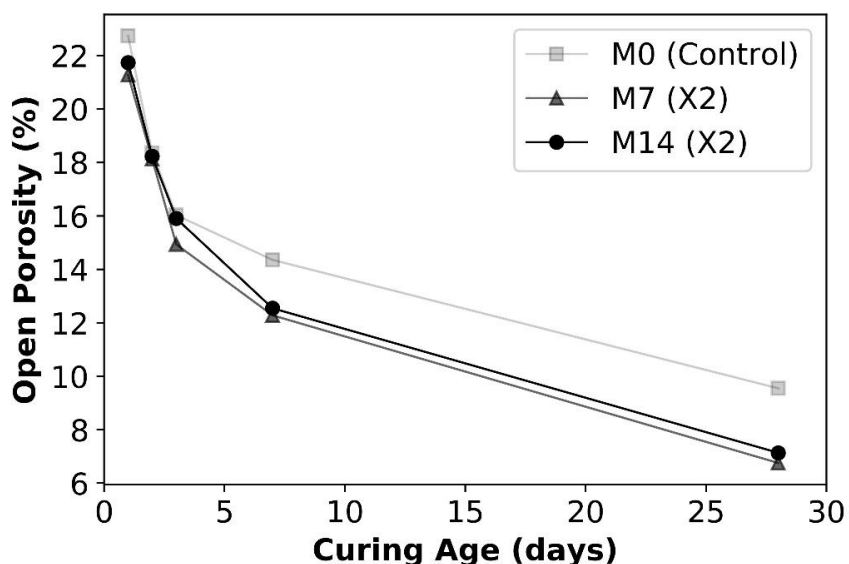
Figure 22. Graph. Open porosity for the control cement paste mixture and two other mixtures with X2 cured at days 1, 2, 3, 7, and 28 (M0 = 0 fl oz/cwt, M7 = 7 fl oz/cwt, M14 = 14 fl oz/cwt).

In addition, two cement paste mixtures blended with two random samples of fly ash picked from IDOT were compared with a control cement's open porosity after curing at different ages, as presented in Table 5. These mixtures were first explained in Chapter 3 under the subtitle "Laboratory Work." Two main observations can be drawn from this data. First, the mixture without fly ash obtained the lowest open porosity, giving insights that this mixture has the lowest permeability and requires the longest time prior to corrosion initiation at all ages except on day 3, where fly ash–based mixture 216ROT-41 obtained the lowest open porosity. Several researchers investigated the porosity

of blended OPC and fly ash cement paste mixtures. They found that total porosity increases when fly ash is replaced with OPC (Chindaprasirt, Jaturapitakkul, & Sinsiri, 2005; Yu & Ye, 2013). This observation agrees with what the researchers observed in this research project. Second, using two different sources of fly ash does not show a significant difference in porosity. This finding allows contractors to use the available sources of fly ash without any restrictions due to porosity development.

Table 5. Open Porosity Development at Days 3, 28, 56, and 90 for a Control Cement Paste Mixture and Two Other Cement Paste Mixtures Blended with Different Sources of Fly Ash

Mixture	Porosity% at 3 days	Porosity% at 28 days	Porosity% at 56 days	Porosity% at 90 days
OPC	15.5 ± 0.2	8.4 ± 0.4	6.6 ± 0.8	5.9 ± 0.7
75-25 OPC/FA (216ROT-41)	12.1 ± 0.6	9.2 ± 0.5	7.2 ± 0.6	6.4 ± 0.5
75-25 OPC/FA (21MSC2-69)	17.3 ± 0.3	10.2 ± 0.7	7.8 ± 0.5	6.8 ± 0.2

Last, open porosity was measured for a matrix composed of four mixtures (100 OPC, 75-25 OPC/FA, 100 OPC + 17 fl oz/cwt X2, and 75-25 OPC/FA + 17 fl oz/cwt X2) to investigate the influence of adding X2 to cement paste with and without fly ash. These mixtures were first explained in Chapter 3 under the subtitle "Laboratory Work." This matrix was evaluated at days 1, 3, 7, 14, 28, and 56, as presented in Figure 23. On the first day of curing, there were slight differences in open porosity among all mixtures. The data indicate that the fly ash mixtures with and without X2 obtained higher porosity and the C-S-H seeds still had no effect compared to the OPC mixtures. On the third day, the trend changed such that the seeded mixture without the fly ash started to show the lowest open porosity. After day 7 of curing, the mixture containing fly ash obtained higher open porosity compared to the mixture without fly ash. Also, the open porosity became even lower for these mixtures when X2 was added, maintaining the same trend in which the mixture containing the fly ash obtained higher open porosity.

To summarize the effect of adding C-S-H in the cement paste, Wang et al. (2020) recently used mercury intrusion porosimetry to evaluate the porosity of hydrating cement doped with C-S-H seeds. They found that the inclusion of these seeds decreased the total porosity and the capillary pore volume at every curing age (day 1 to 28). Hence, the results of this research study with helium pycnometry support the idea of porosity reduction with the addition of C-S-H seeds. Finally, the results strengthen the hypothesis that these C-S-H seeds improve the hydration reaction by adding new nucleation sites in the matrix and thereby resulting in microstructural refinement (John et al., 2018).
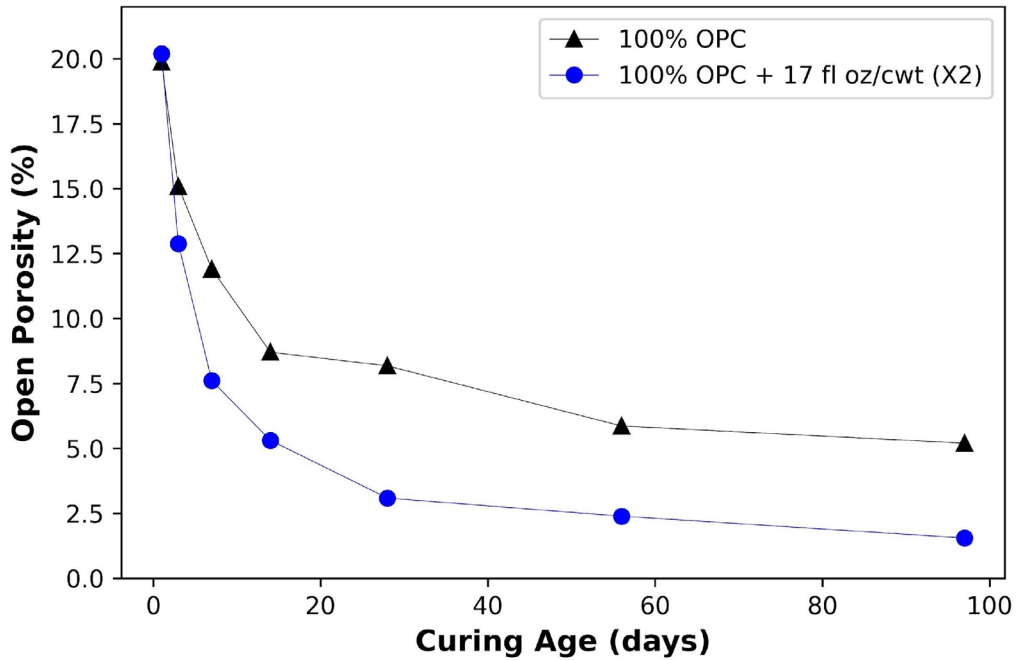
a) Open porosity for two OPC mixtures
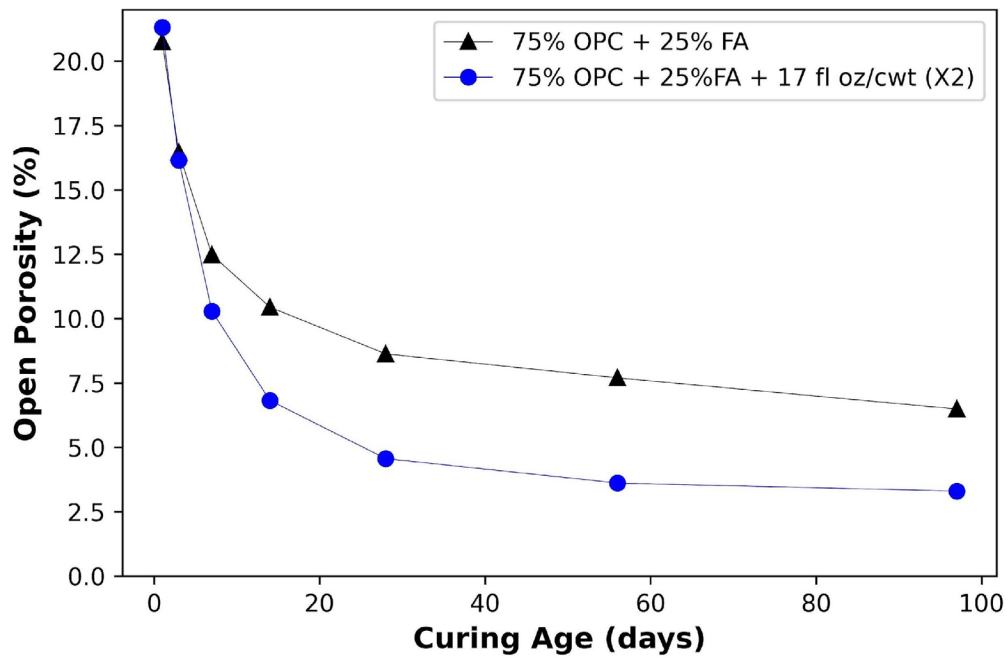
b) Open porosity for two OPC-FA mixtures

Figure 23. Graphs. Open porosity for four mixtures of cement paste cured at different ages: a) two OPC mixtures and b) two OPC-FA mixtures.

Chloride Ion Diffusion

The chloride ion diffusion experiment measures the diffusion rate of chloride within the cement matrix. This rate is impacted by microstructure, which is a function of pore volume, pore size, and the connectivity of the pores (tortuosity of the microstructure). This experiment was conducted two times. The first time evaluated the influence of the water-to-cementitious ratio on diffusion. The second time evaluated the effect of adding X1 into the cement paste mixture. These mixtures were first explained in Chapter 3 under the subtitle "Laboratory Work."

Chloride Ion Diffusion for Mixtures with Different Water-to-Cementitious Ratios

Figure 24 presents chloride ion diffusion for cement paste mixtures prepared with different w/c ratios. Two replicates from each mixture were tested. The researchers noticed that as the w/c ratio decreases, chloride ion penetration decreases.
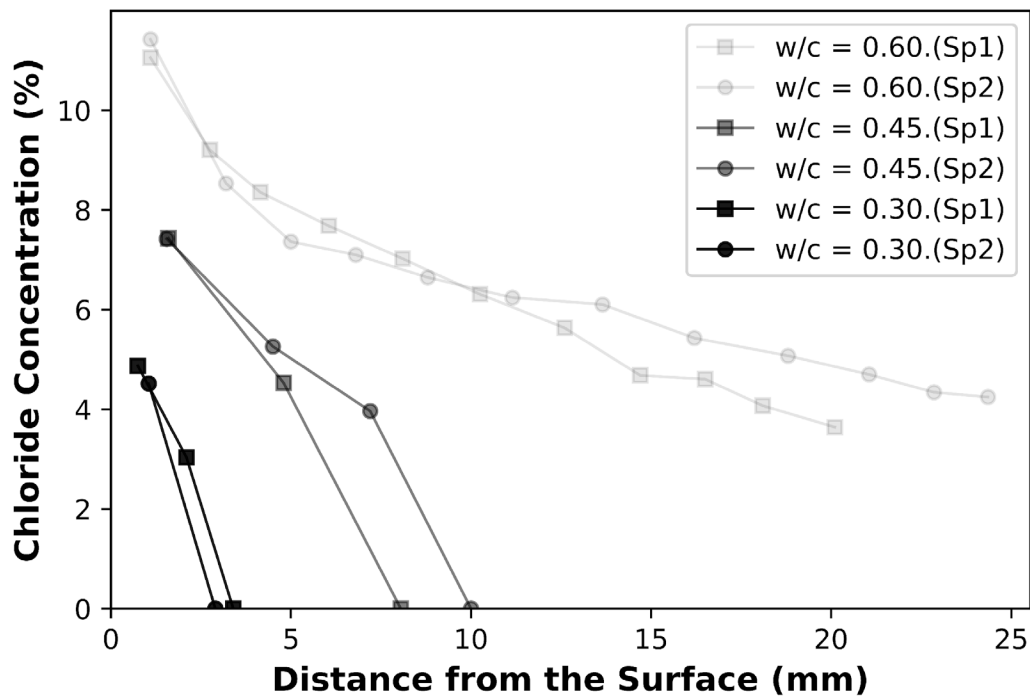
Figure 24. Graph. Chloride ion diffusion for cement paste mixtures with different w/c ratios: (squares represent specimen 1 and circles represent specimen 2).

Chloride Ion Diffusion for Mixtures Prepared with C-S-H Seeds

A control mixture and three mixtures (two replicates from each mixture) with X1 mixed at a w/c ratio equal to 0.40 were analyzed for chloride ion diffusion, as presented in Figure 25. In general, the seeded mixtures demonstrated less penetration depth compared to the control mixture. The cement paste with 8.62 fl oz/cwt demonstrated the least penetration depth among all C-S-H seeded mixtures. This experiment and the previous ones confirm that adding C-S-H seeds into the cement paste refines and densifies the microstructure, which eventually improves durability aspects. These results give insight into the optimal dosage for X1 of 8.62 fl oz/cwt.
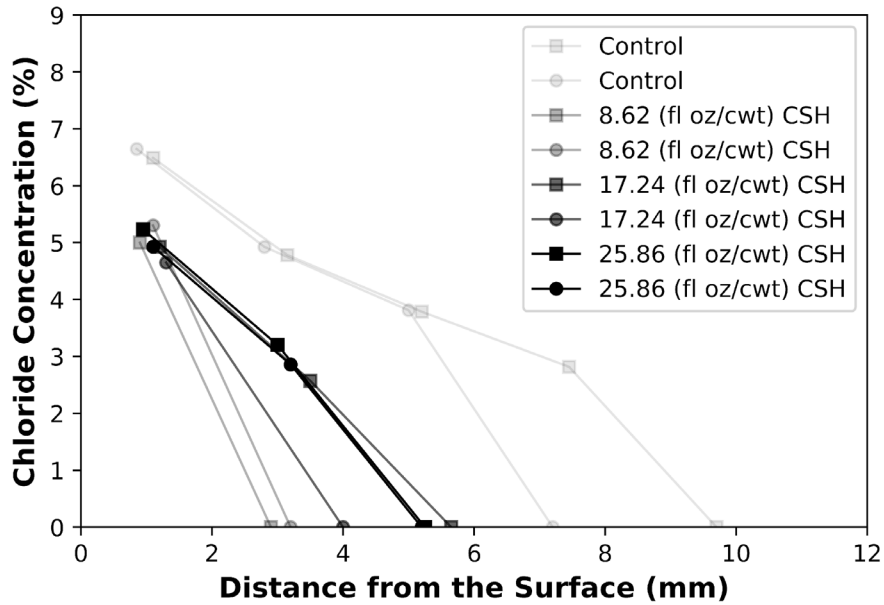
Figure 25. Graph. Chloride ion diffusion for cement paste mixtures with different dosages of X1 at 0.40 w/c ratio.

Thermogravimetric Analysis

Once the cement is mixed with water, a chemical reaction starts and reactants convert to hydration products such as AFt, AFm, calcium hydroxide (CH), and C-S-H. Thermogravimetric analysis (TGA) identifies and quantifies the crystalline and non-crystalline hydration products formed due to hydration of cement. In particular, this test monitors the formation of new phases or diminishing of other phases due to interaction of chemical or mineral admixtures with OPC.

TGA experiment results in a mass degradation curve, which shows the mass reduction due to phase transition while temperature increases. The derived curves can also be obtained, which display the peaks' locations (temperature range of any phase transition/degradation). From the derived curve, peaks demonstrate the degradation of the main hydration products such as AFt, AFm, CH, and C-S-H (Mindess, Young, & Darwin, 2003). The C-S-H phase, which is very small in size and amorphous in structure, contributes significantly to the strength of concrete (Mindess et al., 2003). Most of the phases' degradation curves are overlapped, especially at the low temperature where AFt and AFm degrade (Scrivener et al., 2016). However, CH can be distinguished at temperature ranges between 400–530°C (752–986°F) (Scrivener et al., 2016). The C-S-H phase degrades at different temperatures, but the main degradation takes place around 750–1000°C (1382–1832°F) in the wollastonite ($CaSiO_3$) phase (Scrivener et al., 2016).

X1

A control mixture and one cement paste mixture prepared with X1 were investigated by TGA. These mixtures were first explained in Chapter 3 under the subtitle "Laboratory Work." The mixtures were investigated after three days of curing. Figure 26(a) and Figure 26(b) present the mass degradation and derived curves for the two cement paste mixtures. In the seeded mixture, higher precipitation of

hydration products was observed compared to the control mixture (refer to Figure 26[a]). The derivative thermogravimetric analysis (DTGA) demonstrated that there was no change in the phase assemblage due to using X1, because the same hydration products were formed in both mixtures but with different quantities (refer to Figure 26[b]). Figure 26(c) demonstrates that the seeded mixture obtained a higher amount of bound water, which means that the total degree of hydration was higher in this mixture. Finally, Figure 26(d) demonstrates that the total mass loss in all mixtures was higher in the seeded mixture, which further confirms that there was higher precipitation in the products when X1 was used after three days of curing.

a) TGA

b) DTGA

c) Bound water
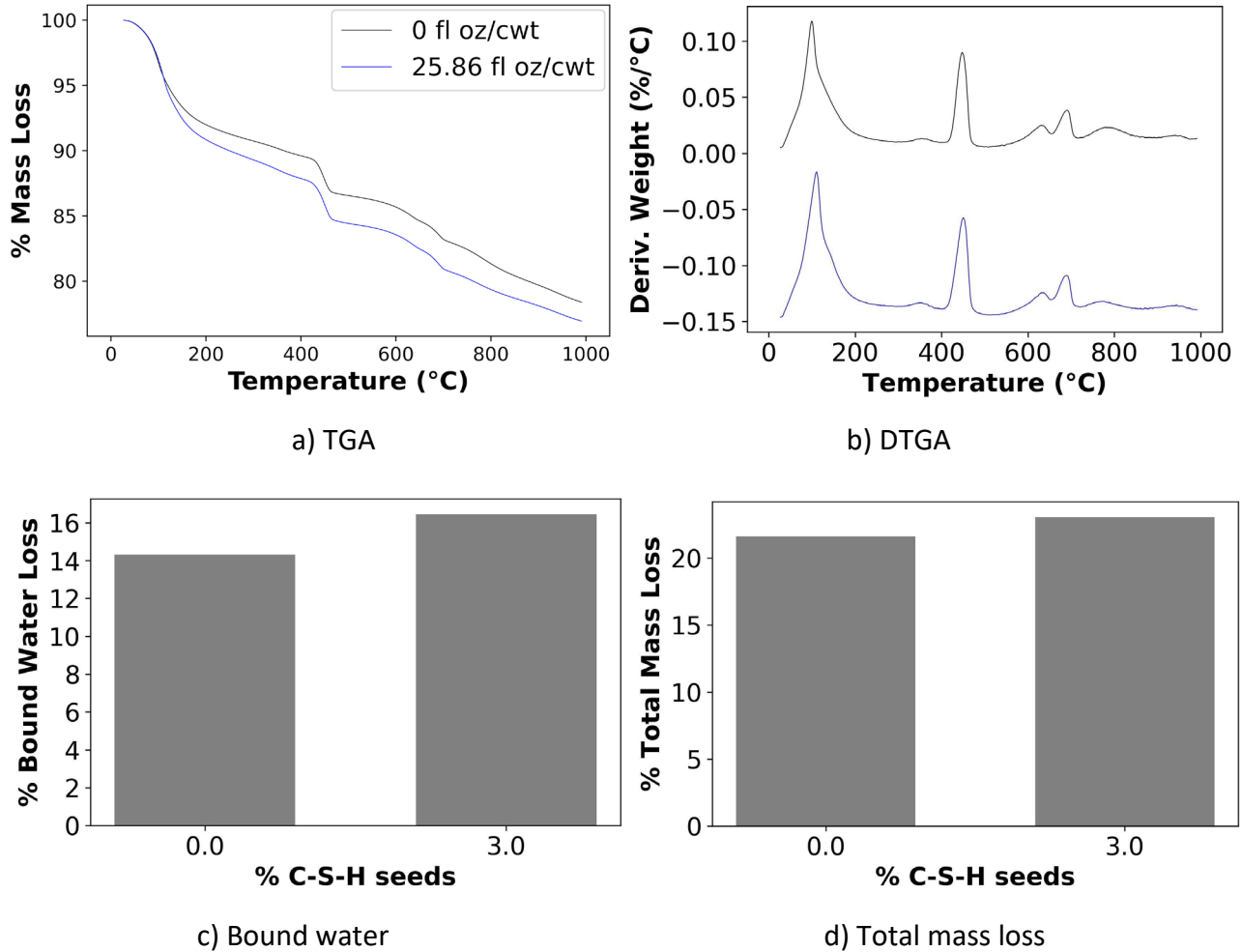
d) Total mass loss

Figure 26. Graphs. TGA experiment for cement paste mixtures mixed with X1 and cured for three days: a) TGA patterns, b) DTGA patterns, c) bound water loss 40–600°C (104–1112°F), d) total mass loss 40–1000°C (104–1832°F). The mixtures are a control and a seeded mixture with 3% C-S-H seeds. Three replicates from each mixture were tested.

X2

The mass degradation with temperature and its derivative were measured for three cement paste mixtures (refer to Table 2) and cured at days 1, 2, 3, 7, and 28 (obtained from Figure 36,

supplementary materials). The graphs demonstrate that all mixtures degrade at the same temperature ranges and follow the same trend. The only difference is that the amount of mass lost at a certain temperature range is different.

Moreover, the data obtained from the total mass loss in the range of 40–1000°C (104–1832°F) are plotted against the ages (1, 2, 3, 7, and 28 days) for all three mixtures, as presented in Figure 27. The total mass loss increased with time due to further precipitation of the hydration products. The seeded mixtures (M7 and M14) had more hydration products precipitated compared to the control mixture (M1). The hydration products M7 and M14 produced after three days were approximately equal to the produced hydration products in M0 after seven days. Furthermore, on the first day, the total mass loss is almost equal among all mixtures, but the gap started to increase between M0 and both M7 and M14 after the seventh day of hydration. This data confirms that using C-S-H seeds further precipitates hydration products, which will eventually contribute to more microstructure refinement. The collected data in Figure 27 demonstrate a trend similar to what the compressive strength and formation factor data demonstrated in previous subsections. This experiment thermally proves the efficacy of using X2 as a strength enhancer to produce early-age strength to remove the falsework or the ability to open roads earlier than the recommended times.
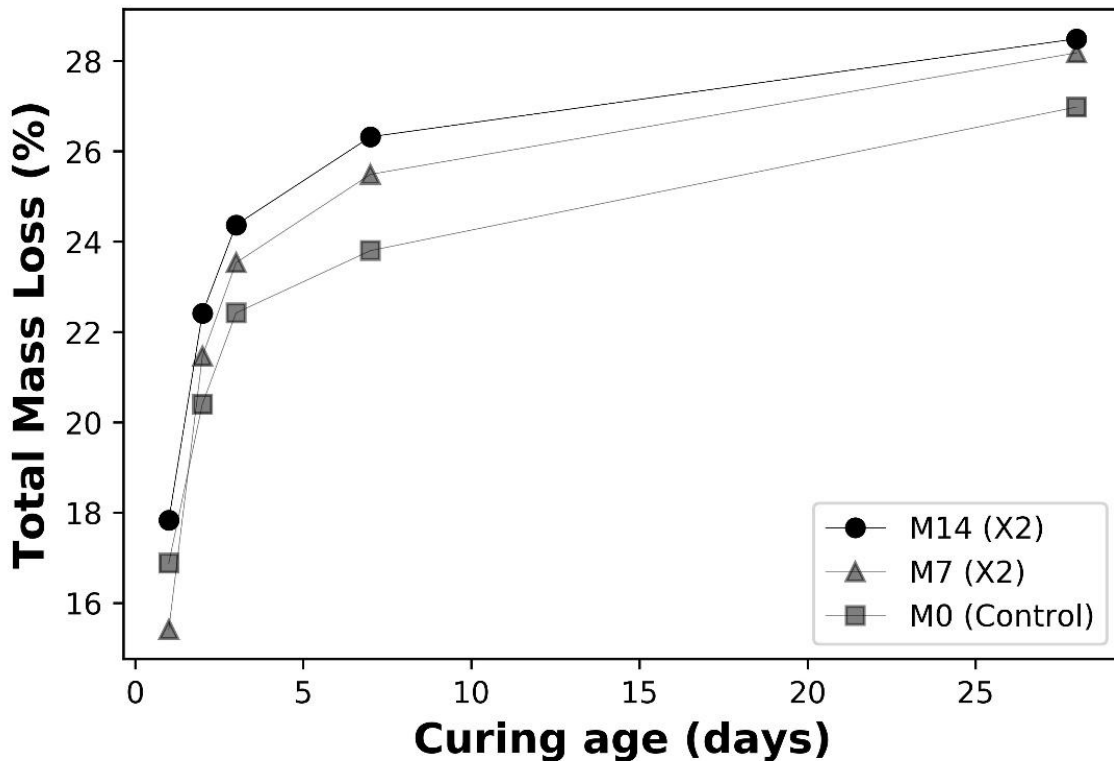
Figure 27. Graph. Total mass loss between 40–1000°C for a cement paste mixture at days 1, 2, 3, 7, and 28 (M0 = 0 fl oz/cwt, M7 = 7 fl oz/cwt, M14 = 14 fl oz/cwt).

Water Sorptivity

The extent and rate of water penetration along with deleterious ions are influenced by the nature of the pore network of the cementitious materials, which in turn affects durability aspects (Hall, 1989; Hanžič & Ilić, 2003). When the pores are big and highly connected with each other, the rate of initial water absorption increases. This measurement is indicative of microstructure refinement. A commonly agreed test used to characterize durability is the sorptivity test (ASTM C1585, 2013). In concrete, 30% of moisture intake occurs through diffusion and 70% through sorption, so sorption is the dominant mechanism for moisture intake (Neithalath, 2006). Therefore, the sorptivity test was used to characterize the microstructure refinement in addition to the previous tests in this research project.

Figure 28 presents the results for water sorptivity for eight cement paste mixtures blended with X1 after seven days from the beginning of testing. These mixtures were first explained in Chapter 3 under the subtitle "Laboratory Work." This figure presents the absorption curve for each mixture individually and demonstrates the total cumulative water absorption by each mixture. This is in addition to the initial rate of water absorption reflecting the refinement of the microstructure. The obtained data presented in Figure 28(a) demonstrate two major findings. First, water penetration depth is lower in all X1 mixtures compared to the control mixture after seven days of sorption. The results prove that the microstructure is becoming denser and more refined with the addition of C-S-H seeds. Second, this test did not seem to distinguish the slight differences between the various seeded cement paste mixtures. In other words, this test only demonstrated that the seeded mixtures behaved better than the control mixture, but it did not demonstrate the optimal X1 dosage or detect any trend when increasing the dosage, as detected by helium pycnometry measurements. From this perspective, it is better to rely on open porosity measurements or isothermal calorimetry measurements to decide the optimal X1 dosage to add to the cement paste. Figure 28(b) presents the cumulative water absorption after seven days. The mixture with no X1 absorbed the highest amount of water compared to all mixtures seeded with X1. Figure 28(c) presents the initial rate of water absorption for all samples. The rate of initial absorption of all mixtures prepared with X1 was lower than the control mixture. The secondary rate of absorption was not of interest in this study for many reasons. The samples became saturated early because they were very small in size, so the obtained data after seven days were compromised. Also, there was significant fluctuation in the collected data after the first 24 hours.

Prior studies have measured water sorptivity in cement paste mixed with different seeds (Du & Pang, 2015; Ehsani, Nili, & Shaabani, 2017; Shaikh & Supit, 2014), but have not measured cement paste doped with C-S-H seeds specifically. In this study, water sorptivity was introduced to investigate the impact of adding C-S-H seeds to cement paste mixtures, proving that adding C-S-H seeds improves transport properties such as water absorption, diffusion, and permeability by refining the microstructure.
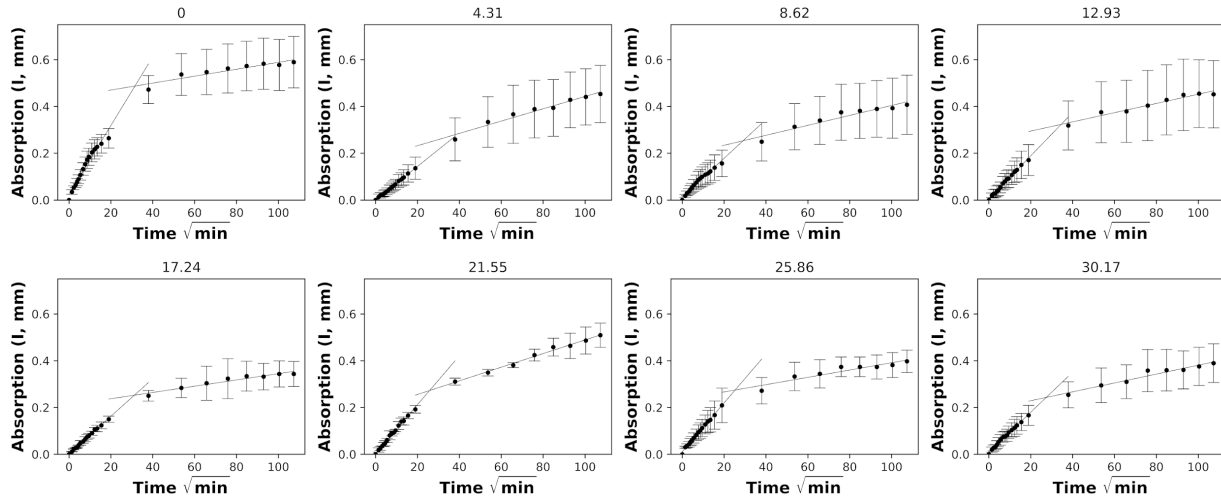
a) Sorptivity measurements for eight cement paste mixtures
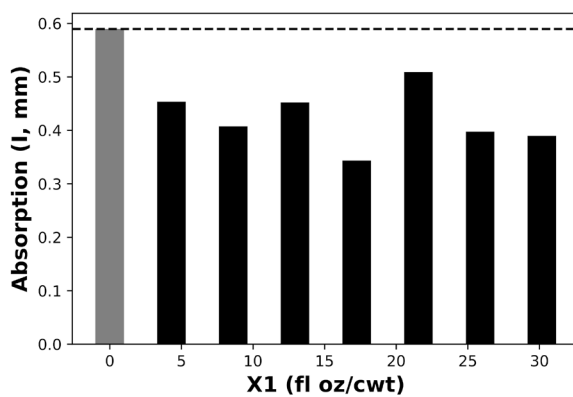
b) Cumulative absorbed water
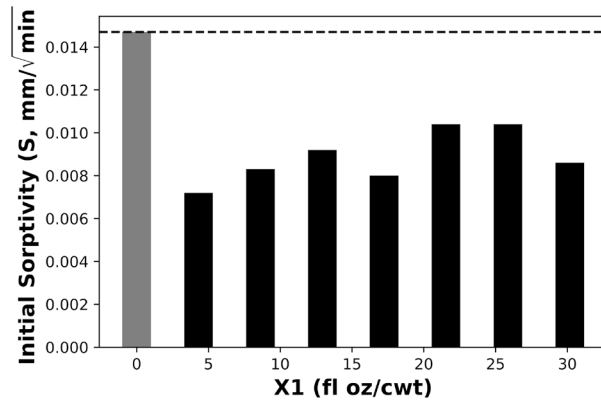
c) initial rate of water absorption

Figure 28. Graphs. a) Sorptivity measurement of all cement paste mixtures mixed with C-S-H seeds (the number on the top of every single figure represents the dosage [fl oz/cwt] of X1), b) the cumulative absorbed water for all cement paste mixtures mixed with X1, and c) the values of the initial rate of water absorption of all cement paste mixtures mixed with X1. The dose percentages of X1 in all graphs range from 0 to 30.17 fl oz/cwt. This experiment is conducted for cement paste specimens after three days of sealed curing.

Correlations between Different Measurement Techniques

X1

For cement paste mixtures cast in the lab with different dosages of X1, there is a good correlation between the final cumulative heat of hydration and the open porosity volume after three days of hydration, as presented in Figure 29. From this figure, the total cumulative heat of hydration increased, which represents the degree of hydration at a certain time, and the open porosity volume decreased with the increase of X1 dosage. A steep correlation (high slope) was also observed until the addition of 12.93 fl oz/cwt of X1. After this dosage, the correlation becomes smooth (small slope).
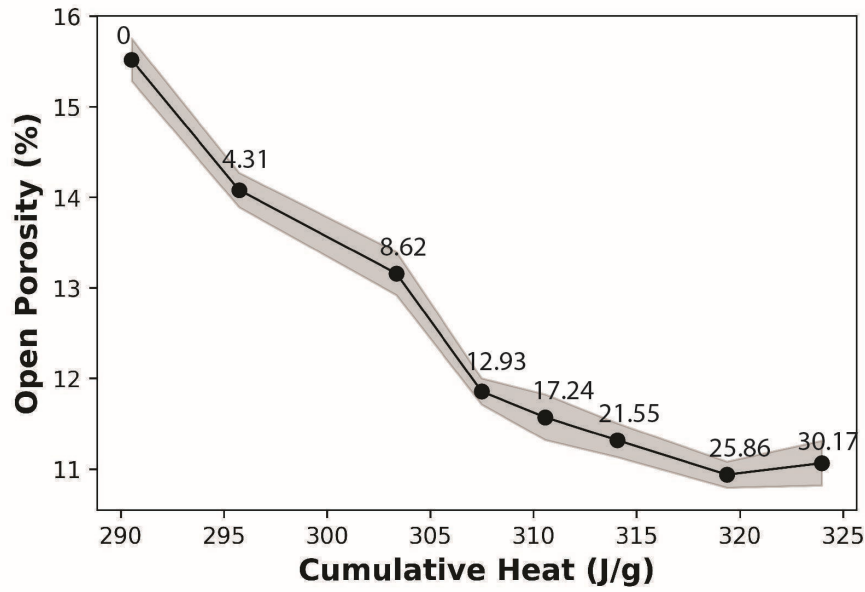
Figure 29. Graph. Relationship between cumulative heat development and open porosity volume at different dosages of X1. The numbers above the markers represent the dosage of the X1 in fl oz/cwt.

X2

For the cement paste and concrete mixtures cast in the lab and mixed with X2, there are several correlations between compressive strength, total mass loss, open porosity, and the formation factor, as presented in Figure 30. These correlations followed a linear path, e.g., the increase in compressive strength was highly correlated with the increase in total mass loss obtained from the TGA experiment, as presented in Figure 30(a). This correlation proves that the increase in hydration products' precipitation caused an increase in compressive strength. In the literature, the relationship between compressive strength and the degree of hydration in different concrete mixtures was found to be linear, which agrees with what the researchers found in this study (Chu et al., 2021; Deboucha et al., 2017). The degree of hydration was calculated based on the total mass loss between 40–1000°C (104–1832°F). These results prove that the TGA results could be used to predict compressive strength when concrete is seeded with C-S-H seeds.

Furthermore, there was an inverse correlation between compressive strength and open porosity, as presented in Figure 30(b). The results demonstrated that the increase in compressive strength was accompanied by a reduction in open porosity volume, which confirms that microstructure refinement increases the strength of concrete. Different studies found that there is a relationship between compressive strength and total porosity. For example, Chen et al. (2013) found there was a negative exponential relationship between compressive strength and total porosity. In this study, the trend seems to be more linear than exponential. This finding gives insight into the effect of adding C-S-H seeds to concrete in regard to porosity reduction measured by helium pycnometry.

Last, the compressive strength and the formation factor measured by electrical resistivity testing followed a direct linear relationship, as presented in Figure 30(c). This correlation further proves that the increase in compressive strength was accompanied by microstructure refinement, which results

in an improvement in transport properties due to an increase in tortuosity and a reduction in pores' volume based on the formation factor measurements.

Good insights are given from this correlation, which means that the compressive strength could be predicted nondestructively using the electrical resistivity and formation factor measurements. A study investigated the correlation between electrical resistivity (not including formation factor) and compressive strength. It found there is no direct relationship between electrical resistivity and compressive strength (Gudimettla & Crawford, 2016). This result contradicts the results of this study, potentially due to not using the formation factor, which is derived from electrical resistivity. In this study, the direct relationship between formation factor and compressive strength is decidedly linear. This finding calls for further studies to investigate this correlation and how to use the formation factor parameter to predict compressive strength.
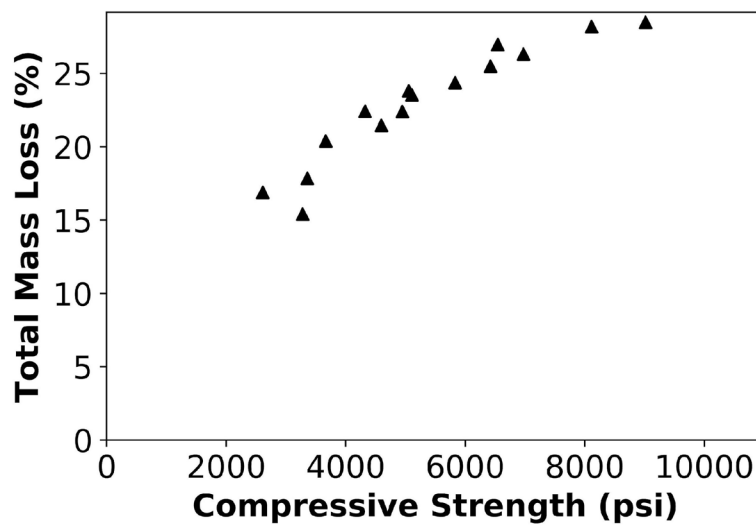
a) Compressive strength versus total mass loss
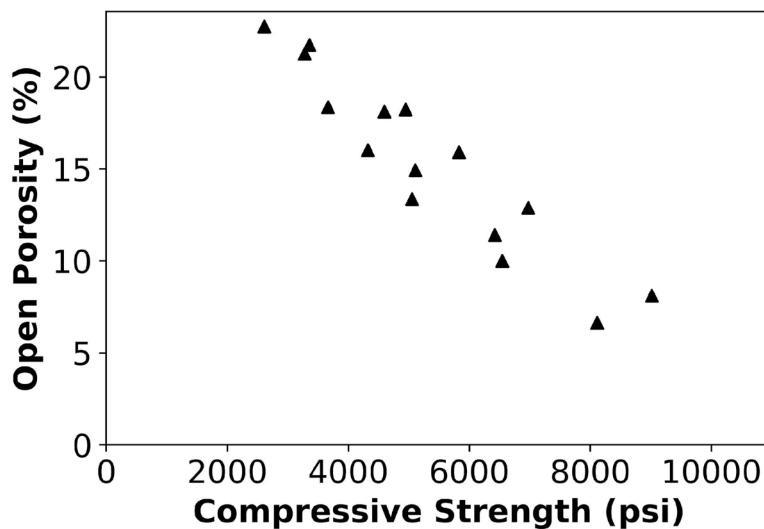
b) Compressive strength versus open porosity
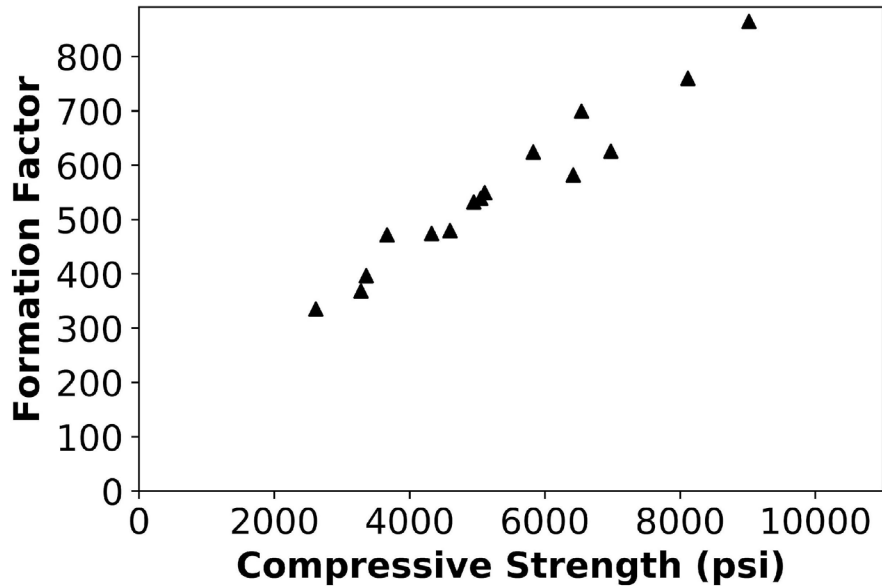
c) Compressive strength versus formation factor

Figure 30. Graph. Several correlations with compressive strength for M0 (0 fl oz/cwt), M7 (7 fl oz/cwt), and M14 (14 fl oz/cwt) concrete mixtures (X2 was used with these mixtures): a) correlation between the total mass loss and compressive strength, b) correlation between the open porosity measured by the helium pycnometry and compressive strength, and c) correlation between the formation factor and compressive strength.

FIELD DATA

In parallel with the lab experiments, data were collected on optimal mixtures designed for the field (refer to Table 3). As the researchers were trying to establish a baseline seven-day cure, concrete samples were cured at different curing times, as explained in Chapter 3 under the subtitle "Field Work." Figure 31, Figure 32, Figure 33, and Figure 34 present results for compressive strength, flexural strength, electrical resistivity, and formation factors, respectively. Tables 7 through 14 in Appendix A present detailed results of the cast-in-place measurements.

Compressive Strength

Figure 31 presents the compressive strength for four structure mixtures (SI Mix), a precast concrete mixture (PC Mix), a concrete mixture obtained from a drilled shaft (DS Mix), and field demo concrete mixtures (Stage I and Stage II) obtained from the box culvert constructed near Armstrong, Illinois, on days 1, 2, 3, 7, 14, 52, and 97.
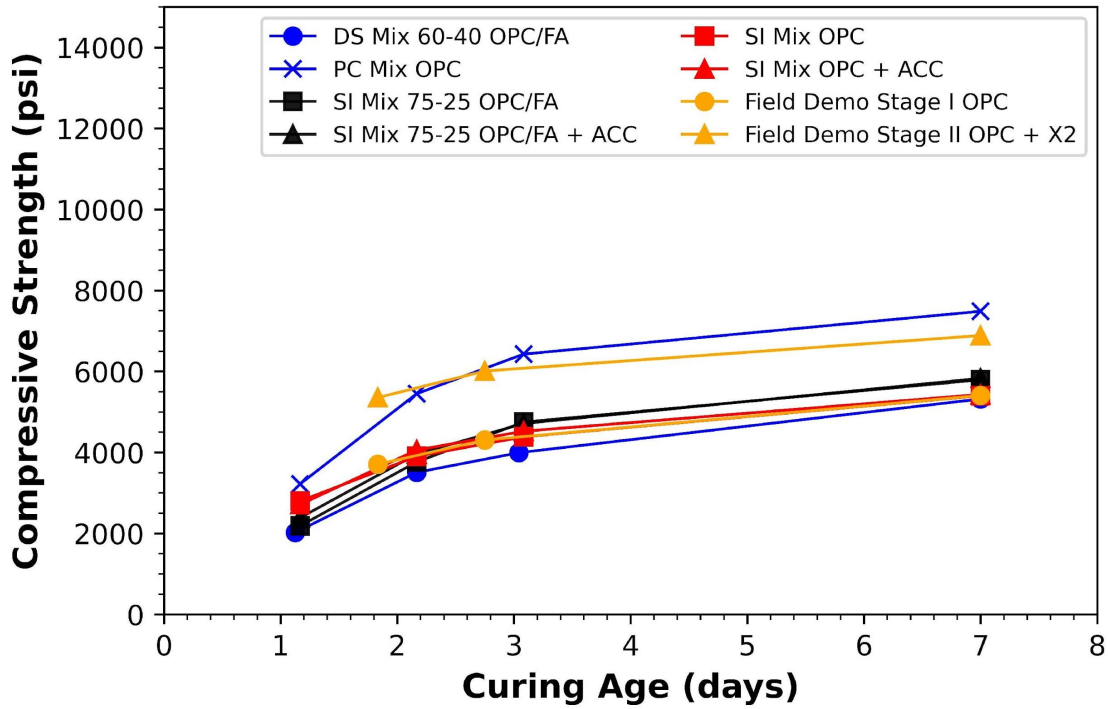
a) Compressive strength development up to 7 days
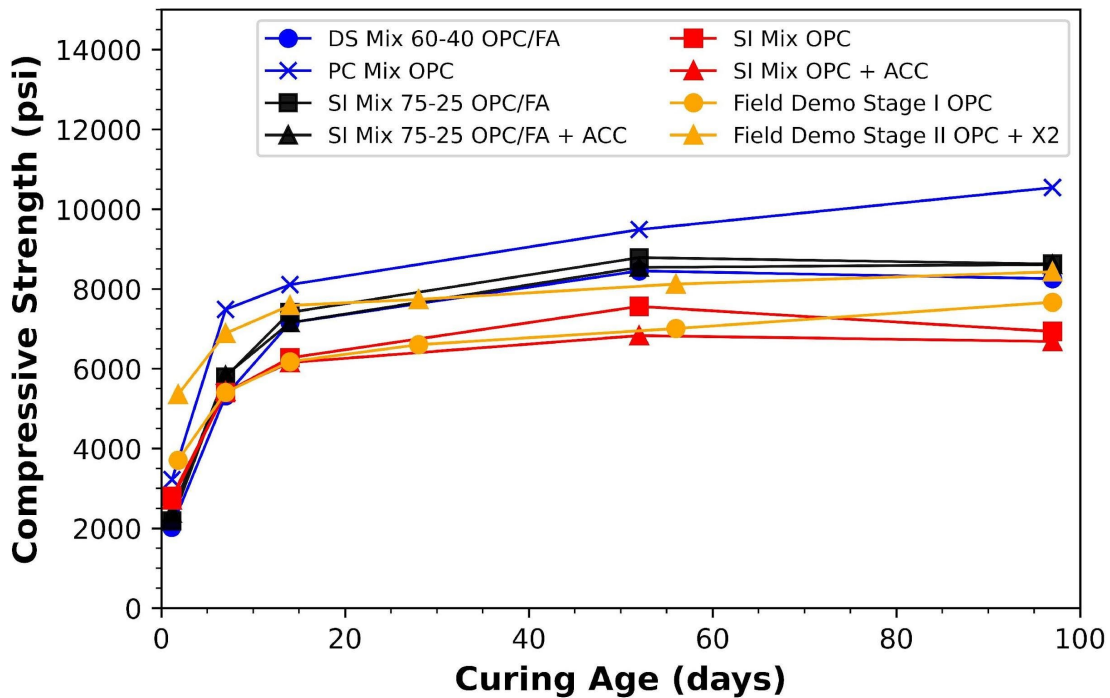
b) Compressive strength development up to 97 days

Figure 31. Graph. Compressive strength development for concrete mixtures: a) measurements for days 1, 2, 3, and 7 and b) measurements from days 1 to 97. (Days 2 and 3 are omitted in this figure.)

Several observations can be drawn from the obtained results. Regarding the SI Mix 75-25 OPC/FA, SI Mix 75-25 OPC/FA + ACC, SI Mix 100 OPC, and SI Mix 100 OPC + ACC concrete mixtures obtained from the ready-mix plant, the compressive strength for all mixtures is similar up to 28 days. From day 29 and onward, the SI Mix 75-25 OPC/FA and SI Mix 75-25 OPC/FA + ACC achieve higher strength. This behavior confirms that the fly ash takes some time to react and contributes to the increase of compressive strength. The precast concrete mixture achieved the highest compressive strength among all concrete mixtures at all ages. The w/c ratio in this concrete mixture was the lowest, and it had the highest total cementitious content, which is why this mixture had the highest compressive strength. The DS Mix 60-40 OPC/FA concrete mixture was comparable to the SI Mix 75-25 OPC/FA and SI Mix 75-25 OPC/FA + ACC mixtures because these mixtures were blended with fly ash.

The Field Demo Stage I and Stage II concrete mixtures were prepared with only OPC and without any fly ash. For all ages, the compressive strength of the Stage II mixture is higher than Stage I. This behavior is due to using X2. For example, the compressive strength of the Stage I mixture after seven days is 37.3 MPa (5,406 psi), whereas it is 36.9 MPa (5,354 psi) for Stage II after only two days. Also, the strength of the Stage I and Stage II mixtures after 97 days is 52.9 MPa (7,667 psi) and 58.1 MPa (8,428 psi), respectively, meaning the compressive strength was boosted by 10% when X2 was added. The difference in the compressive strength between the Stage I and Stage II mixtures is consistent, which confirms that no further hydration takes place at a later age due to adding X2. The effect of adding these seeds appears at an early age and stays consistent over the long term.

Flexural Strength

Figure 32 presents the flexural strength test results for four structure mixtures (SI Mix), a precast concrete mixture (PC Mix), a concrete mixture obtained from a drilled shaft (DS Mix), and Field Demo concrete mixtures (Stage I and Stage II) obtained from the box culvert constructed near Armstrong, Illinois, at days 2, 3, 7, and 14. The flexural strength was measured at 3, 7, and 14 days for all concrete mixtures, except Stage I and Stage II concrete mixtures which were measured at 2, 3, and 7 days.

Several observations can be drawn from the test results. First, the PC Mix OPC and the DS Mix 60-40 OPC/FA mixtures achieved the highest flexural strength, because these concrete mixtures were mixed with the lowest w/c ratio compared to other mixtures. Second, strength on day 14 decreased compared to strength on day 7, a trend observed in all mixtures. This behavior could be contributed to testing the beams in the dry state. Some researchers observed that drying concrete before testing reduces the flexural strength as compared to wet concrete at the time of testing (Yurtdas, Burlion, Shao, & Li, 2011). This trend did not occur in the compressive strength measurements. This finding makes the flexural strength behavior unclear and requires further research. Third, the flexural strength of the Stage II mixture is higher than the Stage I mixture. This behavior is due to using X2.
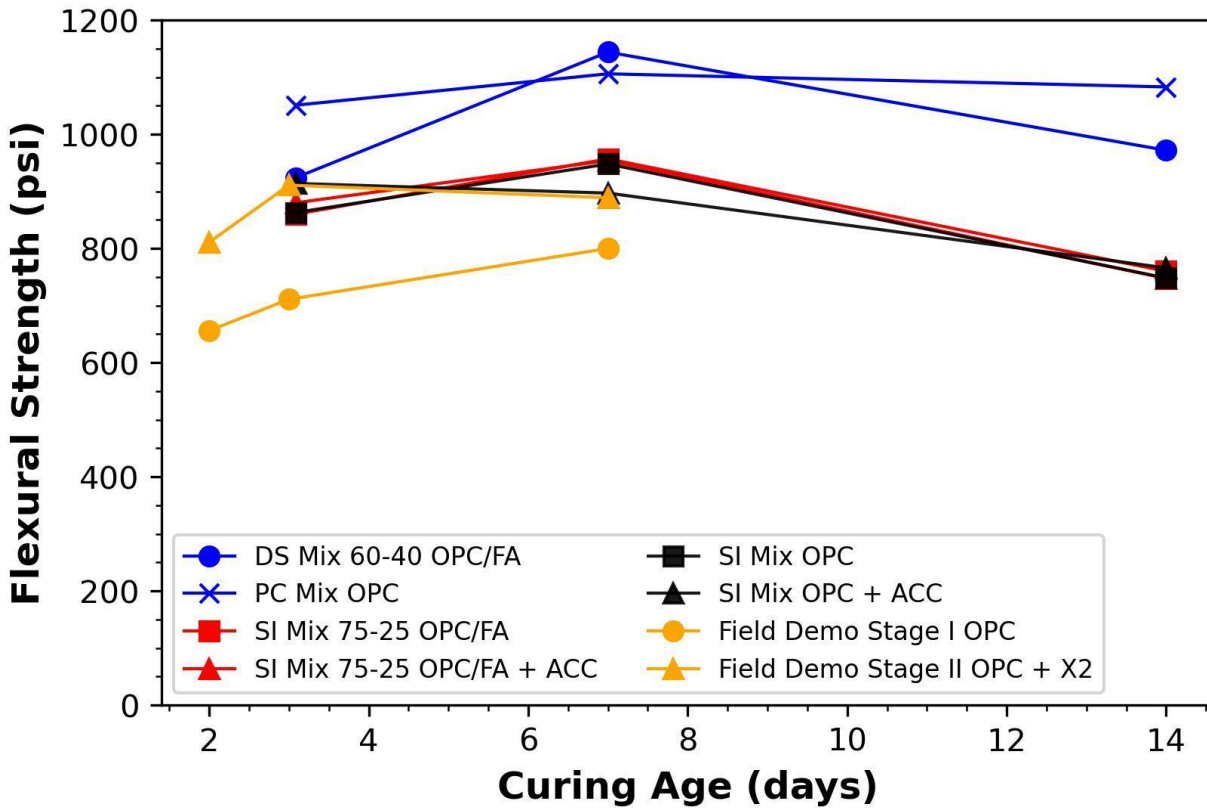
Figure 32. Graph. Flexural strength development for concrete mixtures.

Electrical Resistivity and Formation Factor

Figure 33 presents the electrical resistivity for four structure mixtures (SI Mix), a precast concrete mixture (PC Mix), a concrete mixture obtained from a drilled shaft (DS Mix), and Field Demo concrete mixtures (Stage I and Stage II) obtained from the box culvert constructed near Armstrong, Illinois, on days 1, 2, 3, 7, 14, 29, 52, and 97.
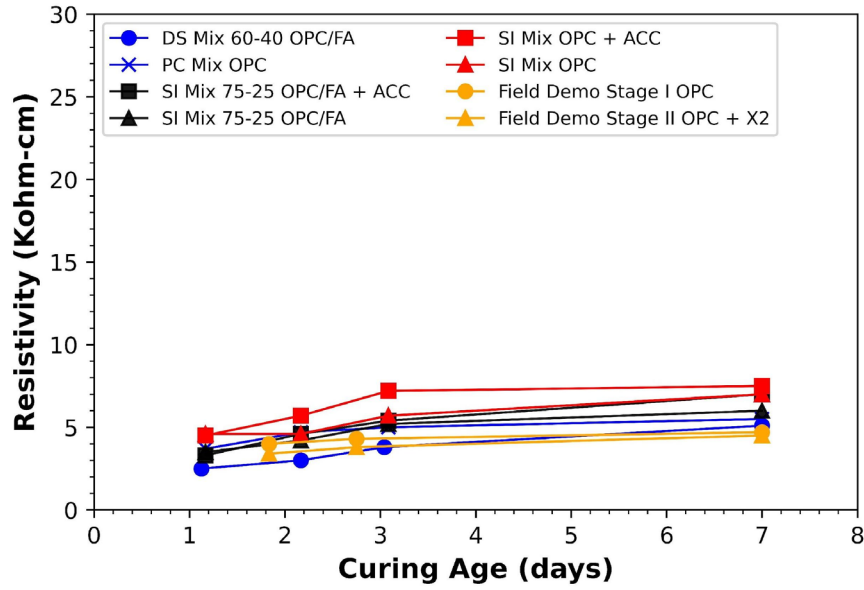
a) Electrical resistivity development up to 7 days
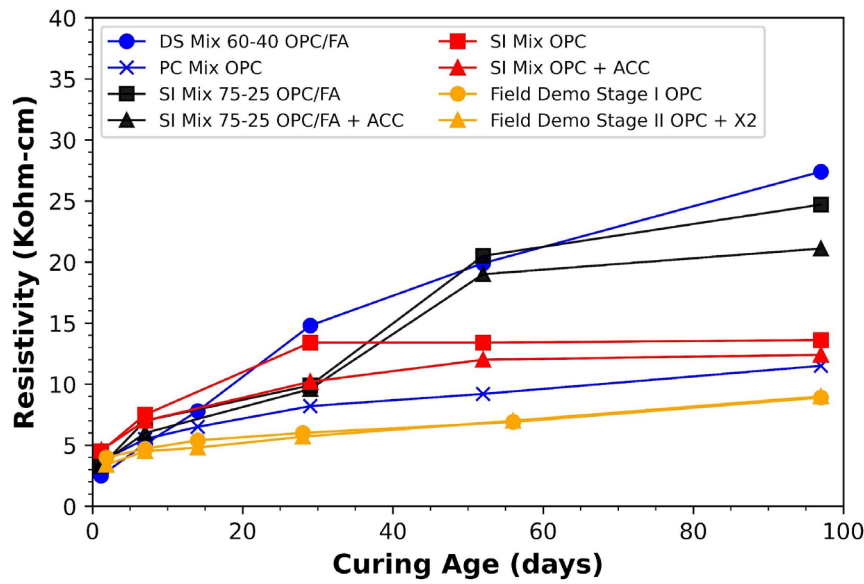
b) Electrical resistivity development up to 97 days

Figure 33. Graphs. Electrical resistivity measurements for concrete mixtures: a) measurements for days 1, 2, 3, and 7 and b) measurements from days 1 to 97. (Days 2 and 3 are omitted in this figure.)

Several observations can be drawn from these results. First, the Field Demo Stage I and Stage II mixtures obtained the lowest electrical resistivity at all ages compared to other mixtures. Second, the mixtures blended with fly ash obtained the highest electrical resistivity, especially after day 29. The concrete mixtures prepared without fly ash obtained electrical resistivity values close to each other. However, the PC Mix OPC obtained electrical resistivity values slightly less than the SI Mix 100 OPC

and the SI Mix 100 OPC + ACC because of the lower w/c ratio in the precast concrete, reflecting the less refined microstructure.

Figure 34 presents the formation factor for four structure mixtures (SI Mix), a precast concrete mixture (PC Mix), a concrete mixture obtained from a drilled shaft (DS Mix), and Field Demo concrete mixtures (Stage I and Stage II) obtained from the box culvert constructed near Armstrong, Illinois, at days 1, 2, 3, 7, 14, 29, 52, and 97.
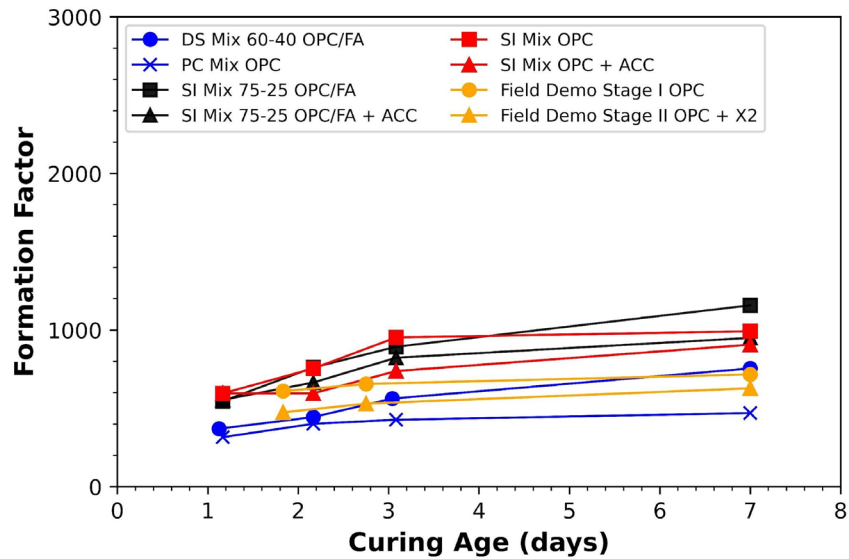
a) Formation factor development up to 7 days
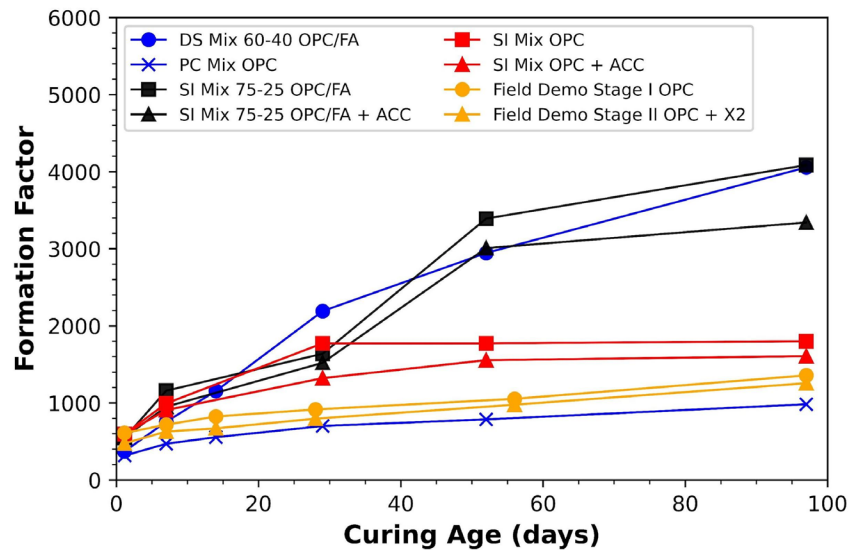
b) Formation factor development up to 97 days

Figure 34. Graphs. Formation factor for concrete mixtures: a) measurements for days 1, 2, 3, and 7 and b) measurements from days 1 to 97. (Days 2 and 3 are omitted in this figure.)

Based on what was introduced in Chapter 3, the formation factor reflects the state of microstructure refinement. The higher the formation factor, the denser and more refined the microstructure. In other words, the higher the formation factor, the less pore volume and less connectivity in the pore microstructure. The formation factor trend for most concrete mixtures was almost similar to what was obtained from the electrical resistivity measurements. Yet, at all ages, the precast concrete's formation factor became less than the Field Demo Stage I and Stage II concrete mixtures. This trend switched in electrical resistivity measurements. The reason behind the change in this data representation is due to the normalization to the pore solution resistivity for each concrete mixture.

Correlations

For all concrete mixtures collected from the field, the relationship between the formation factor and compressive strength was drawn as presented in Figure 35.
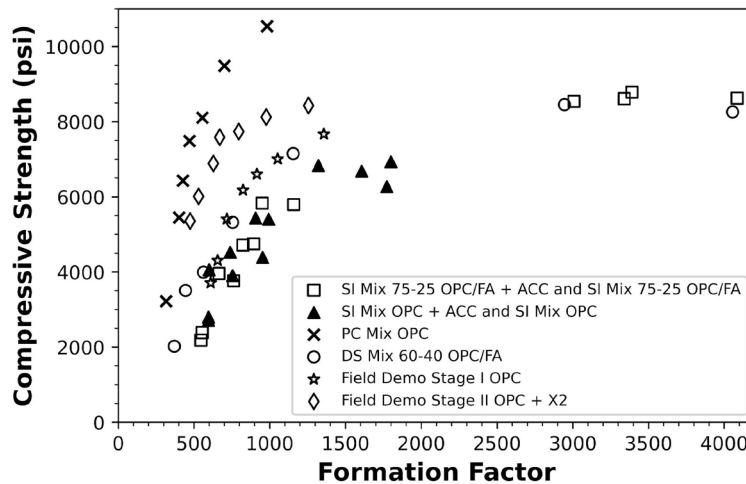
a) Formation factor versus compressive strength for all concrete mixtures collected from the field. Each mixture is shown in a different legend.
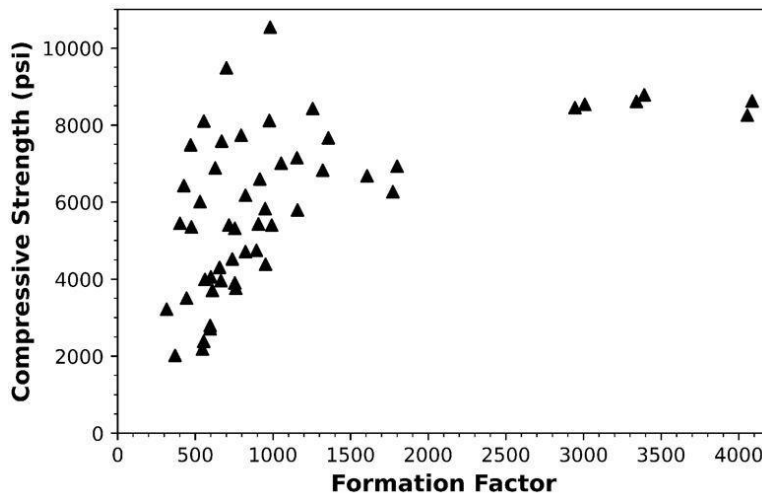
b) Formation factor versus compressive strength for all concrete mixtures collected from the field. All mixtures are shown in the same legend.
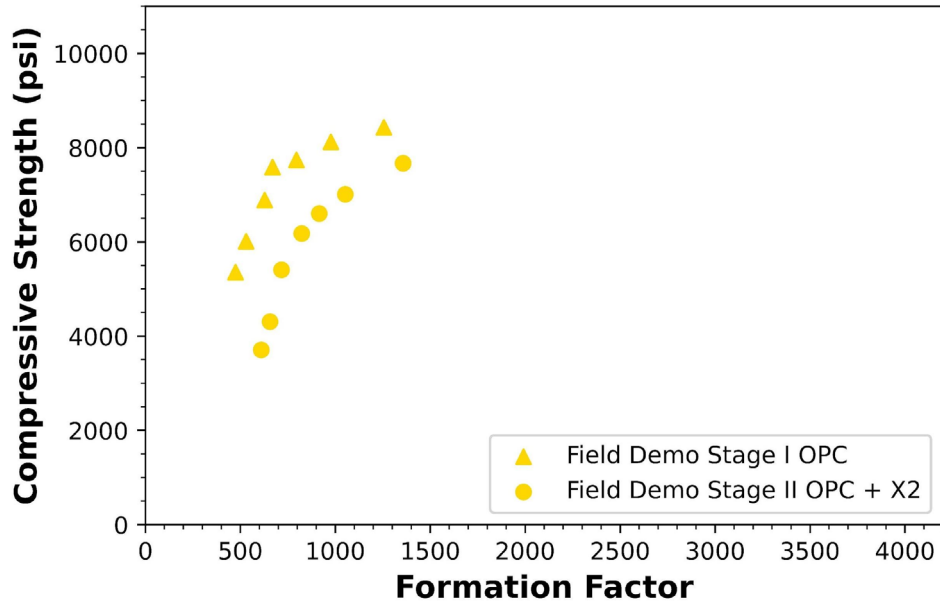
c) Formation factor versus compressive strength for Stage I and Stage II concrete mixtures

Figure 35. Graphs. Relationship between formation factor and compressive strength for all mixtures obtained from the field: a) all mixtures separately, b) all mixtures without distinguishing, and c) only field demo Stage I and Stage II (dosage = 5 fl oz/cwt) mixtures.

At first glance, each concrete mixture had its own trend. All concrete mixtures had a parabolic trend, except the precast concrete mixture, which fits linearly. The results demonstrate that the exact relationship (linear versus parabolic) between the two parameters is highly mixture dependent.

Heat of Hydration

In regard to X2 having a significant influence on maximum concrete temperatures in the field, the following was observed for the field box culvert demo project:

The Stage I (without X2) 0.33 m (13 in.) bottom slab was poured on May 12, 2022. The concrete temperature was 31.1°C (88°F) and the air temperature was 32.8°C (91°F) at the time of concrete placement. The maximum concrete temperature achieved from heat of hydration was 51.5°C (124.7°F). For comparison, the Stage II (with X2) 0.33 m (13 in.) bottom slab was poured on July 21, 2022. The concrete temperature was 26.7°C (80°F) and the air temperature was 18.3°C (65°F) at the time of concrete placement. The maximum concrete temperature achieved from heat of hydration was 57.5°C (135.5°F).

The Stage I (without X2) 0.28 m (11 in.) wall was poured on May 20, 2022. The concrete temperature was 27.8°C (82°F) and the air temperature was 29.4°C (85°F) at the time of concrete placement. The maximum concrete temperature achieved from heat of hydration was 51.5°C (124.7°F). For comparison, the Stage II (with X2) 0.28 m (11 in.) wall was poured on August 11, 2022. The concrete temperature was 28.9°C (84°F) and the air temperature was 31.1°C (88°F) at the time of concrete

placement. The maximum concrete temperature achieved from heat of hydration was 46.5°C (115.7°F).

The Stage I (without X2) 0.30 m (12 in.) top slab was poured on June 8, 2022. The concrete temperature was 23.3°C (74°F) and the air temperature was 18.3°C (65°F) at the time of concrete placement. The maximum concrete temperature achieved from heat of hydration was 47°C (116.6°F). For comparison, the Stage II (with X2) 0.30 m (12 in.) top slab was poured on August 22, 2022. The concrete temperature was 28.9°C (84°F) and the air temperature was 25°C (77°F) at the time of concrete placement. The maximum concrete temperature achieved from heat of hydration was 52.5°C (126.5°F). Detailed information on the pours is available in another ICT-IDOT study, R27-219 (Solanki & Xie, Forthcoming).

A review of this test information does not give a conclusive indication that using the X2 admixture will generate higher heat of hydration concrete temperatures in the field. More research is needed in this area.

CHAPTER 5: CONCLUSIONS AND RECOMMENDATIONS

The main goal of this study was to reduce the curing time of concrete bridge substructure components and concrete box culverts by employing C-S-H-based seeds to enhance the early hydration and improve the strength of seeded mixtures. Two commercially available seeds (X1 and X2) were tested via a series of lab techniques to judge their performance. One seed (X2) was deployed in the field on a box culvert in Armstrong, Illinois, to investigate the field performance of the seeded mixture (Qadri & Garg, 2023). Moreover, fly ash addition and low water-to-cement ratio were evaluated as additional approaches to improve durability and reduce cure time.

Based on the lab and field data collected between August 2020 and February 2022, the researchers draw the following conclusions:

1. X1, at all dosages up to 30 fl oz/cwt, slightly accelerated the reaction kinetics of the cementitious pastes and resulted in an overall higher degree of hydration based on the total cumulative heat recorded from isothermal calorimetry from approximately 290 to approximately 325 J/g. Additionally, increasing the dosage also resulted in a finer microstructure, as evidenced from the reduced open porosity values from approximately 15% to approximately 11%. It also seemed to somewhat limit the chloride ion diffusion into the cement pastes and reduce water sorptivity, although thermogravimetry analysis demonstrated no significant change in the final phase assemblage.

2. In contrast, X2, at all dosages up to 15 fl oz/cwt, slightly retarded the reaction kinetics of the cementitious pastes at the early hours of hydration. However, in the long term, it too resulted in a higher degree of hydration, as presented by the total cumulative heat from calorimetry from approximately 290 to approximately 325 J/g. In terms of porosity reduction, it had an optimal value of 14 fl oz/cwt, where the lowest open porosity value of 10% was recorded. The thermogravimetry analysis data corroborated these results, as a clear increase in bound water was found with increasing the dosage of these seeds up to 14 fl oz/cwt, suggesting a fine microstructure. Finally, concrete mixtures were cast in the lab with X2 at 0, 7, and 14 fl oz/cwt, where increasing the dosage increased early-age strength as well as the formation factor, indicating reduced permeability. Ultimately, strong correlations were observed between almost all measurement parameters as follows: total mass loss via thermogravimetry analysis, cumulative heat, open porosity, formation factor, and compressive strength. Overall, X2 was considered for field testing, given its more relevant performance for the ready-mix concrete and its approval as a Type S chemical admixture by the Illinois Department of Transportation.

3. A series of concrete mixtures were cast in the field to ascertain the range of variability for permeability of different mixes in terms of strength and formation factor development as a function of age. In addition, a demo project conducted under two stages was performed in 2022 to compare the effect of using seeds in the field. The Stage I mixture had no X2 whereas the Stage II mixture used 5 oz/cwt of X2. The X2 mixture consistently had improved compressive and flexural strengths compared to the control mix. Overall, there

are clear relationships between compressive strengths and formation factors for all mixes deployed in the field, suggesting resistivity-based rapid testing can be an approximate indicator of mechanical strength development. However, the relationship between formation factor and strength is highly mix dependent, and formation factors should not be compared across different mixes.

4. Fly ash–based concrete mixtures obtained higher compressive strength at later ages and higher formation factors.

5. Based on porosity measurements, the cement paste mixtures made of only OPC obtained lower porosity than mixtures blended with fly ash. However, the porosity was improved in blended mixtures when X2 was used. This finding further confirms the efficacy of using the X2 chemical admixture with blended concrete mixtures.

6. Referring to Table 11 and 13, both the PC Mix OPC and DS Mix 60-40 OPC/FA compared no curing for 90 days to curing for 90 days. As anticipated, a difference was found, but that would be expected for the very long cure time (90 days). Based on the test results, it is not anticipated that reducing 7 days of curing to 3 days of curing will provide significant harm to permeability.

Based on these conclusions, the researchers recommend that a C-S-H seed admixture is a viable option for enhancing the strength and microstructure of concrete, paving the way for reducing curing durations. The dosage and the type of admixture are two very important parameters that must be carefully chosen based on the desired performance, cost, and feasibility. Other approaches to improve the early-age strength and to reduce the curing duration is to reduce the water-to-cement ratio and to consider using reactive finely divided materials.

Regarding implementation of specification changes based on the field box culvert demo project, a Contractor option to reduce the cure time from 7 days to 3 days for bridge substructure components and box culverts may benefit earlier completion of a project. IDOT's *Standard Specifications for Road and Bridge Construction* (2022) require cast-in-place substructures and cast-in-place box culverts to cure for seven days. For precast structural members and precast box culverts, the producer has the option to discontinue curing when the concrete has attained 80% of the mix design strength or after seven days of curing (IDOT, 2022). Given that the precast mixes are allowed to cure for shorter durations as long as they meet 80% of the design strength, reducing cure time from 7 days to 3 days for cast-in-place bridge substructure components and cast-in-place box culverts appears reasonable. Especially as long as the strength specimens are field-cured and obtain 100% of the design strength at 3 days. It is recommended at the time of casting that the IDOT maximum water-to-cement ratio be reduced from 0.44 to 0.42 to help with early strength and will make the concrete more impermeable (IDOT, 2022).

REFERENCES

AASHTO T 119. (2018). *Standard method of test for slump of hydraulic cement concrete*. AASHTO.

AASHTO T 152. (2019). *Standard method of test for air content of freshly mixed concrete by the pressure method*. AASHTO.

AASHTO T 177. (2017). *Standard method of test for flexural strength of concrete (using simple beam with center-point loading)*. AASHTO.

AASHTO T 22. (2017). *Standard method of test for compressive strength of cylindrical concrete specimens*. AASHTO.

AASHTO. (2020). *AASHTO LRFD bridge design specification*. AASHTO.

Aïtcin, P.-C. (2016). Accelerators. In *Science and technology of concrete admixtures* (pp. 405–413). Elsevier.

Aligizaki, K. K. (2005). *Pore structure of cement-based materials: Testing, interpretation and requirements*. CRC Press.

Alizadeh, R., Raki, L., Makar, J. M., Beaudoin, J. J., & Moudrakovski, I. (2009). Hydration of tricalcium silicate in the presence of synthetic calcium–silicate–hydrate. *Journal of Materials Chemistry*, *19*(42), 7937–7946.

Alzaza, A., Ohenoja, K., Langås, I., Arntsen, B., Poikelispää, M., & Illikainen, M. (2022). Low-temperature (−10° C) curing of Portland cement paste–Synergetic effects of chloride-free antifreeze admixture, C–S–H seeds, and room-temperature pre-curing. *Cement and Concrete Composites*, *125*, 104319

American Concrete Institute. (2016). *Guide to external curing of concrete*. American Concrete Institute.

Amin, M., Tayeh, B. A., & Agwa, I. S. (2020). Effect of using mineral admixtures and ceramic wastes as coarse aggregates on properties of ultrahigh-performance concrete. *Journal of Cleaner Production*, *273*, 123073.

Asaad, M. A., Ismail, M., Tahir, M. M., Huseien, G. F., Raja, P. B., & Asmara, Y. P. (2018). Enhanced corrosion resistance of reinforced concrete: Role of emerging eco-friendly Elaeis guineensis/silver nanoparticles inhibitor. *Construction and Building Materials*, *188*, 555–568.

ASTM C494/C494 M-17. (2020). *Standard Specification for Chemical Admixtures for Concrete*. ASTM International.

ASTM C143. (2012). *Standard test method for slump of hydraulic-cement concrete*. ASTM International.

ASTM C1152. (2020). *Standard test method for acid-soluble chloride in mortar and concrete*. ASTM International.

ASTM C1556. (2016). *Standard test method for determining the apparent chloride diffusion coefficient of cementitious mixtures by bulk diffusion*. ASTM International.

ASTM C1585. (2013*). Standard test method for measurement of rate of absorption of water by hydraulic—cement concretes*. ASTM International.

ASTM C1760. (2012). *Standard test method for bulk electrical conductivity of hardened concrete*. ASTM International.

ASTM C231. (2009). *Standard test method for air content of freshly mixed concrete by the pressure method*. ASTM International.

ASTM C293. (2016). *Standard test method for flexural strength of concrete (using simple beam with center-point loading)*. ASTM International.

ASTM C39. (2018). *Standard test method for compressive strength of cylindrical concrete specimens*. ASTM International.

Balluffi, R. W., Allen, S. M., & Carter, W. C. (2005). *Kinetics of materials*. John Wiley & Sons.

Baral, A., Rodriguez, E. T., Hunnicutt, W. A., Cakmak, E., Sun, H., Ilavsky, J., … Garg, N. (2022). Ultra-high gamma irradiation of calcium silicate hydrates: Impact on mechanical properties, nanostructure, and atomic environments. *Cement and Concrete Research*, *158*, 106855.

Bentz, D. P. (2007). A virtual rapid chloride permeability test. *Cement and Concrete Composites*, *29*(10), 723–731.

Berodier, E., & Scrivener, K. (2015). Evolution of pore structure in blended systems. *Cement and Concrete Research*, *73*, 25–35.

Bonneau, O., & Aitcin, P. C. (2002). Effect of the release of the formworks and of a thermal shock on the temperature and strains gradients in non-reinforced concrete. *PRO 23: International RILEM Conference on Early Age Cracking in Cementitious Systems-EAC'01*, *23*, 103. RILEM Publications.

Bräu, M., Ma-Hock, L., Hesse, C., Nicoleau, L., Strauss, V., Treumann, S., … Wohlleben, W. (2012). Nanostructured calcium silicate hydrate seeds accelerate concrete hardening: A combined assessment of benefits and risks. *Archives of Toxicology*, *86*(7), 1077–1087.

Chaudhary, S. K., & Sinha, A. K. (2020). Effect of silica fume on permeability and microstructure of high strength concrete. *Civil Engineering Journal*, *6*(9), 1697–1703.

Chen, X., Wu, S., & Zhou, J. (2013). Influence of porosity on compressive and tensile strength of cement mortar. *Construction and Building Materials*, *40*, 869–874.

Chen, X., Yang, X., Wu, K., Chen, Q., Yang, Z., Xu, L., & Li, H. (2023). Understanding the role of C–S–H seed/PCE nanocomposites, triethanolamine, sodium nitrate and PCE on hydration and performance at early age. *Cement and Concrete Composites*, 105002.

Cheung, J., Jeknavorian, A., Roberts, L., & Silva, D. (2011). Impact of admixtures on the hydration kinetics of Portland cement. *Cement and Concrete Research*, *41*(12), 1289–1309.

Chindaprasirt, P., Jaturapitakkul, C., & Sinsiri, T. (2005). Effect of fly ash fineness on compressive strength and pore size of blended cement paste. *Cement and Concrete Composites*, *27*(4), 425–428.

Chu, D. C., Kleib, J., Amar, M., Benzerzour, M., & Abriak, N.-E. (2021). Determination of the degree of hydration of Portland cement using three different approaches: Scanning electron microscopy

(SEM-BSE) and thermogravimetric analysis (TGA). *Case Studies in Construction Materials*, *15*, e00754.

Das, B. B., Singh, D. N., & Pandey, S. P. (2007). Some investigations for establishing suitability of watson's strength-porosity model for concrete. *Journal of ASTM International*, *5*(1), 1–10.

Das, S., Ray, S., & Sarkar, S. (2020). Early strength development in concrete using preformed CSH nano crystals. *Construction and Building Materials*, *233*, 117214.

Deboucha, W., Leklou, N., Khelidj, A., & Oudjit, M. N. (2017). Hydration development of mineral additives blended cement using thermogravimetric analysis (TGA): Methodology of calculating the degree of hydration. *Construction and Building Materials*, *146*, 687–701.

Du, H. J., & Pang, S. D. (2015). Effect of colloidal nano-silica on the mechanical and durability performances of mortar. *Key Engineering Materials*, *629*, 443–448.

Ehsani, A., Nili, M., & Shaabani, K. (2017). Effect of nanosilica on the compressive strength development and water absorption properties of cement paste and concrete containing fly ash. *KSCE Journal of Civil Engineering*, *21*(5), 1854–1865.

Ferreira, R. M., & Jalali, S. (2010). NDT measurements for the prediction of 28-day compressive strength. *NDT & E International*, *43*(2), 55–61.

Gaitero, J. J., Campillo, I., Mondal, P., & Shah, S. P. (2010). Small changes can make a great difference. *Transportation Research Record*, *2141*(1), 1–5.

Galan, I., & Glasser, F. P. (2015). Chloride in cement. *Advances in Cement Research*, *27*(2), 63–97.

Galobardes, I., Cavalaro, S. H., Aguado, A., & Garcia, T. (2014). Estimation of the modulus of elasticity for sprayed concrete. *Construction and Building Materials*, *53*, 48–58.

Garg, N., Gomez, J. M., & White, C. E. (2017). Impact of Nano-sized Additives on the Atomic Structure and Reaction Kinetics of Alkali-activated Slag. *37th Cement and Concrete Science Conference,* (pp. 151). At London, UK.

Garg, N., Özçelik, V. O., Skibsted, J., & White, C. E. (2019). Nanoscale ordering and depolymerization of calcium silicate hydrates in the presence of alkalis. *Journal of Physical Chemistry C*, *123*(40), 24873–24883.

Garg, N., & Skibsted, J. (2014). Thermal activation of a pure montmorillonite clay and its reactivity in cementitious systems. *Journal of Physical Chemistry C*, *118*(21), 11464–11477.

Garg, N., & Skibsted, J. (2015). Heated montmorillonite: structure, reactivity, and dissolution. In *Calcined Clays for Sustainable Concrete* (pp. 117–124). Springer.

Garg, N., & Wang, K. (2012). Comparing the performance of different commercial clays in fly ash-modified mortars. *Journal of Sustainable Cement-Based Materials*, *1*(3), 111–125.

Gluth, G. J. G., & Hillemeier, B. (2013). Pore structure and permeability of hardened calcium aluminate cement pastes of low w/c ratio. *Materials and Structures*, *46*(9), 1497–1506.

Gudimettla, J., & Crawford, G. (2016). Resistivity Tests for Concrete—Recent Field Experience. *ACI Materials Journal*, *113*(4).

Hall, C. (1989). Water sorptivity of mortars and concretes: A review. *Magazine of Concrete Research*, *41*(147), 51–61.

Hanehara, S., & Yamada, K. (1999). Interaction between cement and chemical admixture from the point of cement hydration, absorption behaviour of admixture, and paste rheology. *Cement and Concrete Research*, *29*(8), 1159–1165.

Hanžič, L., & Ilić, R. (2003). Relationship between liquid sorptivity and capillarity in concrete. *Cement and Concrete Research*, *33*(9), 1385–1388.

Hewlett, P. C., & Young, J. F. (1983). Physico-chemical interactions between chemical admixtures and Portland cement. *Journal of Materials Education*, *9*(4), 395–435.

Hewlett, P., & Liska, M. (2019). *Lea's chemistry of cement and concrete*. Butterworth-Heinemann.

Hosseini, P., Hosseinpourpia, R., Pajum, A., Khodavirdi, M. M., Izadi, H., & Vaezi, A. (2014). Effect of nano-particles and aminosilane interaction on the performances of cement-based composites: An experimental study. *Construction and Building Materials*, *66*, 113–124.

Houst, Y. F., Bowen, P., Perche, F., Kauppi, A., Borget, P., Galmiche, L., … Schober, I. (2008). Design and function of novel superplasticizers for more durable high performance concrete (superplast project). *Cement and Concrete Research*, *38*(10), 1197–1209.

Hubler, M. H., Thomas, J. J., & Jennings, H. M. (2011). Influence of nucleation seeding on the hydration kinetics and compressive strength of alkali activated slag paste. *Cement and Concrete Research*, *41*(8), 842–846.

Illinois Department of Transportation (IDOT). (2022). *Standard specifications for road and bridge construction.* Illinois Department of Transportation. https://idot.illinois.gov/Assets/uploads/files/Doing-Business/Manuals-Guides-&-Handbooks/Highways/Construction/Standard-Specifications/2022 Standard Specifications for Road and Bridge Construction.pdf

Indiana Department of Transportation (INDOT). (2022). *Standard Specifications*. https://www.in.gov/dot/div/contracts/standards/book/sep21/2022 Standard Specifications.pdf

Jennings, H. M., Bullard, J. W., Thomas, J. J., Andrade, J. E., Chen, J. J., & Scherer, G. W. (2008). Characterization and modeling of pores and surfaces in cement paste: Correlations to processing and properties. *Journal of Advanced Concrete Technology*, *6*(1), 5–29.

John, E., Epping, J. D., & Stephan, D. (2019). The influence of the chemical and physical properties of CSH seeds on their potential to accelerate cement hydration. *Construction and Building Materials*, *228*, 116723.

John, E., Matschei, T., & Stephan, D. (2018). Nucleation seeding with calcium silicate hydrate—A review. *Cement and Concrete Research*, *113*, 74–85.

Juenger, M. C. G., Snellings, R., & Bernal, S. A. (2019). Supplementary cementitious materials: New sources, characterization, and performance insights. *Cement and Concrete Research*, *122*, 257–273.

Justnes, H., & Nygaard, E. C. (1995). Technical calcium nitrate as set accelerator for cement at low temperatures. *Cement and Concrete Research*, *25*(8), 1766–1774.

Kanchanason, V., & Plank, J. (2019). Effect of calcium silicate hydrate–polycarboxylate ether (CSH–

PCE) nanocomposite as accelerating admixture on early strength enhancement of slag and calcined clay blended cements. *Cement and Concrete Research*, *119*, 44–50.

Karagöl, F., Demirboğa, R., Kaygusuz, M. A., Yadollahi, M. M., & Polat, R. (2013). The influence of calcium nitrate as antifreeze admixture on the compressive strength of concrete exposed to low temperatures. *Cold Regions Science and Technology*, *89*, 30–35.

Korpa, A., & Trettin, R. (2007). Nanoscale pozzolans for improving ultra-high performance cementitious binders. *Cement International*, *5*(1), 74–83.

Kosmatka, S., & Wilson, M. (2016). *Design and Control of Concrete Mixtures* (16th ed). Portland Cement Association.

Krus, M., Hansen, K. K., & Künzel, H. M. (1997). Porosity and liquid absorption of cement paste. *Materials and Structures*, *30*(7), 394–398.

Land, G., & Stephan, D. (2012). The influence of nano-silica on the hydration of ordinary Portland cement. *Journal of Materials Science*, *47*(2), 1011–1017.

Land, G., & Stephan, D. (2015). Controlling cement hydration with nanoparticles. *Cement and Concrete Composites*, *57*, 64–67.

Land, G., & Stephan, D. (2018). The effect of synthesis conditions on the efficiency of CSH seeds to accelerate cement hydration. *Cement and Concrete Composites*, *87*, 73–78.

Li, Haoxin, Xu, C., Dong, B., Chen, Q., Gu, L., & Yang, X. (2020). Enhanced performances of cement and powder silane based waterproof mortar modified by nucleation CSH seed. *Construction and Building Materials*, *246*, 118511.

Li, H., Xiao, H., Yuan, J., & Ou, J. (2004). Microstructure of cement mortar with nano-particles. *Composites Part B: Engineering*, *35*(2), 185–189.

Lothenbach, B., Scrivener, K., & Hooton, R. D. (2011). Supplementary cementitious materials. *Cement and Concrete Research*, *41*(12), 1244–1256.

Magarotto, R., Zeminian, N., & Roncero, J. (2010). An innovative accelerator for precast concrete: Crystal seeding to master the current challenges of the precast industry. *Betonwerk Und Fertigteil-Technik*, *76*(1).

Marsh, B. K., & Day, R. L. (1984). Some difficulties in the assessment of pore-structure of high performance blended cement pastes. *MRS Online Proceedings Library (OPL)*, *42*.

Michigan Department of Transportation (MDOT). (2020). *Standard specifications for construction*. https://www.michigan.gov/-/media/Project/Websites/MDOT/Field-Services/FieldServices4/2020-Standard-Specifications-Construction.pdf?rev=1e853edbff15425ca8b4905be4e51dee

Mindess, S., Young, F. J., & Darwin, D. (2003). Concrete, 2nd Ed. *Technical Documents*.

Mondal, P., Shah, S. P., Marks, L. D., & Gaitero, J. J. (2010). Comparative study of the effects of microsilica and nanosilica in concrete. *Transportation Research Record*, *2141*(1), 6–9.

Moon, J., Taha, M. M. R., Youm, K.-S., & Kim, J. J. (2016). Investigation of pozzolanic reaction in nanosilica-cement blended pastes based on solid-state kinetic models and 29Si MAS NMR.

Materials, *9*(2), 99.

Neithalath, N. (2006). Analysis of moisture transport in mortars and concrete using sorption-diffusion approach. *ACI Materials Journal*, *103*(3), 209.

Nguyen, H. G. T., Horn, J. C., Bleakney, M., Siderius, D. W., & Espinal, L. (2019). Understanding material characteristics through signature traits from helium pycnometry. *Langmuir*, *35*(6), 2115–2122.

Nicoleau, L., Gädt, T., Chitu, L., Maier, G., & Paris, O. (2013). Oriented aggregation of calcium silicate hydrate platelets by the use of comb-like copolymers. *Soft Matter*, *9*(19), 4864–4874.

Pedrosa, H. C., Reales, O. M., Reis, V. D., Paiva, M. das D., & Fairbairn, E. M. R. (2020). Hydration of Portland cement accelerated by C-S-H seeds at different temperatures. *Cement and Concrete Research*, *129*(August 2019), 105978. https://doi.org/10.1016/j.cemconres.2020.105978

Powers, T. C. (1958). Structure and physical properties of hardened Portland cement paste. *Journal of the American Ceramic Society*, *41*(1), 1–6.

Price, W. H. (1951). Factors influencing concrete strength. *Journal Proceedings*, *47*(2), 417–432.

Proceq. (2011). *Instructions, Resipod Operating*. Switzerland.

Qadri, F., & Jones, C. (2020). Durable high early strength concrete via internal curing approach using saturated lightweight and recycled concrete aggregates. *Transportation Research Record*, 0361198120920882.

Qadri, F., & Garg, N. (2023). Early-stage performance enhancement of concrete via commercial CSH seeds: From lab investigation to field implementation in Illinois, US. *Case Studies in Construction Materials*, e02353.

Ramachandran, V. S. (1996). *Concrete admixtures handbook: properties, science and technology*. William Andrew.

Romero, P., & Garg, N. (2022). Evolution of kaolinite morphology upon exfoliation and dissolution: Evidence for nanoscale layer thinning in metakaolin. *Applied Clay Science*, *222*, 106486.

Rupnow, T. D., & Icenogle, P. J. (2012). Surface resistivity measurements evaluated as alternative to rapid chloride permeability test for quality assurance and acceptance. *Transportation Research Record*, *2290*(1), 30–37.

Schrag, E., Qadri, F., & Jones, C. (2021). Temperature prediction for high early strength concrete pavement repair. In *Airfield and Highway Pavements 2021* (pp. 155–161).

Scrivener, K., Snellings, R., & Lothenbach, B. (2016). *A practical guide to microstructural analysis of cementitious materials* (Vol. 540). CRC Press.

Shaikh, F. U. A., & Supit, S. W. M. (2014). Mechanical and durability properties of high volume fly ash (HVFA) concrete containing calcium carbonate (CaCO3) nanoparticles. *Construction and Building Materials*, *70*, 309–321.

Shanahan, N., Sedaghat, A., & Zayed, A. (2016). Effect of cement mineralogy on the effectiveness of chloride-based accelerator. *Cement and Concrete Composites*, *73*, 226–234.

Sharma, U., Singh, L. P., Zhan, B., & Poon, C. S. (2019). Effect of particle size of nanosilica on microstructure of CSH and its impact on mechanical strength. *Cement and Concrete Composites*, *97*, 312–321.

Solanki, P., & Xie, H. (Forthcoming). *Field-curing methods for evaluating the strength of concrete test specimens*. Illinois Center for Transportation.

Song, H.-W., Pack, S.-W., Nam, S.-H., Jang, J.-C., & Saraswathy, V. (2010). Estimation of the permeability of silica fume cement concrete. *Construction and Building Materials*, *24*(3), 315–321.

Spragg, R., Bu, Y., Snyder, K., Bentz, D., & Weiss, J. (2013). *Electrical testing of cement-based materials: Role of testing techniques, sample conditioning, and accelerated curing* (Report No. FHWA/IN/JTRP-2013/28). Joint Transportation Research Program. https://doi.org/10.5703/1288284315230

Sun, J., Shi, H., Qian, B., Xu, Z., Li, W., & Shen, X. (2017). Effects of synthetic CSH/PCE nanocomposites on early cement hydration. *Construction and Building Materials*, *140*, 282–292.

Taylor, P. C. (2013). *Curing concrete*. CRC Press.

Theobald, M., & Plank, J. (2022). C–S–H–Polycondensate nanocomposites as effective seeding materials for Portland composite cements. *Cement and Concrete Composites*, *125*, 104278.

Thomas, J. J., Jennings, H. M., & Chen, J. J. (2009). Influence of nucleation seeding on the hydration mechanisms of tricalcium silicate and cement. *Journal of Physical Chemistry C*, *113*(11), 4327–4334.

Todd, N. T., Suraneni, P., & Weiss, W. J. (2017). Hydration of cement pastes containing accelerator at various temperatures: Application to high early strength pavement patching. *Advances in Civil Engineering Materials*, *6*(2), 23–37.

Vehmas, T., Kronlöf, A., & Cwirzen, A. (2018). Calcium chloride acceleration in ordinary Portland cement. *Magazine of Concrete Research*, *70*(16), 856–863.

Wang, F., Kong, X., Jiang, L., & Wang, D. (2020). The acceleration mechanism of nano-CSH particles on OPC hydration. *Construction and Building Materials*, *249*, 118734.

Wei, Y., Wang, Y., Zheng, F., Mu, W., & Huang, T. (2022). Preparation and hydration mechanism of aluminum formate/aluminum sulfate based alkali-free composite accelerator for sprayed concrete. *Materials Research Express*, *9*(5), 55101.

Weiss, W. J., Barrett, T. J., Qiao, C., & Todak, H. (2016). Toward a specification for transport properties of concrete based on the formation factor of a sealed specimen. *Advances in Civil Engineering Materials*, *5*(1), 179–194.

Weiss, W. J., Qiao, C., Isgor, B., & Olek, J. (2020). *Implementing rapid durability measure for concrete using resistivity and formation factor* (Report No. FHWA/IN/JTRP-2020/08). Joint Transportation Research Program Publication. https://doi.org/10.5703/1288284317120

Wyrzykowski, M., Assmann, A., Hesse, C., & Lura, P. (2020). Microstructure development and autogenous shrinkage of mortars with CSH seeding and internal curing. *Cement and Concrete Research*, *129*, 105967.

Xu, C., Li, H., & Yang, X. (2020). Effect and characterization of the nucleation CSH seed on the

reactivity of granulated blast furnace slag powder. *Construction and Building Materials*, *238*, 117726.

Yu, Z., & Ye, G. (2013). The pore structure of cement paste blended with fly ash. *Construction and Building Materials*, *45*, 30–35.

Zhang, G., Yang, Y., & Li, H. (2020). Calcium-silicate-hydrate seeds as an accelerator for saving energy in cold weather concreting. *Construction and Building Materials*, *264*, 120191.

Zhang, Y., Pichler, C., Yuan, Y., Zeiml, M., & Lackner, R. (2013). Micromechanics-based multifield framework for early-age concrete. *Engineering Structures*, *47*, 16–24.

APPENDIX A

Table 6 presents the date and location of each concrete mixture obtained from the field. Also, Tables 7–15 present all measurements of compressive strength, flexural strength, electrical resistivity, and formation factor for cast-in-place concrete; in addition to fresh properties for concrete mixtures collected from field demo project stage I and stage II.

Table 6. Mixture Date and Locations

Mixture	Date	Location
SI Mix OPC[1]	10/21/2020	Peoria, IL
SI Mix OPC + ACC[1]	10/21/2020	Peoria, IL
SI Mix 75-25 OPC/FA[1]	10/21/2020	Peoria, IL
SI Mix 75-25 OPC/FA + ACC[1]	10/21/2020	Peoria, IL
PC Mix OPC[2]	3/31/2021	Champaign, IL
DS Mix 60-40 OPC/FA[3]	6/17/2021	Peoria, IL
Field Demo Stage I OPC[4]	5/12/2022	Near Armstrong, IL
Field Demo Stage II OPC + X2[5]	7/21/2022	Near Armstrong, IL

1: IDOT Class SI structural mix design.

2: IDOT Class PC precast concrete structural mix design.

3: IDOT Class DS drilled shaft mix design for mass concrete pour.

4: Box culvert field demo project using experimental mix without X2.

5: Box culvert field demo project using experimental mix with X2.

Table 7. Compressive Strength for All Mixtures

Compressive Strength (psi)							
Mixture	Age (days)						
	1	2	3	7	14	52	97
SI Mix OPC[1]	2799	3903	4387	5401	6272	7562	6933
SI Mix OPC + ACC[1]	2712	4059	4523	5432	6152	6830	6682
SI Mix 75-25 OPC/FA[1]	2185	3765	4748	5794	7411	8785	8626
SI Mix 75-25 OPC/FA + ACC[1]	2386	3960	4714	5830	7153	8540	8612
PC Mix OPC[2]	3220	5450	6428	7485	8105	9487	10540
DS Mix 60-40 OPC/FA[1]	2022	3507	3993	5320	7151	8452	8256

1: The cylinders were kept in water for 7 days, then they were removed to dry. (For more details, refer to section "Field Work" in Chapter 3.)

2: The cylinders were in the mold until the day of testing. (For more details, refer to section "Field Work" in Chapter 3.)

Table 8. Compressive Strength for Field Demo Stage I and Stage II Experimental Concrete Mixtures

Mixture	Date	Compressive Strength (psi)						
		Age (days)						
		2	3	7	14	28	56	97
Stage I OPC	5/12/2022[1]	3708	4305	5406	6177	6602	7007	7667
Stage II OPC + X2	7/21/2022[1]	5354	6010	6886	7585	7736	8121	8428
Stage I OPC	5/20/2022[2]		4720					
Stage I OPC	5/20/2022[3]		4600					
Stage I OPC	6/8/2022[4]	4086	4493	5325				
Stage I OPC	6/8/2022[5]	3817	4089	5299				
Stage I OPC	6/8/2022[6]	4344	4502	5460				
Stage I OPC	6/8/2022[7]	4279	4736	4923				
Stage II OPC + X2	8/11/2022[2]		5875					
Stage II OPC + X2	8/11/2022[3]		5874					
Stage II OPC + X2	8/22/2022[4]	4927	5974	7096				
Stage II OPC + X2	8/22/2022[5]	5295	5772	6703				
Stage II OPC + X2	8/22/2022[6]	6069	6333	6794				
Stage II OPC + X2	8/22/2022[7]	6070	6267	6498				

1: The cylinders were demolded and kept in a water tank until the day of testing. (For more details, refer to section "Field Work" in Chapter 3.)
2: 100 mm (4 in.) cylinders cured in an insulated cooler until the time of the test. 100 mm (4 in.) cylinders cured in the same cooler as 150 mm (6 in.) cylinders. Refer to ICT-IDOT project R27-219 for more information (Solanki & Xie, Forthcoming).
3: 150 mm (6 in.) cylinders cured in an insulated cooler until the time of the test. 150 mm (6 in.) cylinders were in the same cooler as the 100 mm (4 in.) cylinders. Refer to Solanki and Xie (Forthcoming) for more information.
4: 100 mm (4 in.) cylinders field cured until time of test. Refer to Solanki and Xie (Forthcoming) for more information.
5: 150 mm (6 in.) cylinders field cured until time of test. Refer to Solanki and Xie (Forthcoming) for more information.
6: 100 mm (4 in.) cylinders field cured in insulated cooler until time of test. Refer to Solanki and Xie (Forthcoming) for more information.
7: 150 mm (6 in.) cylinders field cured in insulated cooler until time of test. Refer to Solanki and Xie (Forthcoming) for more information.

Table 9. Flexural Strength for All Mixtures

Mixture	Flexural Strength (psi)		
	Age (days)		
	3	7	14
SI Mix OPC[1]	860	957	760
SI Mix OPC + ACC[1]	880	954	747
SI Mix 75-25 OPC/FA[1]	863	948	748
SI Mix 75-25 OPC/FA + ACC[1]	914	897	766
PC Mix OPC[2]	1052	1107	1083
DS Mix 60-40 OPC/FA[1]	924	1144	972

1: The beams were kept in water for seven days and then were removed to dry. (For more details, refer to section "Field Work" in Chapter 3.)
2: The beams were demolded in the first day after casting and kept dry until the day of testing. (For more details, refer to section "Field Work" in Chapter 3.)

Table 10. Flexural Strength for Field Demo Stage I and Stage II Experimental Concrete Mixtures

Flexural Strength (psi)[2]				
Mixture	Date	Age (days)		
		2	3	7
Stage I OPC_1[1]	5/12/2022	656	711	800
Stage I OPC_2	5/20/2022	650	734	911
Stage I OPC_3	5/27/2022	734	733	856
Stage I OPC_4	6/8/2022	667	734	789
Stage II OPC + X2_1[1]	7/21/2022	811	911	889
Stage II OPC + X2_2	8/11/2022	667	800	889
Stage II OPC + X2_3	8/22/2022	750	734	823

1: Test result was used for Figure 32.

2: The beams were demolded in the first day after casting and placed in water tank for curing.

Table 11. Electrical Resistivity for All Mixtures

Electrical Resistivity (Kohm-cm)								
Mixture	Age (days)							
	1	2	3	7	14	29	52	97
SI Mix OPC[1]	4.5	5.7	7.2	7.5	–	13.4	13.4	13.6
SI Mix OPC + ACC[1]	4.6	4.6	5.7	7.0	–	10.2	12	12.4
SI Mix 75-25 OPC/FA[1]	3.3	4.6	5.4	7.0	–	9.9	20.5	24.7
SI Mix 75-25 OPC/FA + ACC[1]	3.5	4.2	5.2	6.0	–	9.6	19	21.1
PC Mix OPC[1]	3.7	4.7	5.0	5.5	6.5	8.2	9.2	11.5[1]/14.3[2]
DS Mix 60-40 OPC/FA[1]	2.5	3.0	3.8	5.1	7.8	14.8	19.9	27.4[1]/30.8[2]

1: The cylinders were kept in water all the time until testing. (For more details, refer to section "Field Work" in Chapter 3.)
2: The cylinders were in the mold for 90 days and subsequently saturated for seven days. (For more details, refer to section "Field Work" in Chapter 3.)

Table 12. Electrical Resistivity for Field Demo Stage I and Stage II Experimental Concrete Mixtures

Electrical Resistivity (Kohm-cm)								
Mixture	Date	Age (days)						
		2	3	7	14	28	56	97
Stage I OPC[1]	5/12/2022	4	4.3	4.7	5.4	6	6.9	8.8
Stage II OPC+X2[1]	7/21/2022	3.4	3.8	4.5	4.8	5.7	7	9

1: The cylinders were kept in water all the time until testing. (For more details, refer to section "Field Work" in Chapter 3.)

Table 13. Formation Factor for All Mixtures

Mixture				Formation Factor				
				Age (days)				
	1	2	3	7	14	29	52	97
SI Mix OPC[1]	595	754	953	992	–	1773	1773	1800
SI Mix OPC + ACC[1]	596	596	738	907	–	1321	1554	1606
SI Mix 75-25 OPC/FA[1]	546	761	843	1158	–	1637	3391	4085
SI Mix 75-25 OPC/FA + ACC[1]	554	665	823	950	–	1120	3008	3340
PC Mix OPC[1]	316	401	427	470	555	700	786	982[1]/1221[2]
DS Mix 60-40 OPC/FA[1]	370	444	560	755	1154	2190	2945	4055[1]/4558[2]

1: The cylinders were kept in water all the time until testing. (For more details, refer to section "Field Work" in Chapter 3.)
2: The cylinders were in the mold for 90 days and subsequently saturated for seven days. (For more details, refer to section "Field Work" in Chapter 3.)

Table 14. Formation Factor for Field Demo Stage I and Stage II Experimental Concrete Mixtures

Mixture	Date	Formation Factor						
		Age (days)						
		2	3	7	14	28	56	97
Stage I OPC[1]	5/12/2022	610	656	717	823	915	1052	1357
Stage II OPC+ X2[1]	7/21/2022	474	530	628	700	795	977	1256

1: The cylinders were kept in water all the time until testing. (For more details, refer to section "Field Work" in Chapter 3.)

Table 15. Fresh Properties of Concrete Mixtures Collected from Field Demo Project Stage I and Stage II

Mixture	Date	Slump (inches)	Air Content (%)	Concrete Temperature (°F)	Air Temperature (°F)	w/c ratio
Stage I OPC	5/12/2022	6.5	5.1	88	91	0.38
Stage I OPC	5/20/2022	–	8.0	82	85	0.37
Stage I OPC	5/27/2022	–	5.0	73	58	0.39
Stage I OPC	6/8/2022	6.5	5.9	74	65	0.38
Stage II OPC + X2	7/21/2022	4.75	5.4	80	65	0.42
Stage II OPC + X2	8/11/2022	7.5	5.6	84	88	0.43
Stage II OPC + X2	8/22/2022	6.5	5.3	84	77	0.39

1: The calculated water-to-cement ratio includes water from the admixtures. It was assumed 70% of the chemical admixture dosage was water.

Table 16. Concrete Mixture Proportions Collected from the Field Demo Project Stage I and Stage II

Concrete Mixtures	Quantity Batched per Cubic Yard									
	Cement, kg (lb)	Fly Ash, kg (lb)	Water, L (gal)	FA[8], kg (lb)	CA[9], kg (lb)	AEA[10], mL (fl oz)	Water Reducer, mL (fl oz)	Retarder, mL (fl oz)	HRWR[11], mL (fl oz)	RCA[12], mL (fl oz)
Field Demo Stage I OPC[1]	286 (630)[13]	–	107 (28.3)	533 (1,174)[13]	831 (1,831)[13]	192 (6.5)	654 (22.1)	467 (15.8)	840 (28.4)	–
Field Demo Stage I OPC[2]	286 (630)[13]	–	103 (27.3)	523 (1,152)[13]	838 (1,848)[13]	204 (6.9)	745 (25.2)	467 (15.8)	1263 (42.7)	–
Field Demo Stage I OPC[3]	286 (630)[13]	–	111 (29.2)	523 (1,152)[13]	838 (1,848)[13]	183 (6.2)	745 (25.2)	–	–	–
Field Demo Stage I OPC[4]	286 (630)[13]	–	107 (28.3)	523 (1,152)[13]	838 (1,848)[13]	160 (5.4)	671 (22.7)	–	379 (12.8)	–
Field Demo Stage II OPC + X2[5]	286 (630)[13]	–	119 (31.5)	529 (1,166)[13]	822 (1,812)[13]	296 (10.0)	651 (22.0)	186 (6.3)	420 (14.2)	932 (31.5)
Field Demo Stage II OPC + X2[6]	286 (630)[13]	–	120 (31.7)	529 (1,166)[13]	822 (1,812)[13]	296 (10.0)	742 (25.1)	467 (15.8)	630 (21.3)	932 (31.5)
Field Demo Stage II OPC + X2[7]	286 (630)[13]	–	110 (29.0)	529 (1,166)[13]	822 (1,812)[13]	296 (10)	742 (25.1)	467 (15.8)	630 (21.3)	932 (31.5)

1: Cast on 5/12/2022
2: Cast on 5/20/2022
3: Cast on 5/27/2022
4: Cast on 6/8/2022
5: Cast on 7/21/2022
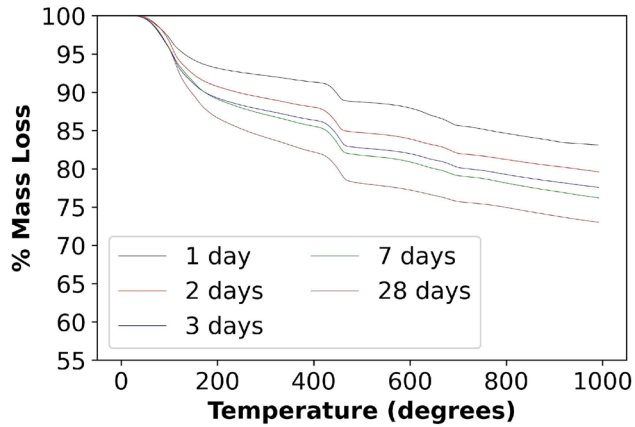6: Cast on 8/11/2022
7: Cast on 8/22/2022
8: Fine aggregate
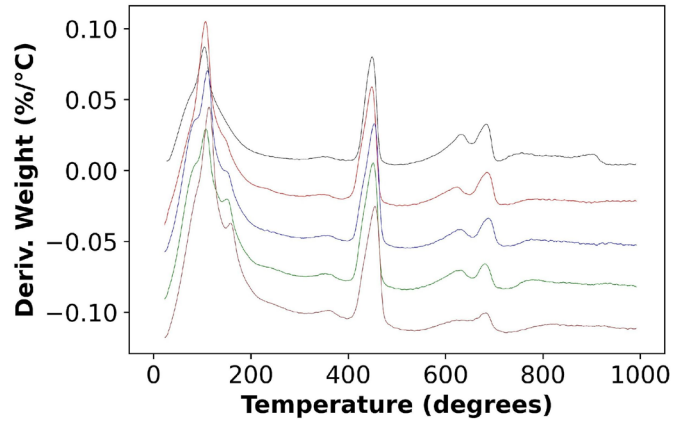9: Coarse aggregate
10: Air-entraining admixture
11: High-range water reducer
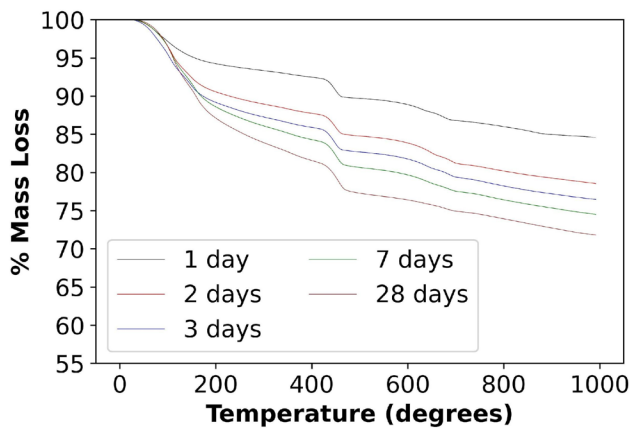12: Rheology-controlling admixture (X2)
13: Theoretical batch weight provided since actual batch weight was unavailable.
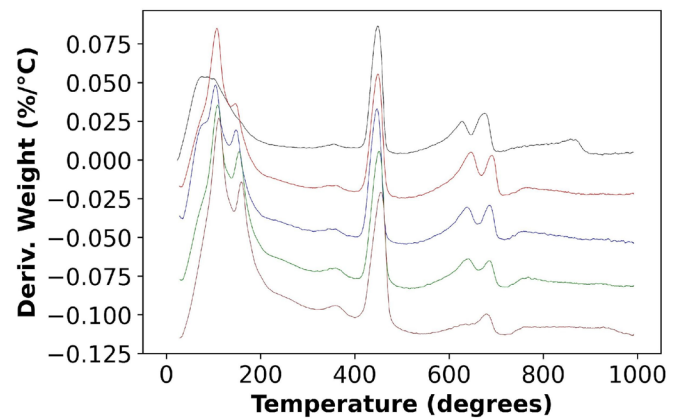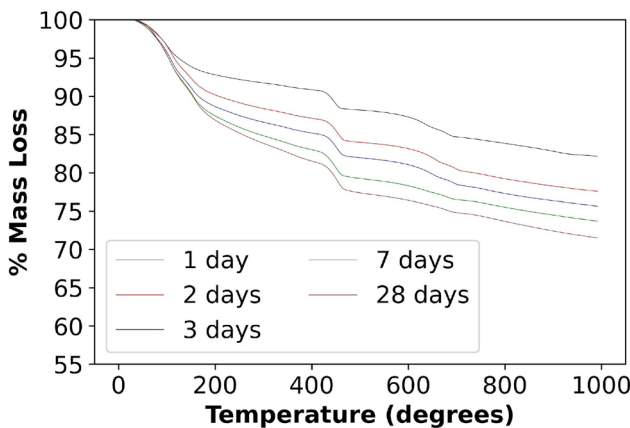
a) TGA for M0 mixture

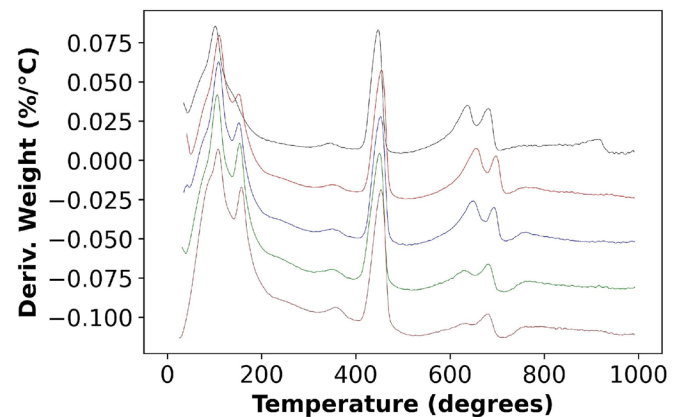b) DTGA for M0 mixture

c) TGA for M7 mixture

d) DTGA for M7 mixture

e) TGA for M14 mixture

f) DTGA for M14 mixture

Figure 36. Graphs. a) Mass degradation for M0, b) derivative mass degradation for M0, c) mass degradation for M7, d) derivative mass degradation for M7 e) mass degradation for M14, and f) derivative mass degradation for M14. These data are measured at days 1, 2, 3, 7, and 28.

APPENDIX B

The following is the special provision for the box culvert demo project. The box culvert (Structure # 092-2045) was completed under Illinois Department of Transportation Contract # 70905. The box culvert is located on Illinois Route 49, 0.5 miles north of US 136 East in Vermilion County.

CAST-IN-PLACE BOX CULVERT CONCRETE (CLASS SI - SHORT CURE PERIOD (SCP))

Effective: August 13, 2021

Description.

The Contractor is advised this is a demonstration project for a new concrete mix design. This work shall consist of the construction of a cast-in-place box culvert using Class SI concrete with a cure period in the range of 24 to 72 hours for Stage I and Stage II, as well as construction of trial batches for concrete testing with disposal of the excess concrete. The work shall be according to the applicable portions of Section 540 of the Standard Specifications.

Materials.

The materials shall be according to Article 540.02(a) except the following revisions shall apply to Section 1020.

For Stage I construction of the box culvert, the Class SI mix design parameters per Article 1020.04 (Table 1) are revised as follows: the cement factor shall be a minimum 6.05 cwt/cu yd (360 kg/cu m) and a maximum 6.50 cwt/cu yd (385 kg/cu m); the water/cement ratio shall be 0.36 to 0.38, the strength shall be a minimum 3500 psi (24,000 kPa) compressive or 650 psi (4500 kPa) flexural at 72 hours; and a high range water-reducing admixture shall be used.

For Stage II construction of the box culvert, the Class SI mix design parameters shall be the same as Stage I except the rheology-controlling admixture (X2) will also be required. The dosage shall be in the 7-10 oz/cwt. (456-652 ml/100 kg) range. A technical representative shall be available for assistance when establishing the dosage rate.

For each concrete pour, the Engineer will perform all concrete testing. Sufficient compressive and flexural strength specimens will be molded to perform six separate compressive tests and six separate flexural tests.

The curing period for Culverts as indicated in Article 1020.13 shall be revised to end at 72 hours. However, this specified curing period may be terminated earlier if the concrete has attained 80 percent of the specified mix design strength. The minimum cure period shall be 24 hours.

Trial Batch.

A trial batch for the Class SI – SCP concrete shall be scheduled a minimum of 21 calendar days prior to anticipated use for Stage I construction of the box culvert and 14 calendar days prior to anticipated

use for Stage II. The trial batch shall be performed in the presence of the Engineer, and the Engineer will perform all testing.

A minimum 4 cubic yard (3.0 cubic meter) trial batch shall be produced and placed off site. The Contractor may propose alternative locations for approval by the Engineer. The trial batch will be evaluated for slump, air content, and strength without the rheology-controlling admixture. Sufficient compressive and flexural strength specimens will be molded to perform nine separate compressive tests and nine separate flexural tests.

The same trial batch will subsequently be evaluated for slump, air content, and strength with the rheology-controlling admixture. Sufficient compressive and flexural strength specimens will be molded to perform nine separate compressive tests and nine separate flexural tests.

 Based on one or more trial batches, the final admixture dosages and mix design parameters will be determined and approved by the Engineer. A mix design capable of obtaining the full specified strength at 72 hours will be selected.

Instrumentation.

The Engineer shall have free access for installation of thermocouples and other instrumentation on or within the structure. The testing equipment will be provided by the Engineer. As a minimum, three thermocouples per pour will be installed. Two will be installed in the concrete and one will be used to measure ambient air temperature. This information is for determining the maximum temperature differential as discussed under Falsework and Form Removal. The Contractor shall cooperate with the Engineer and take necessary steps to prevent damage to the instrumentation.

Falsework and Form Removal

Falsework and form removal shall be according to Articles 503.05 and 503.06 except only flexural strength test results will be accepted for self-supporting box culvert components. The cure period shall be as specified under Materials herein.

When the Contractor performs form removal, the maximum temperature differential between the internal concrete core and the ambient air temperature shall not exceed 50 °F (28 °C). If this maximum temperature differential is exceeded, the Contractor shall wait until the concrete is within the maximum temperature differential range before form removal is performed. The Engineer will provide the heat of hydration temperature differential information.

Method of Measurement.

Cast-in-place concrete box culverts will be measured for payment according to Article 540.07.

Concrete for cast-in-place box culverts which contain a rheology-controlling admixture will be measured for payment in cubic yards (cubic meters) as specified in Article 540.07

Trial batches will be measured for payment in units of each.

<u>Basis of Payment.</u>

Cast-in-place concrete box culverts will be paid for according to Article 540.08.

Cast-in-place concrete box culverts which contain a rheology-controlling admixture will be paid for at the contract unit price per cubic yard (cubic meter) for CONCRETE BOX CULVERTS (RHEOLOGY-CONTROLLING ADMIXTURE).

Trial batches will be paid for at the contract unit price per each for TRIAL BATCH.